

POLITECNICO DI TORINO

Dipartimento di Energia

**Corso di Laurea Magistrale
in Ingegneria Energetica e Nucleare**

Tesi di Laurea Magistrale

System analysis of a polygeneration plant integrated by a chemical
looping unit for dimethyl ether and power production



Relatori

Prof. Massimo Santarelli
Dott. Azharuddin E. Farooqui

Candidato

Felice Di Tomaso

A.A.2017-2018

Abstract

Chemical looping syngas production has gained attention in recent times as an alternative to the fuel crises and CO₂ emission reduction by converting CO₂ into fuel or hydrocarbons. Methane reduction of metal oxides for subsequent CO₂/H₂O dissociation provides a significant advantage to the liquid hydrocarbon and fuel production strategies which was found to be hindered by the only-thermal reduction step in existing approach for solar thermochemical syngas production. The present study proposes to utilise an integrated methane driven chemical looping unit for CO₂-H₂O dissociation for syngas production from exhaust gases in a novel polygeneration plant for power and dimethyl ether production. The thesis aims to investigate the feasibility of the plant through simulation studies using Aspen Plus[®]. In this regard, a full assessment of the plant was performed adopting both thermodynamic and kinetics of chemical looping syngas production with ceria as an oxygen carrier. The analysis is carried out based on energy, exergy and economic study. Through thermodynamic sensitivity analyses of the main parameters of the plant, the optimal point of operation of the plant was calculated. It results in an overall efficiency of 50.2% and a production of 102 MW and 2.14 kg/s of power and DME respectively. An exergy efficiency of 45% was also calculated. A detailed techno-economic and exergo-economic assessment was performed. Results show a total overnight cost of the plant as 537 million\$, with the Air Separation Unit being the primary contributor with 22% of the total cost. A payback period of 20 years was achieved with electricity and DME selling price of 220 \$/MWh and 72 \$/MWh respectively.

The chemical looping unit with two reactors is highly depended on the type of reactor system chosen which reflects the syngas production. Based on the literature, a moving bed reactor model was selected. The corresponding performance was evaluated based on the thermodynamic and the kinetic assessments. A 20% lower efficiency for the kinetic assessment was found compared to thermodynamics. Later, the CL unit with the kinetic model was integrated with the polygeneration plant to access the overall system performance. It is found that for similar ceria circulating flow the DME production reduces from 2.14 kg/s for thermodynamic CL unit model to 1.48 kg/s for kinetic moving bed CL unit. Similarly, there is a drop in power production when considering the kinetic model from 102 MWe to 71 MWe. The kinetics of redox ceria cycle has a very strong effect on the chemical looping unit which limits the whole process layout but still can reach a high efficiency of 51.8%. In addition, it also reflects the strong potential of chemical looping syngas production pathways to integrate with polygeneration system to increase the overall efficiency with reduced cost of carbon capture from the baseline.

Contents

Abstract	1
Contents.....	i
1. Introduction.....	1
1.1. Objectives of the thesis.....	3
1.2. Structure of the thesis	3
2. Theory Background	4
2.1. Carbon Capture and Sequestration	4
2.2. Carbon Capture and Utilization (CCU).....	7
2.3. Chemical looping process.....	8
2.3.1. CO ₂ /H ₂ O dissociation based on chemical looping process.....	9
2.3.1.1 Materials	11
2.3.1.2 Reactors.....	14
2.3.2. Chemical looping process by fuel reduction.....	21
2.4. Polygeneration.....	22
2.5. Dimethyl ether	23
3. Methodology.....	27
3.1. Process modelling and simulation tools	27
3.2. Exergy analysis.....	27
3.2.1. Exergy analysis indicators.....	29
3.3. Techno-economic and discounted cash flow analysis.....	30
3.3.1. Economic assumption	31
3.4. Exergo-economic analysis.....	33
3.5. Water consumption estimation	35
4. Plant simulation and results	37
4.1. Process and plant description	37
4.1.1. Simulation Assumption.....	38
4.1.2. Chemical looping syngas production Unit (CL unit).....	40
4.1.3. Air separation unit (ASU)	40
4.1.4. Oxyfuel Combustion unit.....	42
4.1.5. Dimethyl ether production (DME) unit.....	42
4.1.6. DME distillation unit.....	42

4.1.7.	Steam cycle	43
4.2.	Synthesis of DME.....	43
4.2.1.	Kinetic Model.....	44
4.2.1.	Reactor design	47
4.3.	Performance results	48
4.3.1.	Effect of operating conditions	48
4.3.2.	Heat integration in the plant	55
4.4.	Exergy analysis.....	56
4.5.	Economic analysis	62
4.5.1.	Discounted Cash Flow analysis.....	64
4.5.2.	Exergo-economic analysis.....	64
4.5.3.	Water consumption	67
5.	Chemical looping unit analysis	68
5.1.	Analysis of the thermodynamic model of the CL unit	69
5.1.1.	Reactor model design	69
5.1.2.	Reduction reactor results	70
5.1.3.	Oxidation reactor results	72
5.1.4.	Heat Requirement results	74
5.2.	Kinetic model of CL unit.....	76
5.2.1.	Ceria oxidation kinetic	77
5.2.2.	Ceria reduction kinetic	78
5.2.3.	Reactor model	79
5.2.4.	Simulation Assumption	80
5.2.5.	Reactor sizing and performance sensitivity	80
5.2.5.1	Reduction Reactor	80
5.2.5.2	Oxidation reactor.....	82
5.3.	CL unit performance results - thermodynamic and kinetic model comparison	84
6.	Integration of the kinetic model in the polygeneration plant	86
6.1.	Reactors sizing.....	86
6.2.	Performance results	86
7.	Conclusion	90
	References	91

List of Figures

Figure 1: a) Conceptual scheme of the solar chemical looping syngas production through solar thermal reduction and corresponding splitting of water and carbon dioxide, usually present in waste gas from industrial applications. b) Conceptual scheme of the chemical looping syngas production through methane reduction and corresponding splitting of water and carbon dioxide, usually present in waste gas from industrial applications	2
Figure 2: main route for carbon capture [27]	4
Figure 3: Historical progression of oxyfuel combustion technology [42].	6
Figure 4: syngas utilization routes in the industrial sector	8
Figure 5: Schematic of the sulphur-iodine thermochemical cycle for hydrogen production proposed by General Atomics [64]	10
Figure 6: Tubular packed bed solar reactor for H ₂ production proposed by Tamaura et al. [85]	15
Figure 7: Honeycomb multi-channels reactor proposed by Roeb et al. [70]	16
Figure 8: a) Multi-chambers reactor proposed by Roeb et al. [86], b) lamellae shutter for temperature regulation.....	17
Figure 9: Internally circulating bed proposed by Kodama et al. [87]	17
Figure 10: a) Foam reactor proposed by Gokon et al. [88] b) Iron foam sample, c) ceria foam sample.....	18
Figure 11: proposed reactor by Chueh et al. [90] for H ₂ O-CO ₂ dissociation.....	19
Figure 12: a) Rotator reactor concept proposed by Kaneko et al. [92], b) pilot scale rotating reactor.....	20
Figure 13: CR5 reaction proposed by diver et al.[93].....	20
Figure 14: reactor design for chemical looping methane reduction. a) solar cavity receiver proposed by Warren et al. [102] b) tubular packed bed proposed by Krenzke et al. [104]	22
Figure 15: Road load test data comparing engine emissions using DME and diesel [120].....	25
Figure 16: Tank-to-wheel efficiency of various vehicle technologies [24]	25
Figure 17: Tank-to-wheel GHG emission for various fuels and vehicles [24].	26
Figure 18: plant general concept	37
Figure 19: Detailed Plant Layout for Power and DME Production from Natural Gas Utilizing the CL Unit.....	39
Figure 20: Detailed plant of the Air Separation Unit	41
Figure 21: influence of the H ₂ /CO ratio on the equilibrium synthesis of DME at T=250°C and p=50 bar.....	46
Figure 22: a) influence of the CO ₂ on the equilibrium synthesis of DME at T=250°C and p=50 bar, b) influence of the H ₂ O on the equilibrium synthesis of DME at T=250°C and p=50 bar.....	47
Figure 23: DME yield from DME reactor varying reactor length (L)	48
Figure 24: influence of chemical looping unit pressure on efficiency η , W_{NET} , Ce ₂ O ₃ outlet from RED and $W_{COMP,tot}$ ($=W_{COMP-1}+ W_{COMP-2}+ W_{COMP-3}$).	49
Figure 25: influence of the outlet temperature of RED on efficiency (η), net power (W_{NET}), gas turbine power (W_{GT}), heat need from RED (Q_{RED})	50
Figure 26: effect of the initial gas mixture composition fed into OXI on a) final syngas CO/H ₂ ratio, b) CO ₂ content in the syngas after water removal	50

Figure 27: influence of the as mixture composition into the inlet of OXI on the plant performance b considering a metal outlet temperature from the RED equal to 900°C.	51
Figure 28: effect of the gas mixture inlet composition and metal oxide inlet temperature ($T_{OC,OXI}$ inlet) on the temperature of the metal oxide outlet	52
Figure 29: effect of the gas turbine inlet temperature TIT on the efficiency of the plant (η), power produced by the steam turbine (W_{ST}), by the gas turbine GT (W_{GT}) and the power absorbed by the COMP-3 (W_{COMP-3}).....	53
Figure 30: pinch point analysis, hot and cold composite curve	56
Figure 31: exergetic efficiency and total irreversibilities generated varying a) the operating pressure of the CL unit, b)the temperature of the inlet metal into the reduction reactor ($T_{MET,in}$) c) the temperature inlet into the gas turbine (TIT).....	57
Figure 32: effect of the gas mixture composition feed into the OXI on the exergetic efficiency η_{ex} and irreversibilities I_{dest}	58
Figure 33: contribution of the components to the TOC	63
Figure 34: (a) Economic performance varying DME and electricity price. (b) Payback period (PBP) varying DME and electricity price	64
Figure 35: Schematic of Interconnected CL unit for ceria reduction with methane and subsequent oxidation with CO ₂ and H ₂ O splitting using moving bed reactors.....	69
Figure 36: Effect of the CH ₄ /CeO ₂ ratio and the isothermal temperature of the reduction reactor over the equilibrium of the main species, a) Ce ₂ O ₃ , b) CH ₄ , c) CO, d) H ₂	70
Figure 37: effect of the CH ₄ /CeO ₂ ratio and the isothermal temperature of the reduction reactor over the equilibrium of the sub-products, a) CO ₂ , b) H ₂ O, c) C	71
Figure 38: the effect of the inlet temperature of the fed Ce ₂ O ₃ and of an equimolar (50% H ₂ -50% H ₂ O, with a gas-mixture/Ce ₂ O ₃ ratio fixed to 1.05) inlet gas mixture on a) CeO ₂ production, b) CO/H ₂ ratio, c) CO ₂ dilution, d) H ₂ O dilution.....	73
Figure 39: effect of the gas-mixture/Ce ₂ O ₃ ratio on the production of CeO ₂ by an equimolar gas inlet with a temperature inlet of 1000°C and a metal inlet temperature of 1000°C.....	73
Figure 40: effect of varying the metal inlet temperature $T_{metal,inlet}$ and the composition of the inlet gas stream (the remaining part of the gas mixture is composed by water) on a) CO/H ₂ ratio of the outlet syngas, b) CO ₂ content after syngas dehydration (gas-mixture/Ce ₂ O ₃ ratio equal to 1.05 and $T_{gas,inlet}$ equal to 500°C).....	74
Figure 41: effect of the CH ₄ /CeO ₂ ratio and isothermal temperature of the reduction reactor (T_{RED}) on the heat need by the reactor (Q_{RED}) (a) and effect of both inlet temperature of the methane ($T_{in,methane}$) and CeO ₂ ($T_{in,CeO2}$) on the heat need by the reactor (Q_{RED}) (b)	75
Figure 42: a) effect of the composition of the inlet gas and metal temperature inlet ($T_{metal,in}$) on the heat from oxidation reactor (Q_{OXI}), b) effect of the metal inlet temperature ($T_{metal,in}$) and Gas.mixture/Ce ₂ O ₃ ratio on the heat from the oxidation reactor (Q_{OXI})	75
Figure 43: ASPEN Plus model for moving bed reactor with 10 RCSTRs (only oxidation reactor shown), where with OXYG it is intended the gas flow and OXY the metal oxide flow	79
Figure 44: Logic diagram of moving bed reactor model in ASPEN Plus hooked with user kinetics written in an external FORTRAN Code	80
Figure 45: effect of the reactor volume on the degree of advancement of the reduction reaction (X_{RED}).....	81

Figure 46: effect of the reactor volume on the degree of advancement of the oxidation reaction (X_{OXI}) with different gas mixture (with a 5% excess from the stoichiometric value) at the inlet of the reactor considering a gas temperature inlet of 500°C and a metal inlet temperature of 800°C.....	82
Figure 47: effect of the inlet temperature of the fed Ce_2O_3 ($T_{OC,inlet}$) and of the equimolar (50% H_2 -50% H_2O , with an excess of 5% with respect to the stoichiometric) inlet gas mixture ($T_{gas,inlet}$) on a) CeO_2 production, b) CO/H_2 ratio, c) H_2O molar fraction, d) CO_2 molar fraction at the outlet.....	83
Figure 48: effect of the gas mixture inlet composition into OXI (with an excess of 5%) and the metal oxide inlet temperature on the H_2/CO ratio of the syngas outlet from OXI, considering a gas temperature inlet into OXI equal to 500°C.....	84
Figure 49: effect of the CH_4/CeO_2 ratio and isothermal temperature of the reduction reactor (T_{RED}) on a) first efficiency parameter (η_{CL}), b) second efficiency parameter (η_{CL2}), with an equimolar gas feed in the oxidation reactor (excess of 5%) for thermodynamic and kinetic model.....	85
Figure 50: effect of the size on the degree of the advancement of a) oxidation reactor (X_{OXI}) b) reduction reactor (X_{RED}), with a gas mixture into OXI composed by 52%-48% CO_2 - H_2O with an excess of 5%.....	86
Figure 51: effect of the operation condition T_{RED} and inlet methane flow on a) advancement of the reduction reaction (X_{RED}) and hear needed Q_{RED} , b) efficiency and total power produced W_{NET} , c) DME production and CO_2 recirculation into OXI.....	88

List of Tables

Table 1: the oxygen storage capacity of the described oxygen carriers.....	11
Table 2: Comparison of DME properties to commonly used fuel [24]	24
Table 3: environment state and dead state data and assumptions	29
Table 4: CEPCI index	32
Table 5: main assumption in CAPEX estimation.....	32
Table 6: main assumption in OPEX estimation	32
Table 7: economic assumptions	33
Table 8: main assumption made in water consumption calculation.....	36
Table 9: main assumptions and hypothesis used in the process simulation.....	39
Table 10: thermodynamics properties and composition of ASU streams.....	41
Table 11: distillation unit operation parameters.....	43
Table 12: kinetic parameters	45
Table 13: fixed parameters for DME reactor design.....	47
Table 14: Plant results	54
Table 15: thermodynamics properties and composition of selected streams.....	55
Table 16: specific chemical exergy of the gas mixture streams.....	56
Table 17: chemical, physical and total exergy of the plant's streams.....	59
Table 18: results from the exergetic analysis of the main components	60
Table 19: equipment cost	62

Table 20: productive structure of the plant and auxiliary equations	65
Table 21: main results of exergo-economic analysis	66
Table 22: results of water consumption calculation.....	67
Table 23: kinetic parameters of Ce_2O_3 oxidation with H_2O and CO_2 [181].....	77
Table 24: final results of the best point of operation of the polygeneration plant integrated with the moving bed CL unit (KM-LAYOUT) compared with the results of the layout with the thermodynamic CL unit (TM-LAYOUT)	89

1. Introduction

Climate change presents a global risk to society, it menaces the basic elements of life for living beings. This, by increasing the risk of irreversible and large-scale changes to the climatic and ecological system, can subsequently have significant consequences for human life as well. With this focus, the 21st Conference on the Climate Change in Paris, resulting in the so-called Paris Agreement of December 2015, has achieved significant milestones, with 195 participants agreeing “to strengthen the global response to the threat of climate change, [...]. Holding the increase in the global average temperature to well below 2°C above pre-industrial levels and pursuing efforts to limit the temperature increase to 1.5°C above pre-industrial levels, recognizing that this would significantly reduce the risks and impacts of climate change.”[1]. Among the causes of climate change, the emission of greenhouse gases (GHG), primarily from anthropogenic activities, is the primary attribute [2]. Of the several GHGs that are emitted, carbon dioxide is of the highest concern due to its highest volume rate of emission and persistence in the atmosphere [2,3]. Several literature works which have been published over the last couple of years reported that the global-mean temperature is nearly linearly proportional to the total cumulative CO₂ emitted [4]. Therefore, emissions need to be capped to a specific value, which in literature is usually called carbon budget. In the fifth Assessment Report of the Intergovernmental Panel on Climate Change (IPCC) was estimated, in order to have a likely chance to stay below the 2°C, a maximum emission of 2900 GtCO₂ [5]. From the pre-industrial era to 2011 an amount of 1900 GtCO₂ has been already emitted, 65% of the total estimated carbon budget [5]. Without drastic measures, proceeding with the current pace of emissions, it is expected to overshoot the limits of the Paris agreement by 2050 [6].

The greatest part of emissions comes from the combustion of fossil fuel, especially for energy production purpose [5]. For this reason, a big effort is given towards a low carbon energy sector. Different pathways have been proposed and are still studied such as: increase the efficiency in the industrial sector, increase the use of renewable energy sources, increase the use of the nuclear power, switch to less carbon-intensive fuels, enhance CO₂ uptake in biomass, CO₂ capture, and storage (CCS). Of the several possible alternatives, Carbon capture and storage (CCS) technologies have been studied to provide considerable benefits towards decreasing the anthropogenic emissions [7–9]. Indeed the significance of CCS in a low carbon economy has been predicted to be considered by the scientific community [10], especially in a midterm pathway in which fossil fuels are still the main sources. Nevertheless, unlike all other pathways, CCS suffers from its own drawbacks including the need for compression of CO₂ to high pressures of usually 110 bar, large storage space requirement and high efficiency and economic penalty on the power plant among others [11–13]. Therefore, an alternate pathway, to recycle and reuse the captured CO₂ via innovative process integrations through the chemical formation for subsequent use has received much attention (CCU) [14–16]. In fact, reuse of CO₂ not only permits to avoid sequestration issues but generates a monetary return from CO₂ [17]. In this regard, polygeneration systems, combining a number of utilities in a single system in an efficient way, to produce multiple products (power, chemical, fuel etc.) has received particular

interest in recent years [18]. In general, polygeneration is more efficient than stand-alone plant due to a better integration of the multiple utilities in term of mass and heat. Thus, the integration of CCS in a polygeneration plant can reduce the energy and economic penalty of carbon capture. The captured CO₂ from exhaust gas instead to be sent to the sequestration, it is recycled as feedstock for new products (syngas, chemicals, fuels etc.), increasing the efficiency and profitability of the overall system.

One intriguing approach to recycle exhausts within the plant and hence produce chemicals in addition to power is through chemical looping (CL) technology [19,20]. Chemical looping technology for CO₂/H₂O splitting usually utilizes metallic oxygen carriers (OCs) to convert the thermochemical energy into chemical energy [21]. Both thermally driven cycles (by concentrated solar power, (Figure 1.a) or by fuel reduction (by methane, Figure 1.b) are feasible alternatives [22]. Methane-driven cycles, however, besides being able to operate at low-temperature, [22,23] are also able to operate round the clock, unlike solar driven cycles. Moreover, they don't require costly solar field and challenging reactor design.

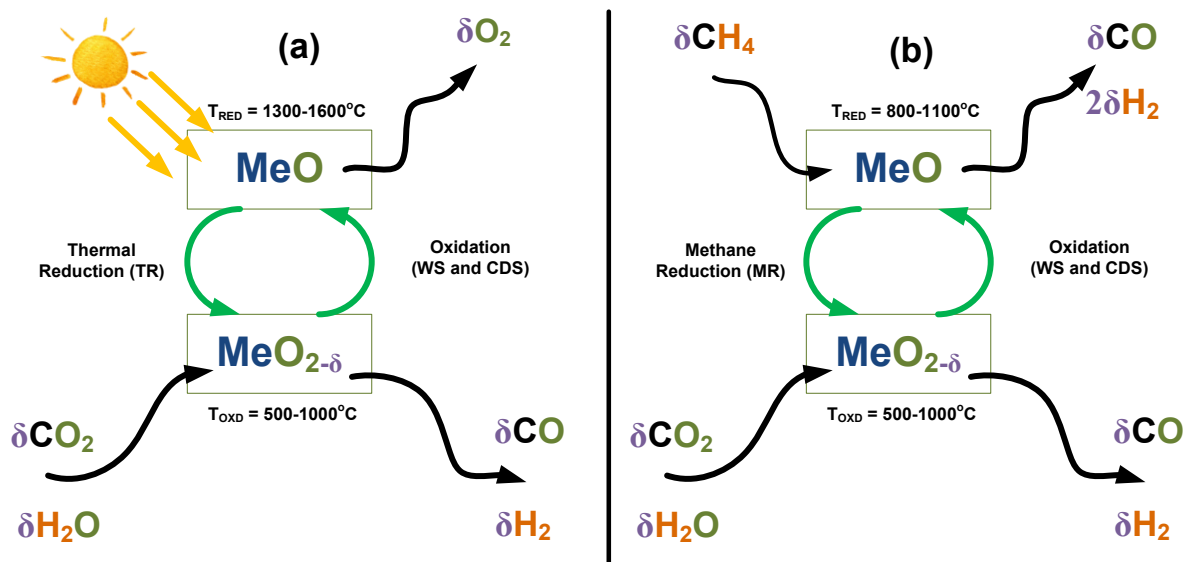


Figure 1: a) Conceptual scheme of the solar chemical looping syngas production through solar thermal reduction and corresponding splitting of water and carbon dioxide, usually present in waste gas from industrial applications. b) Conceptual scheme of the chemical looping syngas production through methane reduction and corresponding splitting of water and carbon dioxide, usually present in waste gas from industrial applications

By optimally combining the composition of the exhaust gas (a mixture of water and CO₂), and by controlling the temperature of reaction, the desired composition of syngas can be obtained, which can subsequently be utilized to produce multiple products through industrial processes. Of the most interesting options, the production of synthetic fuels, able to generate electrical power in high efficient devices such as fuel cells or direct implementation in automotive applications is an interesting alternative [24,25]. Dimethyl Ether (DME), is, in fact, one of the strongest candidates as a synthetic fuel due to its similarity with diesel. While, thanks to its physical properties and chemical structure – produces low NO_x, limited HC and almost no SO_x and particulate subject to combustion [24].

1.1. Objectives of the thesis

Considering the features described in the previous section, the aim of the thesis is to propose and deeply analyze a novel polygeneration plant integrated with a chemical looping unit for the production of power and dimethyl ether. The following are the specific goals:

- I. Development of a flowsheet model for the DME polygeneration plant based on a thermodynamic equilibrium for the chemical looping $\text{CO}_2\text{-H}_2\text{O}$ splitting;
- II. Optimization of the layout investigating the effect of the main operation conditions;
- III. Perform detailed energy and exergy analysis to assess the feasibility of the plant;
- IV. Perform a techno-economic and exergo-economic study to investigate the economic performance of the plant;
- V. Development of a moving bed reactor model with kinetics for the chemical looping unit;
- VI. Comparison of the performance of the thermodynamic and kinetic model for the chemical looping unit;
- VII. Integration of the polygeneration plant with the moving bed reactor for chemical looping;

1.2. Structure of the thesis

The thesis is organized into 6 chapters:

- *Chapter 1* introduce the general topic and the object of the thesis.
- *Chapter 2* contains the theoretical background of the technology used in the polygeneration plant. It presents an overview of the current status of carbon capture and sequestration, carbon capture and utilization, chemical looping cycle, polygeneration plant and DME production technologies.
- *Chapter 3* describes the tools and methodology adopted during the plant investigation.
- *Chapter 4* describes the plant layout and the related sub-system. It contains the results of the plant integrated with the thermodynamic model of the chemical looping and the effect of the main operation parameters.
- *Chapter 5* describes the moving bed reactor model and the kinetic model for chemical looping reactions.
- *Chapter 6* reports the results of the integration of the moving bed within the polygeneration plant.

Finally, the last part of the thesis gives the summary of the work followed by the conclusion and the further work to extend the current study.

2. Theory Background

2.1. Carbon Capture and Sequestration

Carbon capture was proposed in the late 1970s in the USA, after the global crisis, to enhance the oil recovery. Later, the use of CCS was shifted to capture CO₂ emitted from fossil fuel for climate change tackling. At the current status, there are 26 facilities integrated with CCS technology, which account for more than 30 Mtpa of CO₂ emission avoided [26]. The CO₂ produced in a power or industrial plant is previously captured, conditioned, transported through pipeline, railways or roadways and stored in a suitable body for several decades. According to the point where CO₂ is separated, CCS is referred to as post-combustion, oxyfuel-fuel or pre-combustion as shown in Figure 2.

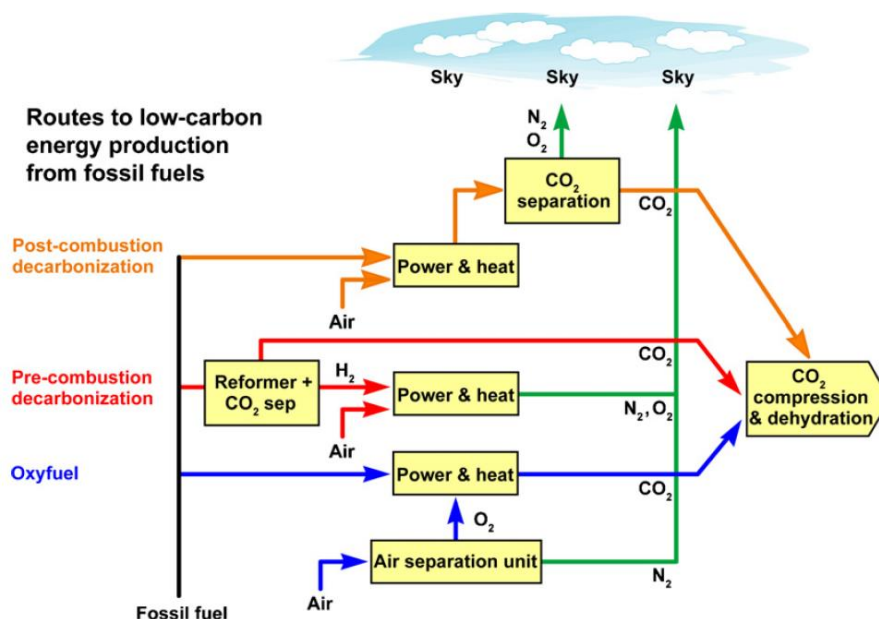


Figure 2: main route for carbon capture [27]

In post-combustion CCS, CO₂ is separated downstream from the flue gases after the combustion of fossil fuel [11]. The main advantage of this technology is that it can be adapted to retrofit existing fossil fuel plants such as a coal power plant. However, its use implies a plant efficiency penalty and cost addition due to the fact that CO₂ is present in the flue gases with a low partial pressure, since the use of air in the combustion. In addition, flue gases coming from the combustion chamber are at ambient pressure, making the CO₂ separation highly energy consuming [27]. The most used separation processes are physical and chemical absorption in which CO₂ is scrubbed through a liquid solvent. In physical absorption, CO₂ is physically captured at the surface of the solvent, which has an increased absorption ability at high pressure. The high-pressure allows to regenerate the CO₂ rich solvent and release the CO₂ in a stripper, just decreasing the operation pressure [28]. In general, physical absorption is used when CO₂ content in flue gas is higher than 15% vol. [29].

In chemical absorption process, the flue gases are scrubbed through an aqueous alkaline solvent (MEA, DEA, MDEA etc.) in an absorber, where CO₂ is captured by the solvent via chemical reactions. A subsequent stripper column is used to regenerate the rich-in CO₂ solvent through heating up and release a high content CO₂ stream (>85%) [30]. Since the flue gas from fossil fuel power is at ambient pressure and CO₂ content is lower than 15% vol, chemical absorption is preferred.

An oxyfuel CCS based process consists in burn the fuel in a pure oxygen atmosphere (>95%) so that the flue gas is not diluted by nitrogen but it is only composed by CO₂ and water which can be easily separated by condensation. For this reason, oxyfuel-combustion permits to achieve a 100% CO₂ capture. In addition, since N₂ is present in low amount, NO_x production is limited [31]. Differently, from air combustion plant, where N₂ absorbs the heat of combustion, in oxyfuel combustion plant, in order to control the adiabatic flame temperature, a recirculation of the exhausted gases is required (>80%) [31]. This technology can be used for novel plants or can retrofit existing power plants with few modifications [32]. The main drawback is the energy required to produce a pure oxygen stream in an air separation unit (ASU), it is estimated a consumption of 0.16-0.25 kWh per kg of O₂ for the production of 95% pure O₂ stream [33]. Separation of oxygen from nitrogen can be either obtained by the cryogenic process and non-cryogenic process. For industrial process where a high amount of O₂ is required, cryogenic separation is used. Nevertheless, most of the research is direct to non-cryogenic technology such as membrane separation, which with its adoption will reduce the energy penalty [29,32]. Cryogenic separation takes advantage of the different condensation temperatures of gases. The air is firstly compressed (4-6 bar), cooled down to its condensation temperature (-172°C at 6 bar) and sent continuously to two stripper columns where N₂ and O₂ are separated [34]. The energy cost of this cycle is due to the air compression, which is required to have an appropriate level of cooling power to drive the separation [35]. In the current state of the art, big scale oxyfuel combustion is not yet in the commercial status, most of the projects are pilot or demonstrative plants based on coal combustion [36]. As shown in Figure 3, after the construction of pilot plants of 1 MWe and lower size in the first decade of 2000's, big size demonstration plant such as White Rose in the UK [37] or Shenhua in China [38] are now in the phase of projection and construction. Regarding the oxyfuel combustion process integrated with the natural gas-driven cycle, they are in a lower stage of development with respect to above-listed coal fed projects. Few proposed plants such as the one from Allam et al. [39] or Anderson et al. (CES) [40] has reached the demonstrative phase.

In pre-combustion CCS process, the fuel, normally coal or natural gas, is pre-treated before the combustion. For coal, it firstly undergoes low-O₂ gasification process which produces a syngas mainly composed of H₂ and CO. A water gas shift (WGS) reaction is secondly used to increase the H₂ content converting CO in CO₂ (reaction 1). In case of methane, which is in gaseous form, it undergoes steam reforming (reaction 2) and then the H₂ content is increased by a WGS reaction [41].

of new chemicals and fuels [51]. This concept opens to a new branch referred to as Carbon Capture and Utilization (CCU), which will be discussed in the following subsection.

2.2. Carbon Capture and Utilization (CCU)

As an alternative to storage, CO₂ utilization has achieved a great attention in the scientific and industrial field in last years [52]. In fact, the concept of CCU not only permits to make fuel exploitation cleaner but also gives the opportunity for a more sustainable energy economy [53]. CO₂ can be recycled and used as a product directly or converted into a new one. Several industries use directly the CO₂. For example, in the food and beverage sector, it is used as a carbonating agent, packaging gas or in the pharmaceutical sector as an intermediate for drug synthesis [54]. However, this market does not have a potential size to be considered a valid solution in limiting CO₂ emission in a crucial way. Vice versa the conversion of CO₂ to chemicals and fuels is a promising and attractive market since allows to cut a portion of the capture cost and create a closed-loop carbon cycle [17]. Aresta estimated that the CO₂ recycle can contribute to a 7% reduction in overall emissions [55]. The main drawback of CO₂ is that it is thermodynamically high stable and so its conversion requires high energy input, active catalyst and optimum reaction conditions [56]. CO₂ can be used as co-reactant in carboxylation reactions, in which the all carbon dioxide molecule is built into products without entirely cut the C=O bonds [57]. Among carboxylation process mineral carbonation and utilization of CO₂ as a precursor to organic carbonates, carbamates, acrylates, carboxylic acids, and polymers can be cited [58]. For example, the production of urea, for fertilizers and polymers synthesis, is an organic carboxylation reaction that is already present at industrial scale (more than 100 Mt of urea are produced yearly) [52]. Alternatively to carboxylation, CO₂ can be reduced, breaking one or both the C=O bonds and used for the synthesis of new species like syngas. Syngas, a mixture of H₂ and CO, is one of the most valuable resources in the industry field since its versatility. As shown in Figure 4 the syngas can be used in multiple processes for either chemical, fuel and power generation.

Nevertheless, as already written, CO₂ is a highly stable molecule, so in order to break one of the C=O bonds an high energy carrier is required. Of great interest, it is when this energy vector, either heat, electricity, high-energy reactants (H₂, CH₄ etc.) are produced by renewable resources. This rends the reaction of dissociation a chemical storage for a renewable source [57]. Several processes have been proposed for CO₂ dissociation, one that has received great consideration in the research, especially for its application at large scale, is the chemical looping [19,20]. In the following, a detailed description of the state of the art of technology with the related challenges is illustrated.

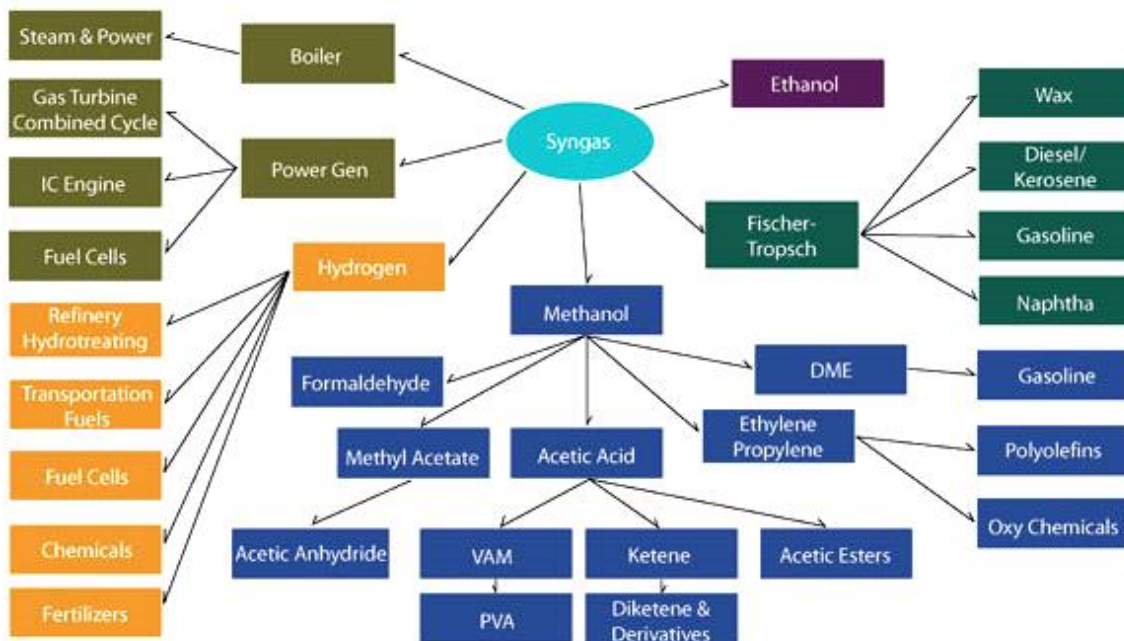


Figure 4: syngas utilization routes in the industrial sector

2.3. Chemical looping process

Chemical looping process is based on multiple sets of chemical reactions which are carried on in different reactors. The main concept consists of a closed loop where one of the reactants is continuously recirculated between the process reactors. In general being this reaction either exothermic or endothermic, the reactors doesn't work at isothermal conditions. Moreover, due to possible temperature swing between the different reactors of hundreds of degree, a thermal integration is required.

Several set-ups of the reactors and reactants allow, at the present, to exploit chemical looping process in the power generation or petrochemical field as the main principle of operation. One of the most mature application is the Fluid Catalytic Cracking (FCC). In this process, the circulating reactant is the catalyst. It is firstly used in the cracking reactor to break up the hydrocarbons in the shorter chain than it is sent to the regeneration reactor to recover the catalyst's potential and thus recirculated [59]. The catalytic cracking is performed in a fluidized bed, in particular, the regenerative process is carried in a circulating fluidized bed. This configuration helps in temperature control since the regeneration reaction is highly exothermic [60].

Another example of utilization of the chemical looping is the already described chemical absorption (via MEA) in section 2.1. Still, in this field, the so-called chemical looping combustion (CLC) is being studied as a new generation of the CCS process. In the CLC process the oxidant and the fuel never enter in contact and thus the exhaust gases are not diluted by N_2 , facilitating the CO_2 separation. The task of bringing oxygen from air to fuel is performed by the oxygen carrier: in the fuel reactor, it is reduced by the fuel, while in the air reactor is regenerated in its oxidated form. The total amount of heat released in the cycle is of the same order of magnitude of a standard fuel-air combustion, thus suitable for power production. Such

a process can be used for, the so-called, fuel decarbonization. In this case, the chemical energy of the fuel is exploited to produce hydrogen. An example of this process was reported by Chiesa et al. [28], which used a three reactors configuration with an iron oxide cycle. As the by-product of the process, an excess of heat is generated, suitable for a steam cycle. Furthermore, these are few examples of chemical looping application, however, one of the most intriguing process, which is under study, is for the CO₂/H₂O splitting for syngas production.

2.3.1. CO₂/H₂O dissociation based on chemical looping process

An easy concept of water-carbon dioxide dissociation is the thermolysis. Thermolysis is based on heating water and carbon dioxide till the $\Delta G_{\text{reaction}} \leq 0$ and thus till reaction becomes spontaneous [61].



However, the required temperatures are extremely high, the thermodynamics of H₂O and CO₂ estimates that thermolysis occurs completely at a temperature higher than 4000°C and 3000°C, respectively [16]. Literature states [62] a temperature range of 2000-2500°C for water dissociation, even though the equilibrium constant reported is only 0.02 and a 50% dissociation of CO₂ at 2700°C [63]. Since this high temperature, special material like zirconia and zeolite [61] are used. Still, these materials undergo rapid sintering at 1900-2100°C, so are unsuitable for this operation conditions. Thus, at the moment, there is no material that can sustain the high temperature for the thermolysis. As a consequence, a great effort was directed to lower the operation condition using particular catalysts. Nevertheless, experimental studies revealed that water can be split at a lower temperature (800°C) using an acid material such as Al₂O₃, CaCO₃ or TiO₂ but with a maximum pick of 0.3% ([62]). In addition, since the oxygen and the CO/H₂ are produced in the same reactor, there is the issue of separating them. The recombination of the two products can reduce the total yield of the process and in the particular case of the O₂-H₂ there might be safety problem since this mixture is explosive. That is why at the moment thermolysis is not considered as a candidate for the production of syngas from CO₂ and H₂O.

A solution of this two major problems is the application of the chemical looping process. The overall process produces CO and/or H₂ with the net input of the only CO₂ and/or H₂O, while the other products are recirculated cyclically. They require a lower temperature than thermolysis and since O₂ and CO/H₂ are produced in different stages, there are no separation issues. In general chemical looping process can be divided into two categories according to the total number of steps, two or more. The latest group is the results of many studies carried out during 1960s-1970s by many institutes of research. The scope was to find the most promising low-temperature thermochemical cycle suitable to work with heat produced by nuclear power plants for hydrogen production. Since the highest temperature obtainable by a nuclear plant is around 1000 K (HTGR), from a thermodynamics perspective, all this process are based on a minimum of three steps ([62]). Few cycles were investigated, hybrid copper-chlorine ([62]), sulphur iodine [64] (Figure 5), calcium bromide (UT3) and hybrid sulphur (HyS). Although the

lower temperature, it can be noticed, that these type of cycles are difficult to be exploited due to the occurrence of several reactions at different temperatures which would demand thermal integration and the use of corrosive chemicals that would imply advanced materials utilization.

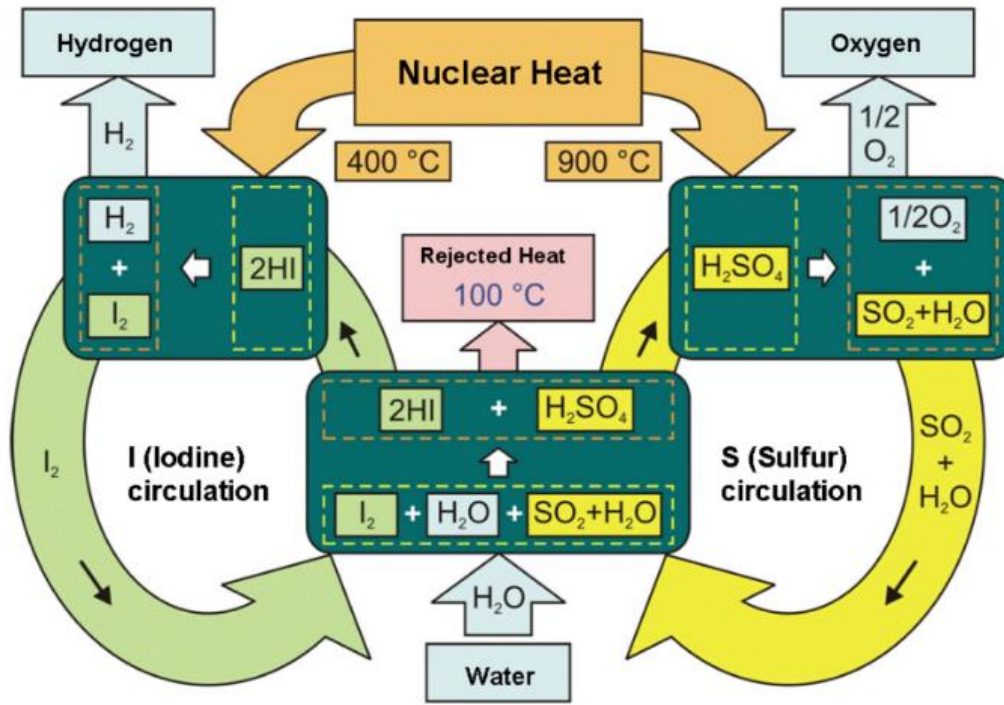


Figure 5: Schematic of the sulphur-iodine thermochemical cycle for hydrogen production proposed by General Atomics [64]

Two steps metal oxide based chemical looping cycles can eliminate this issues. These cycles were proposed in the late 1970s ([65]. The process consists in a closed loop redox reactions in which a metal exhibiting multiple oxidation states is bring continuously from its oxidized form (higher-valance, MeO_{oxi}) to the reduced one (lower-valance MeO_{red}).



The first step is a high temperature (1600-2100 K) endothermic reaction, where a spontaneous release of oxygen from the crystalline's structure of the metal creates vacancies in the solid (eq. 5). The reduced metal oxide is generally dragged out by an inert sweep gas and, consequently, in the second reactor, it is re-oxidized by taking oxygen from the steam or carbon dioxide producing hydrogen or carbon monoxide. This reaction is carried at a lower temperature than in the reduction reactor (800-1100 K) and in addition are exothermic. Due to the high temperature required in the endothermic step, most of the proposed studies for chemical looping process are direct towards the application of concentrated solar power, the so-called thermochemical looping cycles. Moreover, the utilization of a renewable source as solar allows reducing the carbon footprint of the produced syngas (or the fuel/chemical produced with the syngas as intermediate), enhancing a complete environmental friendly process. However, as it will be explained in the following sections an alternative to solar power is the utilization of a

chemical looping process driven by fuel reduction. The main challenges for a disruptive evolution of chemical looping cycle are discussed in the following.

2.3.1.1 Materials

The cornerstone on which chemical looping process are based are the oxygen carriers. Several studies have been and are still conducted in order to find materials able to enhance syngas production by CO₂-H₂O dissociation. Oxygen carriers can be grouped in different ways, whether it is the temperature of reduction and oxidation, the potential oxygen storage or the phase in which they operate during the process. According to the last property, oxygen carriers can be divided in volatile or non-volatile if they melt or not during the loop.

2.3.1.1.1. Volatile carriers

Volatile redox pairs used in the two-step dissociation exhibit a phase transition in the reduction reactor due to the lower boiling temperatures [65]. From a thermodynamics point of view, this has a beneficial because a high entropy gain is obtained. Since the reduction process is not spontaneous ($\Delta G > 0$), an increment of the ΔS reduces the Gibbs free energy of the reaction and consequently the heat required. On the other end, there is the issue that the melted metal can be carried from the sweep gas. A separation is required. At high temperature, the easiest way to do it is solidifying the gaseous carrier. Thus, an intermediate quenching process between the reduction reactor and the oxidation reactor is needed. Unfortunately, during the quenching process, a certain amount of oxygen recombines with the metal oxide reducing the overall efficiency [66].

Palumbo et al [67]. reported that in order to enhance the reduction yield (80%) of zinc oxide a fast quenching rate higher than 1.6×10^7 K/s is required, otherwise only 20-25% total yield can be achieved. An under-vacuum condition (2 kPa) was proposed by Charvin et al.[68] to increase the yield to 90% for SnO. Kang et al. [69] proposed a GeO₂/GeO cycle with the advantage of reducing considerably the reduction temperature (1500°C compared to 1900°C for zinc and 1600°C for tin). However, due to the quenching issue, this types of metal oxide were not considered in the present work.

Table 1: the oxygen storage capacity of the described oxygen carriers

Oxygen carrier	Storage capacity [kgO ₂ /kg]
ZnO/Zn	0.197
SnO ₂ /Sn	0.106
GeO ₂ /GeO	0.153
Fe ₃ O ₄ /FeO	0.069
CeO ₂ /Ce ₂ O ₃	0.046

2.3.1.1.2. Non-volatile carriers

The non-volatile oxides, unlike the volatile oxides, do not undergo phase changing and so remain solid during the reduction cycle. Hence, quenching step is avoided and so solids and

sweep gas separation can be done in mechanical separators, i.e cyclones, lowering structural complexity and system losses. Nevertheless, it is worth mentioning that volatile materials, due to their lower molecular weights, have a higher oxygen atom share and so a better oxygen capacity storage per unit of mass (Table 1).

Several non-volatile cycles were and are investigating in literature such as iron cycles, ceria cycles, perovskite etc. The magnetite/wustite redox cycle was firstly proposed in 1977 by Nakamura for the water dissociation ([70]). In this cycle, water reacts with wustite (FeO) to form magnetite (Fe₃O₄) and H₂. Then the magnetite is thermally reduced regenerating its oxidated form and releasing oxygen:



In his work, Nakamura conducted a thermodynamic analysis of the proposed process. The first reaction is slightly exothermic and occurs at a temperature above 1000°C at ambient temperature. The thermal reduction instead, is carried on at a temperature higher than 2200°C in the air. This temperature is higher than the melting point of both wustite (1370°C) and magnetite (1535°C), as a result, a liquid carrier is obtained during the reduction process. It implies a decrease of the iron oxide surface area and consequently a deactivation of the metal. The temperature reduction might be reduced at 1350°C if the partial pressure of the oxygen is reduced to 10⁻⁷ bar. However, the production of such a pressure condition can be done by vacuum pumps that are high energy intensive and causes an increment in the total cost of the hydrogen production. An alternative is to mix the iron solid with transition metal as manganese (Mn), cobalt (Co), nickel (Ni) or zinc (Zn) forming a ferrite oxide at the form (Fe_{1-x}M_x)₃O₄ with a reduced form (Fe_{1-x}M_x)_{1-y}O. Various ferrite synthesis process has been pursued, starting from either solid, liquid or gaseous precursors such as co-precipitation, sol-gel, atomic layer deposition and spray pyrolysis [71]. Different comparative analysis for the thermal reduction was realized to evaluate the optimal operation parameter of ferrite cycle [71]. Their reduction temperature resulted lower than the pure iron metal (1350-1500°C) but the sintering problem was detected. Tamura et al. [72], deeply analyzed the Zn-ferrite cycles. The study was carried on in a solar reactor with an inert argon atmosphere and in the air afterwards. Decomposition started at 1225°C and increased with the temperature, producing gaseous Zn, O₂ and solid Zn_xFe_{3-x}O₄ [70] in the argon atmosphere. The experiments with air revealed a higher reduction temperature (1525°C) and the formation of gaseous ZnO. The formation of ZnO suggested that in air atmosphere the gaseous Zn rapidly recombines with the oxygen presents in the air. Lorentzou et al [73] studied doped iron oxide with Ni, Mn, and Zn for water splitting. Metal oxide performance was found affected by the dopant type and stoichiometry. Ni-Zn and Zn ferrite cycle resulted in the best materials, achieving a hydrogen yield of 60-80% at a temperature of 800°C and able to be regenerated for the reduction step at 1000-1300°C.

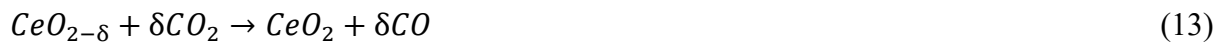
The biggest issue of ferrite cycles is the sintering of the particles. Sintering of the oxides alters the surface area of the particles, the porosity and size influencing the total product yield and

leading to the deactivation of the particles itself. An attempts to tackle this concern have been to support the oxygen carriers with zirconia (ZrO_2) fine particles or supports. Kodama [74] worked on Ni-ferrite on zirconia support cycles to prevent sintering during water splitting chemical looping process. The particles were tested at $1400^\circ C$ for the reduction and $1000^\circ C$ for the water dissociation. What was noted is that the transformation from Fe_3O_4 to FeO occurred in the crystals of the zirconia. $NiFeO_2O_4$ resulted in the most suitable for water splitting with respect of other ZnO_2 coated ferrite (i.e Co-, Mn-, Mg-) averaging a 69% hydrogen yield for repeated cycles. Similar testing of iron oxides and ferrites were performed for CO_2 dissociation alone and combined with water splitting [71]. In [75] iron oxide supported with Al_2O_3 were tested with a different mixture of CO_2 - H_2O . The oxidation process was performed for a range of temperature from $650^\circ C$ to $1150^\circ C$. Statnatiou et al.[76] reported that H_2O splitting exhibited higher reaction rates with respect to carbon monoxide reduction.

Another metal oxide cycle investigated, due to the ceria crystallographic stability [23], is the ceria-based chemical looping cycle. In the beginning, ceria reduction was performed at high temperature ($T=2000^\circ C$, $p=100$ - 200 mbar) [77] so that the reaction 10 could be achieved:



It was noted that during the ceria dissociation, the metal oxide was in a melted state with consequent vaporization issues. Therefore, the interest was shifted towards lower temperature in the range of 1300 - $1500^\circ C$, where ceria doesn't sublimate and its non-stoichiometric reduction occurs (Eq. 11).



In non-stoichiometric reaction, only a portion of ceria atoms changes their oxidation state while the ceria particle maintains its crystalline structure. In this type of reaction, it is released, during the reduction step, only the oxygen content in the lattice structure. A limiting factor for the crystalline structure preservation was reported by Kümmerle et al. [78] with $\delta=0.35$. The advantage of this type of reaction is that melting issues are avoided and, as reported by Chueh et al. [79], the high rates of oxygen chemical diffusivity enhance the redox kinetics. Ceria suffers from the sintering at high temperature. Considering that with the non-stoichiometry reaction oxygen is delivered only from the surface, the thermal stability is one of the critical barriers to be overcome. As for iron, a solution is the mix of the pure ceria particle with other metal such as Mn, Ni, Fe, Cu etc.. The formation of a solid mixture was found to improve the oxygen-releasing at a lower temperature compared to the pure CeO_2 [65]. Gokon et al. [80] investigated the performance of pure ceria with respect of $NiFe_2O_4$, both supported and unsupported on m- ZrO_2 . As expected, they revealed that ceria has a better thermal stability. Thermal reduction and oxidation reactions gave a higher O_2 and H_2 yield for six consecutive cycles. Moreover, they reported that ceria achieves a better yield when reduced at temperature

T=1450°C. A not significant enhancement was noted when the reduction was performed from 1450°C to 1550°C. The non-stoichiometric coefficients varied from 0.034 to 0.11. Sheffe et al. [81] performed a thermodynamic analysis of various doped ceria oxide for water and carbon dioxide splitting. It is reported that above 930°C oxidation reactions are enhanced as the dopant concentration is increased. Abanades et al. [82], investigated the possibility of reducing the reduction temperature by addition other of zirconia in ceria. They reported that the addition of zirconia powder improves significantly the reduction at a temperature below 1500°C, increasing its content the reduction yield up to 70% from 10%. One negative effect noted was that the mixed metal increase the water dissociation temperature to 800°C, which is higher than pure Ce₂O₃. Jiang et al. [83] studied thermochemical cycles with doped ceria for CO₂ dissociation. They reported similar improvement effect as in Abanades et al. [82]. The addition of metal oxide to pure ceria enhance the O₂ evolution activity during reduction, while the synthesized Ce_{0.75}Zr_{0.25}O₂ doubled the CO yield during the cycle (4.5 ml/g for CeO₂ to 10.6 ml/g for the mixed oxide).

In general, as reported in [80,84], ceria-based oxygen carriers tend to have better performances in terms of thermal stability and reduction kinetics than ferrite oxide. For this reasons, ceria oxide has been selected as an oxygen carrier for the chemical looping process of the proposed plant.

2.3.1.2 Reactors

Solar thermochemical cycles employ the same solar concentrating reactors aimed to produce power. Four kinds of optical configurations using movable mirrors are used to track the sun's ray: Parabolic trough collectors, Linear Fresnel reflectors, Power tower and Dish-engine systems. Since these reactors are used to provide heat for the reduction reactions which require a temperature above 1000°C, only solar tower and dish technology are choose. Moreover, considering that syngas synthesis demands a certain size and, knowing the size limitation of dishes, most studies are focussed on the implementation of thermochemical cycles with solar towers.

The solar receivers can be grouped in, directly and indirectly, receivers according to the mechanism of transferring the solar heat to the fluid. The indirect receivers consist of absorbing surfaces exposed to concentrated sun's beams which conduct heat across their walls to the thermal fluid (i.e. tubular receiver). Vice versa in directly receivers the thermal fluid is exposed to the concentrated rays. They are also called "volumetric" receivers due to the fact that is able to trap the solar source within the entire volume of the absorber. As previously written, in redox chemical looping process there is a reaction between a solid, the oxygen carrier, and a gas. According to how the metal oxide is placed, there are two reactor categories: structured reactors where the oxygen carrier is arranged in particular space and non-structured reactors where it is distributed randomly. At the first group are listed reactors such as honeycomb, foam or membrane reactor while the letter is included packed and fluidized beds. Finally, since chemical looping cycles are made by two steps, is it possible to categorize the used reactor according to if it is able to perform both reactions or just the reduction one.

There are several challenges combining redox reactions with concentrated solar reactors. The high temperature for the reduction reaction implies a high concentration ratio, the utilization of special material, issues with reactor thermal losses and reaction between the reactants and material which composed the reactor itself. In addition since the reduction and the oxidation are favoured by different temperature, there are complications with reactor design, handling of metal oxide and heat integration between the two steps. In the following are reported the main reactor design and solution proposed in the years for a solar application to chemical looping process.

A first reactor was proposed in 1995 by Tamaura et al. [85]. It consisted of a small (diameter 2 cm) quartz tubular packed bed reactor heated up by a solar furnace. A secondary concentrator is placed behind the solar reactor for an uniform irradiation of the external surface (Figure 6). As a reactive particle bed, a charge of 5 g of $\text{Ni}_{0.5}\text{Mn}_{0.5}\text{Fe}_2\text{O}_4$ powder mixed with 7.5 g of Al_2O_3 was used. During the reduction step, an anoxic sweep gas stream made by argon was used. After the reduction step, the reactor was cooled down ($500\text{-}700^\circ\text{C}$) and a stream of argon and water was sent to the oxidation reactor. As reported by the author, even though the thermal cycle was demonstrated with the O_2 and H_2 evolution curve, one of the main drawbacks of the work is the low amount of oxygen released with respect of using a reduction step to a lower valence oxide. Furthermore, the requirement of an oxygen-free atmosphere during the reduction step is described as another disadvantage. Due to these reasons, this reactor concept was not followed up. No information about the solar to H_2 efficiency was reported.

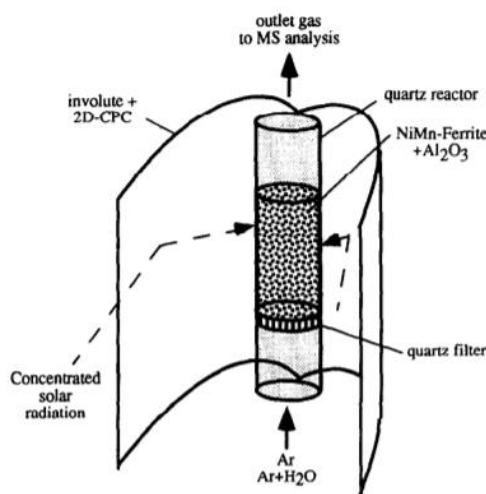


Figure 6: Tubular packed bed solar reactor for H_2 production proposed by Tamaura et al. [85]

Different prototype reactors incorporating fixed coated ceramics in a structured reactor form have been developed in the past years within the scope of the HYDROSOL project. The basic concept of the project was to connect a concentrated solar reactor with a redox pairs system for cyclical water splitting and metal oxide regeneration. Roeb et al. [70], proposed a structured solar reactor in which both the reduction and dissociation reactions take place. It is a compact honeycomb monolith reactor made by a plurality of channels which can be coated by a surface of the active metal oxide compound (Figure 7). Such a reactor is composed of ceramic (SiSiC) coated with ferrite oxide. In this case, the metal oxide is directly irradiated by the concentrated

sun rays. The reactor was tested within a solar furnace, reduction reaction was performed at 1200°C, while water dissociation where performed in the range of 800-1200°C. The reactor where able to perform six cycles producing hydrogen. It is reported that oxidation reaction performs better at a higher temperature (1200°C) however, the higher production is due to precipitation which degrades the support material. For this reason, water splitting has to be conducted at a lower temperature, even if the kinetic is slower. The final results were encouraging, the reactor was capable to split 80% of the injected steam with a solar to hydrogen efficiency of 40%. The main drawback is that the cycle is made in the same reactors, so the two thermal step has to be performed alternatively, producing hydrogen discontinuously.

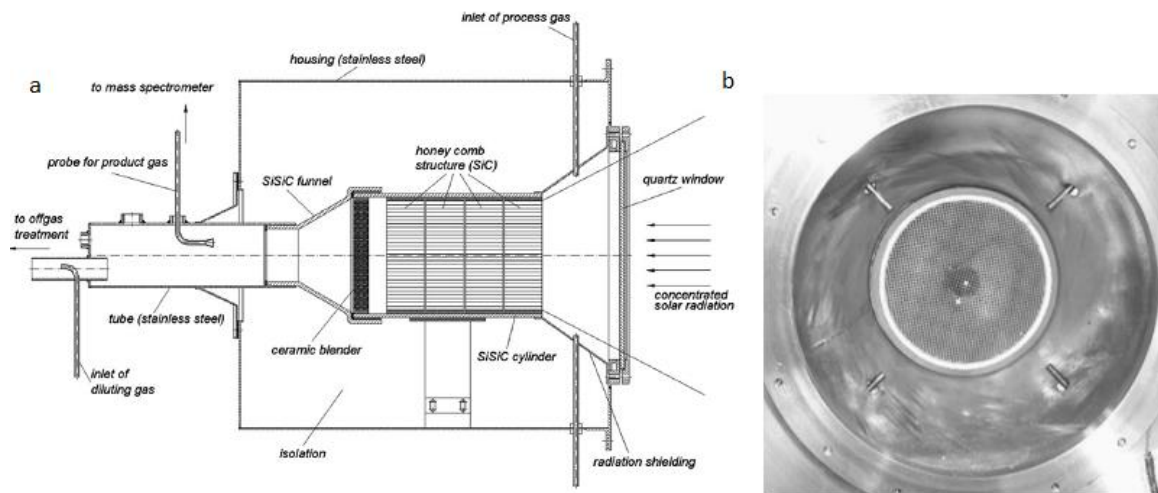


Figure 7: Honeycomb multi-channels reactor proposed by Roeb et al. [70]

For this reason, Roeb et al. [86] proposed later a quasi-continuum reactor for hydrogen synthesis. The reactor consisted of two separate chambers with the same honeycomb structure previously described [70]. The difference is that since the reactor is constituted by two chambers in parallel, it is possible to perform both reduction and splitting together (Figure 8.a). The reactor was tested in a solar furnace. The two reactions were performed respectively at 1200°C and 800°C, using a lamellae shutter in order to regulate the different temperature (Figure 8.b). The outcomes of laboratory tests encouraged researchers to demonstrate the technology at pilot scale. A scaled-up plant of 100 kW_{th} coupled with a solar tower where installed on the Plataforma Solar de Almeria. During the operation, the hydrogen produced was measured from the outlet gas of the oxidation reactor. About 35 g per cycle of H₂ were registered, that in a day would be 500 g. However, the initial plant objective was a daily production of 3 kg. It was noted that the production was not constant during the operation, due to deactivation of the metal oxide and non-homogeneous temperature distribution inside the coated channels.

Kodama et al. [87] proposed an internally circulating fluidized bed combined with a beam-down solar concept (Figure 9). The reactor is composed of two coaxial tubes. The redox particles are circulated through an internal annulus from the bottom to the top, where are irradiated by the concentrated beam entering from the upper window. Then they are moved

downward through the external tube. The general idea was to fluidize the metal particles in order to prevent sintering and agglomeration issues and enhance the heat transfer inside the reactor. During the reduction, a pure N_2 stream was used as the fluidizing gas, while for the reduction a mixed N_2 - H_2O stream was used.

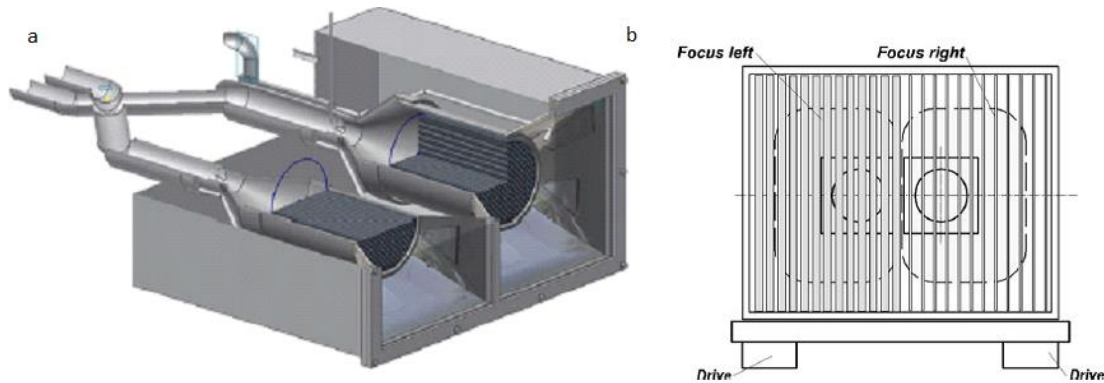


Figure 8: a) Multi-chambers reactor proposed by Roeb et al. [86], b) lamellae shutter for temperature regulation

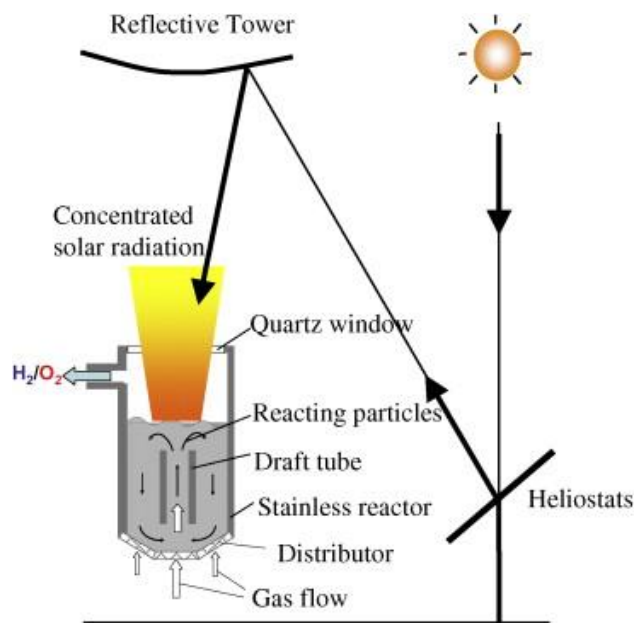


Figure 9: Internally circulating bed proposed by Kodama et al. [87]

The reactor was tested with unsupported $NiFe_2O_4$ and supported $NiFe_2O_4/ZrO_2$ at laboratory scale, using a high-powered sun-simulator equipped with three 6 kW Xe lamps. During these tests, different surface particle temperature was detected due to inhomogeneous solar radiation. Only in the upper part of the draft tube was measured a sufficient temperature for the reduction step. So the heat transfer was not sufficient to heat up the whole bed. In fact, in the annulus zone, a temperature lower of about $200^\circ C$ with respect to the draft tube was registered. Finally,

with an overall 30 minutes cycle, it was reported a 35% conversion of the supported ferrite oxide during the reduction phase and completely re-oxidation during the H₂ production.

The same researchers proposed another reactor design that includes a coated foam device [88]. The foam sample was placed in a quartz plate inside the reactor and heated up by a solar beam-down simulator (Figure 10.a). The reactor was tested with a ceramic foam coated with NiFe₂O₄/m-ZrO₂ (Figure 10.b) or CeO₂/MPSZ (Figure 10.c). The reduction was carried on in a range of 1450-1550°C while the oxidation reaction at 1100°C. The reactor was able to perform 7 cycles but a large temperature distribution was observed. Moreover, it is reported that the hydrogen yield was higher with the ceria foam due to sintering of iron foam during the reduction step.

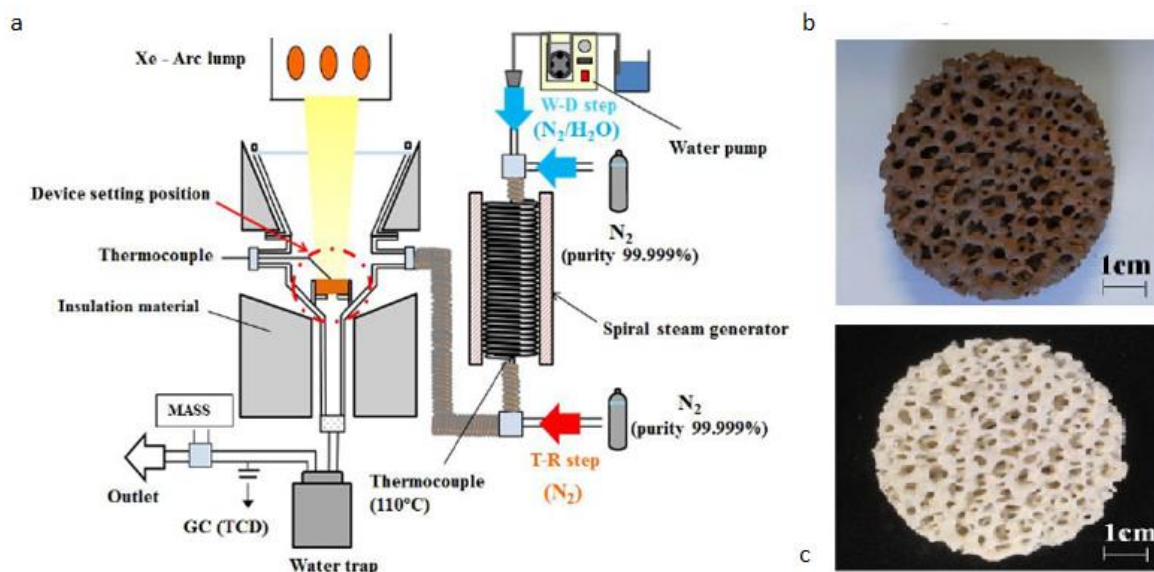


Figure 10: a) Foam reactor proposed by Gokon et al. [88] b) Iron foam sample, c) ceria foam sample

This concept of the reactor was later advanced at pilot scale coupled with a solar furnace of 45 kW_{th} [89]. Only ceria was used due to the reported better performance at lab-scale. Hydrogen was successfully produced in continuous cycles and the rate of its production was 215. ml/min and 443 ml/min using a ceria sample of respectively 15 and 20 cm in diameter. Similarly, Chueh et al. [90] extended the use of porous ceria for H₂O-CO₂. The proposed reactor was a cavity reactor irradiated from the top through a quartz window (Figure 11), the gases are introduced radially flowing through the ceria elements and exit at the bottom.

The tested metal oxide was monolithic porous ceria collected in cylinder form. The solar to fuel pick efficiency calculated was 0.8%, not heat recovery was considered. In further experiments, the monolithic ceria was replaced by porous ceria felt [91]. With this improvement, the calculated efficiency was doubled. Nevertheless, the efficiency remained low. This is due to the cycle irreversibilities resulting from material properties and solar reactor design and operation. With an energy balance, Chueh et al. [90] reported that 50% of the energy losses came from conduction through the reactor wall, while 41% from windows re-radiation. The first losses can be reduced by improving the reactor insulation, while the latter redesigning the

reactor in such a way as to reduce the windows surface. The reactor was able to produce H₂-CO with no interruption for 500 cycles, the steady state was achieved after 200 cycles.

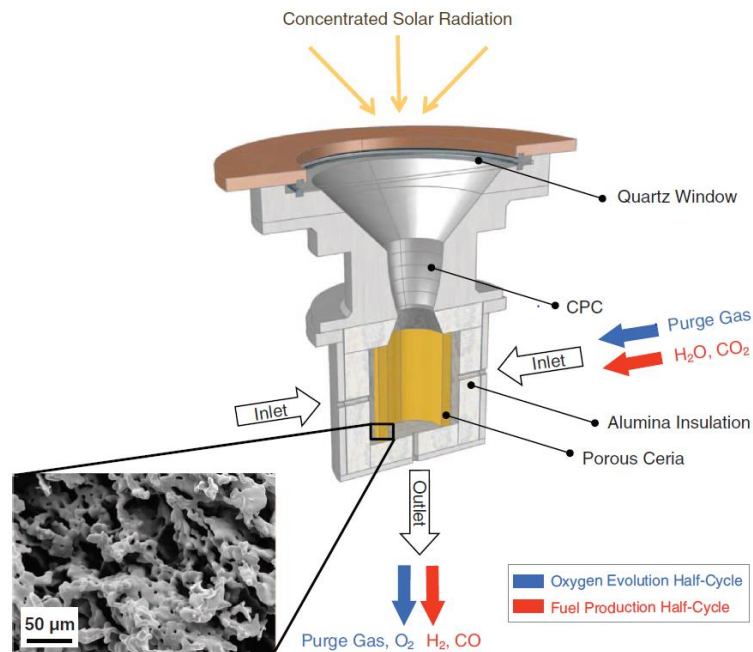


Figure 11: proposed reactor by Chueh et al. [90] for H₂O-CO₂ dissociation

The tested metal oxide was monolithic porous ceria collected in cylinder form. The solar to fuel pick efficiency calculated was 0.8%, not heat recovery was considered. In further experiments, the monolithic ceria was replaced by porous ceria felt [91]. With this improvement, the calculated efficiency was doubled. Nevertheless, the efficiency remained low. This is due to the cycle irreversibilities resulting from material properties and solar reactor design and operation. With an energy balance, Chueh et al. [90] reported that 50% of the energy losses came from conduction through the reactor wall, while 41% from windows re-radiation. The first losses can be reduced by improving the reactor insulation, while the latter redesigning the reactor in such a way as to reduce the windows surface. The reactor was able to produce H₂-CO with no interruption for 500 cycles, the steady state was achieved after 200 cycles.

As for Roeb et al. [70] and Kaneko et al. [92] proposed a reactor able to carry on both reduction and oxidation. This scope was achieved by designing a rotating reactor between two chambers. In one chamber the water splitting is performed while in the other the thermal reduction is achieved under solar irradiation (Figure 12). Such reactor concept was tested firstly in lab scale and then in pilot scale using a coated rotor by Ni-ferrite oxide. The optimum temperatures were found respectively equal to 1200°C and 900°C for the reduction and oxidation reaction. At this condition, it is reported, that 2.1 cm³ of O₂ were produced in 30 minutes.

Diver et al. proposed another rotating reactor, the so-called Counter-Rotating-Ring-Receiver-Reactor-Recuperator (CR-5) [93] can be seen in Figure 13. The reactor consists of a stack of counter-rotating rings with metal oxide fins along the circumference irradiated in the upper part by solar beams. Each ring rotates in the opposite direction of the neighbour. The speed is less than 1 RPM in order to enhance the heat recovery. The main concept is that as the ring rotates, the metal oxide passes from the high-temperature reduction zone to the water split zone and back again. The registered solar to fuel efficiency is 29%. Kim et al. proposed the CR5 for

combining H_2O-CO_2 splitting into a project called “Sun to Petrol” (S2P) [94]. The project had the target to produce liquid fuel (ie. methanol, diesel etc.) starting from H_2-CO produced by solar chemical looping.

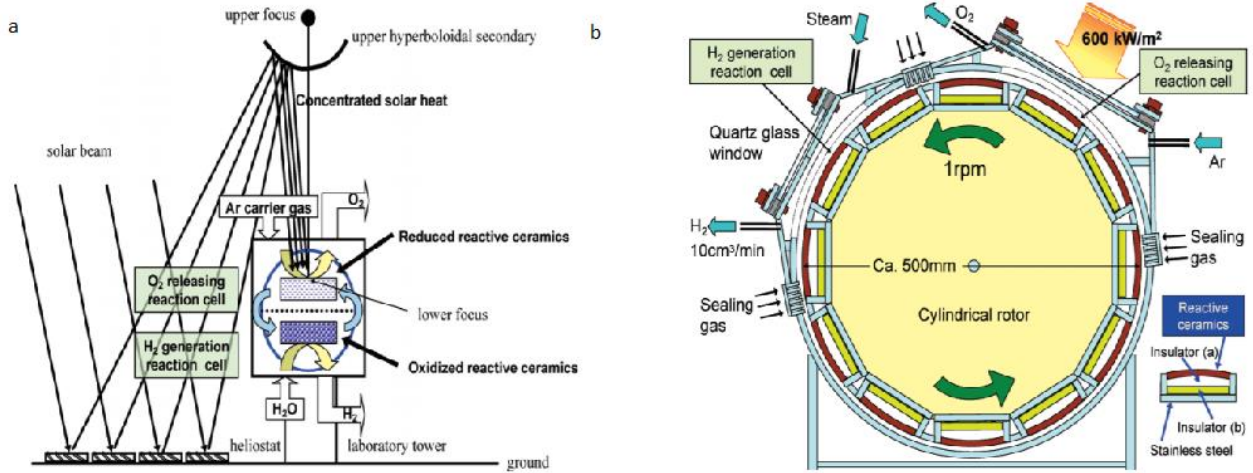


Figure 12: a) Rotator reactor concept proposed by Kaneko et al. [92], b) pilot scale rotating reactor

Diver et al. proposed another rotating reactor, the so-called Counter-Rotating-Ring-Receiver-Reactor-Recuperator (CR-5) [93] can be seen in Figure 13. The reactor consists of a stack of counter-rotating rings with metal oxide fins along the circumference irradiated in the upper part by solar beams. Each ring rotates in the opposite direction of the neighbour. The speed is less than 1 RPM in order to enhance the heat recovery. The main concept is that as the ring rotates, the metal oxide passes from the high-temperature reduction zone to the water split zone and back again. The registered solar to fuel efficiency is 29%. Kim et al. proposed the CR5 for combining H_2O-CO_2 splitting into a project called “Sun to Petrol” (S2P) [94]. The project had the target to produce liquid fuel (ie. methanol, diesel etc.) starting from H_2-CO produced by solar chemical looping.

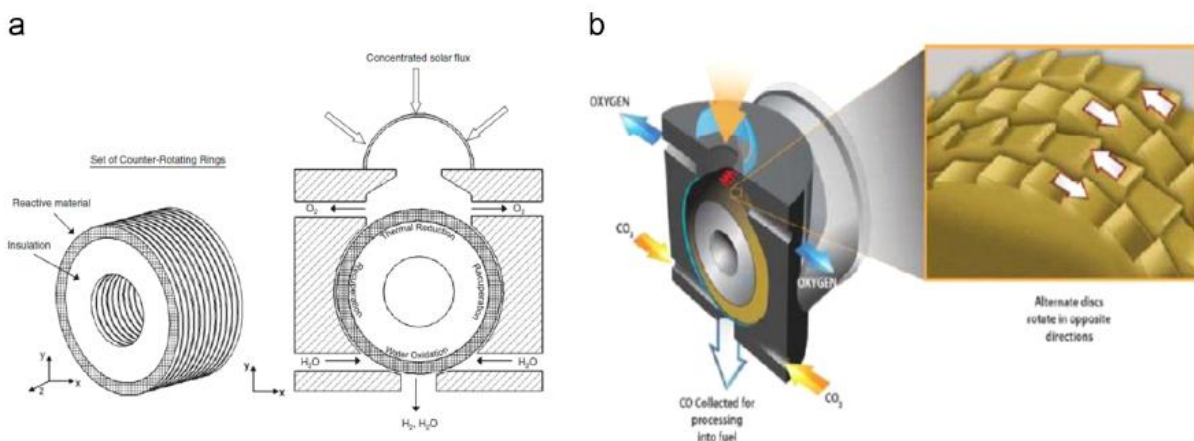


Figure 13: CR5 reaction proposed by diver et al. [93]

2.3.2. Chemical looping process by fuel reduction

Thermochemical looping cycles require high temperatures that might enhance metal oxide melting and sintering issues. In order to reach this operation conditions, solar towers are required. As listed before, coupling solar technology with chemical looping process is challenging. Of the described solar reactors, just a few of them has reached the demonstrative scale while most of the theme remained at lab scale. Besides the high temperature that requires elevated concentration ratio and particular material, the main challenge, especially in a scale-up for industrial application, is to guarantee isothermal conditions in big reactor volume.

An alternative is to perform the first step of the process by fuel reduction. In fact, still with existing limitations, the introduction of a reducing agent effectively lowers the oxygen partial pressure shifting the equilibrium towards lower temperatures [23]. So the overall reduction step results in a kinetically enhanced reaction at a lower temperature with significantly improved extent of metal reduction and, hence, larger oxygen releasing. The temperature swing between the two reactors is reduced, thus eliminating the heat recuperation from the solid resulting in a lower structural complexity and higher efficient process. The need of an inert sweep gas or vacuum condition to remove the released oxygen is eliminated [22]. Finally, the need of fast remove the released oxygen in order to avoid recombination with the metal is neglected.

Due to the abundance, low price and gaseous form, methane is the best candidate carbonaceous source for fuel reduction. However, in the future, the methane might be replaced by bio-methane increasing further the environmental benefits of the cycle. In methane reduction, methane is partially oxidized by the oxygen stored in the metal oxide. The overall reaction is an endothermic reaction which produces a syngas composed by H₂ and CO (2:1) and the reduced metal oxide (reaction 15). With the subsequent CO-H₂ formation in the oxidation reactor, the overall cycle offers a simple and promising alternative of producing syngas in both steps. The produced syngas can be exploited for chemical/fuel synthesis or used for power generation.



This type of cycle has been studied for cerium-based oxide (reaction 16) [95–99] and other materials [100]. Among all the materials, the advantage of pure ceria as an oxygen carrier that it is more thermodynamically favoured as per selectivity [23]. Krenzke et al. [22] performed a thermochemical analysis of ceria chemical looping process driven by methane reduction. The reported reduction non-stoichiometry coefficient δ ranged from 0.2 to 0.25 with a temperature between 950-1000°C. Moreover, Li et al. [101] reported an high selectivity of partial methane oxidation with CeO₂ at a temperature above 850°C [101].



Ceria reduction with methane has been demonstrated at lab scale by Warren et al. [102] and Krenzke et al. [103] which used similar solar reactor described in section 0 (Figure 14) with the main difference in the concentration ratio. In fact, the lower temperature of operation can be obtained with a lower concentration ratio and furthermore, this implies the possibility to work at isothermal condition [23]. However, even though the fuel reduction chemical looping has

been demonstrated only driven by solar source, the low temperatures of operation allow using as a heat source for the endothermic reduction different technologies such as nuclear or fossil fuel combustion. This implies the possibility to work round the clock and use reactor design already present in the industrial market such as a fluidized bed or packed bed reactor.

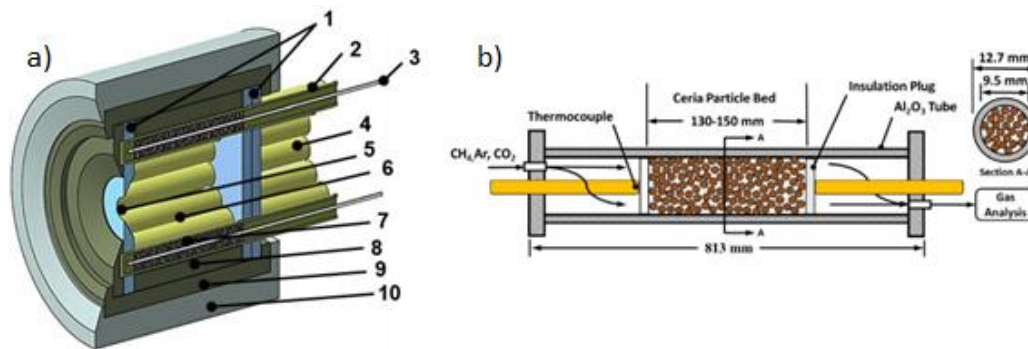


Figure 14: reactor design for chemical looping methane reduction. a) solar cavity receiver proposed by Warren et al. [102] b) tubular packed bed proposed by Krenzke et al. [104]

2.4. Polygeneration

A polygeneration plant combines different process in one system to produce multiple output products (power, heat, fuel, chemical etc.). The scope is twofold. Firstly, a tight integration of the multiple processes in terms of mass and energy allows achieving a higher efficiency than the stand-alone process [105]. For examples an exothermic reaction in one process can be used to carry on an endothermic reaction or, a certain mass stream that in the stand alone process would have been a waste can be used as a source for another subsystem. Secondly, an enhancement in profitability can be realized varying the proportion of the feedstock and products in response to the market status [106]. A plant that produces power and chemicals, might reduce the electricity production during the daily hours where it is cheaper and increase the chemicals production. Vice versa, when chemicals are cheaper, it might increase the electricity production. In addition, the economic gains can be increased due to the reduction of capital cost investment since some equipment might be shared among different process [107]. So polygeneration plants give the opportunity to exploit fossil fuels in a more sustainable and rational way, reducing their impact to the environment. For this reasons, polygeneration has attracted attention in research. Most of the literature is related to theoretical studies: modelling process, thermodynamics, exergy, techno-economic analysis and design optimization [18].

As reported in the previous sections, the main disadvantage of CCS is the efficiency penalty and economic expenditure for CO_2 sequestration. For this reason, the idea to perform CCS in a polygeneration plant to reduce these drawbacks is becoming considerable. Many studies demonstrated higher energy, economic and environmental performance of polygeneration plant

with respect of the stand-alone process integrated with CCS [108]. For examples for coal power plant, comparing an IGCC with CCS with a polygeneration system it is estimated that the latter is in average 7-10% more efficient, and the total CO₂ capture cost is 70-80% lower than the IGCC with CCS [108]. Moreover, the environmental impact of the fuel used to drive the plant can be further decreased if the captured CO₂ is recycled to produce new chemicals and fuels. Especially fuel synthesis from CO₂ allows to reduce the carbon footprint of the energy sector and tackle the fossil fuel scarcity. In addition, performing CCU inside the same plant where the CO₂ capture has been performed permits to avoid compression, transportation and storage issues.

Hu et al. [109] demonstrated that the integration of an IGCC system in a polygeneration plant for power and methanol production can reduce the cost of the CO₂ capture to 2.7 \$/ton_{CO2} which is lower than conventional CCS plant. Zhu et al. [110] integrated a coal IGCC process with a chemical looping unit for the production of H₂ and electricity. The proposed plant was compared to a classical IGCC and an IGCC with CCS, the result was that the polygeneration plant performs better in term of thermodynamic efficiency. Zhang et al. [111] studied an IGCC plant integrated with fuel production process. The CO₂ captured from the flue gases through CCS was recycled for syngas generation followed by methanol synthesis. The economic and thermodynamics improvement with respect to a classical coal-fired power plant was demonstrated. Bose et al. [14] introduced a cost-effective production of urea and power combined with CCS using coal gasification. Li et. [112] proposed different plant design for the combined production of methanol and electric power and compared them with a stand-alone methanol process. The exergy analysis of the different polygeneration plant design resulted in a lower exergy loss (7-20%) with respect of the methanol synthesis alone.

2.5. Dimethyl ether

One of the most interesting fuels that can be synthesized in the industrial sector is the dimethyl ether. DME (CH₃OCH₃) is the simplest ether, in which the oxygen atom (O) is connected to two methyl groups (CH₃). It has similar physical properties to liquefied petroleum gases such as propane and butane. A comparison of the main properties of DME with other fuel is shown in Table 2.

It is produced from methanol (produced from syngas) dehydration via a single step or two-steps catalyst process. Both processes are well established in the market sector, with companies such as JFE Holdings, Haldor Topsoe, Korea Gas Corporation, Air products, Lurgi and Udhe ('MegaDME'), Toyo and NKK that own their technology [113]. The majority of global DME production is currently in China where it is present one of the greatest DME plant (made by Toyo [114]). Furthermore, Japan, Korea, and Brazil have significant new production facilities, and major new capacity additions are planned or under construction in Egypt, India, Indonesia, Iran, and Uzbekistan. China's National Development and Reform Commission is calling for 20 million tons of DME production capacity by 2020 [115].

Table 2: Comparison of DME properties to commonly used fuel [24]

	DME	Methane	Methanol	Ethanol	Gasoline	Diesel
Formula	CH ₃ OCH ₃	CH ₄	CH ₃ OH	CH ₃ CH ₂ OH	C ₇ H ₁₆	C ₁₄ H ₃₀
Molecular weight [g/mol]	46.07	16.04	32.04	46.07	100.2	198.4
Density [g/cm ³]	0.661	0.00072	0.792	0.785	0.737	0.856
Normal boiling point [°C]	-24.9	-162	64	78	38-204	125-400
LHV [kJ/g]	28.82	47.79	19.99	26.87	43.47	41.66
Carbon content [wt. %]	52.2	74	37.5	52.2	85.5	87
Sulfur content [ppm]	0	7-25	0	0	200	250

Few works are present in the literature about polygeneration process which involves DME production. Larson et al. [116] proposed a polygeneration plant for power and DME using switchgrass as fuel. The plant is able to produce 207 MWe and 6 kg/s of DME with an efficiency higher than 50% using a gasification unit for the syngas production. A similar plant was proposed by Clausen et al. [117] with the scope of produce DME and power, reducing the total emissions of CO₂ by carbon capture. The proposed plant is able to produce the DME with a biomass-to-fuel efficiency of 48% to 66% and a cost of 11.9 to 12.9 \$/GJ_{LHV}, depending on the DME reactor configuration (recirculation cycle or once through). Cocco et al. [118] proposed a polygeneration plant for DME and power production using a coal gasification unit for syngas production. The reported overall efficiency ranged from 54.4% to 56.6%, with a DME cost of 6-6.5 \$/GJ_{LHV}.

DME can be used, either blended with LPG or alone, in the residential sector for heating and cooking or burnt in engines for power production. However, the main attractive application is in the transport sector. Since the 90s, DME has been proposed as one of the most valid alternatives to diesel. The advantage of DME is in lower emission of NO_x, hydrocarbons, and CO. Further, due to the high oxygen content and the absence of C-C bonds DME combustion does not emit soot, which is the Achilles' heel of diesel [119]. Figure 15 is shown CIDI (compression ignition direct injection) engine test results for diesel and DME reported by McCandless [120].

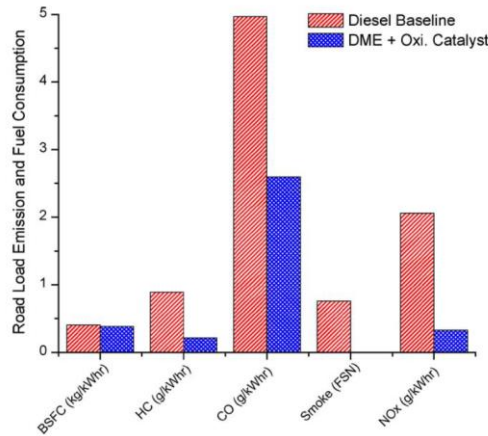


Figure 15: Road load test data comparing engine emissions using DME and diesel [120]

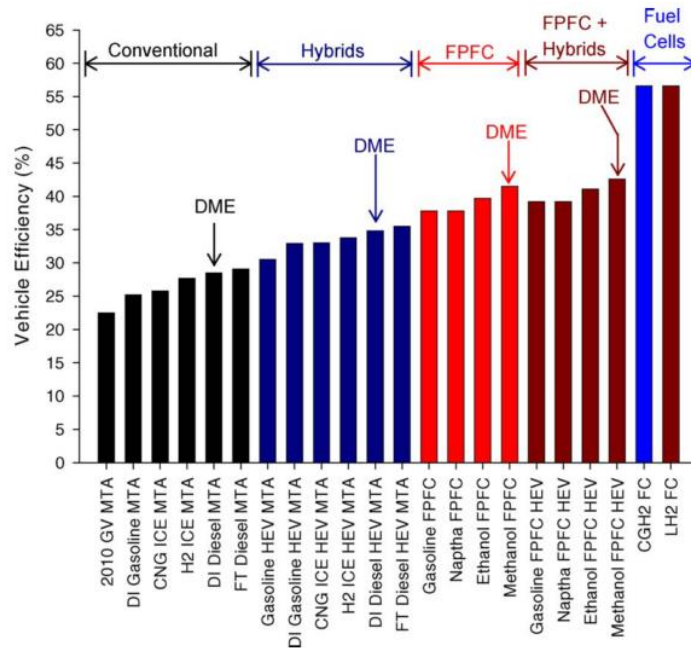


Figure 16: Tank-to-wheel efficiency of various vehicle technologies [24]

The engine designed for diesel combustion does not require any modification to host DME. On the contrary, due to the lower energy density, fuel storage must be twice in size with respect to a traditional diesel tank. In addition with respect to novel fuel for an automotive application like H₂, DME does not require the building of completely new infrastructure for storage and transportation. In fact, due to its similar properties of LPG fuels, dimethyl ether can use existing land-based and ocean-based LPG infrastructure [24]. Figure 16 and Figure 17 are reported the tank-to-wheel efficiency and the tank-to-wheel GHG emissions of different vehicle technologies driven by different fuels [24]. The data reported demonstrating the worth of using DME as an alternative fuel, in fact, each vehicle technology fuelled by dimethyl ether results as one of the most efficient vehicles and lowest GHG emitting.

One of the major initiatives about DME used in transportation sector called BioDME was launched in Sweden [121]. The projects, involving the participation of Volvo and Chemrec, was one of the greatest pilot project involving production, transportation and use of DME per

auto-traction purpose. The Chemrec facility, combined its daily black liquor by-product with multiple bio-waste to generate, through Topsoe process, enough DME to power 10 trucks. The produced DME was transported to existing LPG distribution facilities that were able to handle DME distribution with few modifications. The results of the two years tests were so encouraging that in 2013 Volvo announced the begin of a new line of a vehicle driven by DME combustion. However, later, the same company changed their plans announcing further study about alternative fuels vehicles. At the present a new project is ongoing in New York City for DME trucks produced by Mack Trucks, a sister line's of Volvo. In 2015, Ford Motor Company announced a three years project co-founded by the German government to develop and test the world's first production passenger car to run on DME. The 3.5 million \$ project involves an international collaboration by Ford's Research & Innovation Center and other entities including Oberon fuel.

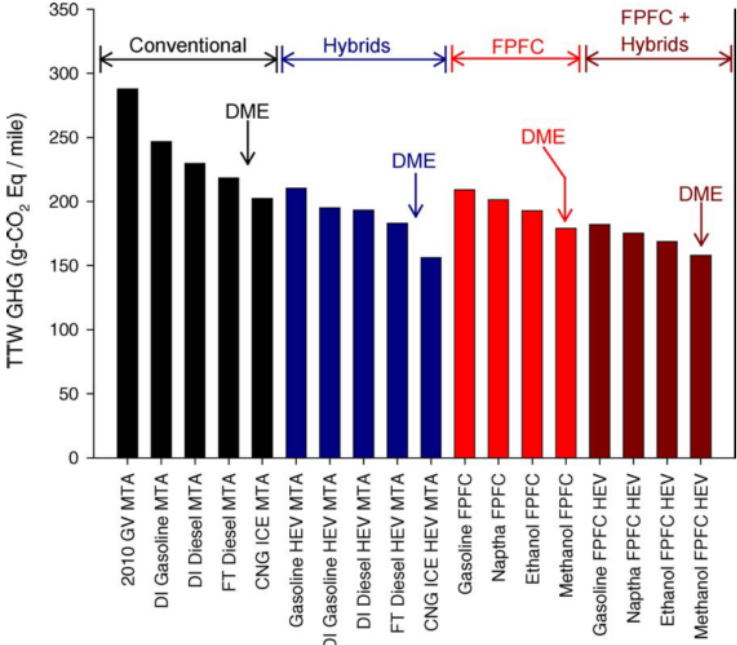


Figure 17: Tank-to-wheel GHG emission for various fuels and vehicles [24].

3. Methodology

3.1. Process modelling and simulation tools

Process modelling is a key element of process design, it permits to mathematically replicate a simple or complex system. A process simulation, instead, allows evaluating the behaviour of the proposed system. Generally, it is performed placing the model in a simulator tool which, through the application of mass and energy balance, gives as output the complete operation condition map of the system. This is a crucial step in process design, since knowing the behaviour of the model, it is possible to understand which are its weak points that can be optimized in order to achieve the prefixed results.

Aspen Plus® made by AspenTech is an example of the simulation tool. It is widely used in the industrial sector for chemical, petrochemical, and oil refining process analysis or in the academic field. Aspen Plus® gives the opportunities to design, analyze and optimize an engineering process. For this scope, it has built-in equipment models like exchangers, reactors, pumps, turbines or additionally FORTRAN subroutines that allows to include further information or, even create from the beginning new models. Furthermore, combining mass and energy equations balance, reaction kinetics and reaction equilibrium to the reliable thermodynamics database and realistic operation conditions, it permits to well simulate the plant behaviour.

The proposed plant was modelled and simulated using Aspen Plus® v8.8. The model described in the following is based on whether the built-in models or subroutine written in FORTRAN which are connected together by streams or Aspen Plus® calculation blocks. The results of the various flowsheets were extrapolated and used for further analysis (exergy analysis, economic and exergo-economic analysis, water consumption analysis) in order to have a complete assessment of the process.

3.2. Exergy analysis

The environment can be described as a large body in the state of perfect thermodynamic equilibrium. This conceptual environment has no gradients in pressure, temperature, chemical potential, kinetic or potential energy, thus, there are no possibilities of producing work from any interaction between parts of them. Any system which has different values of the previously listed parameters with respect to the environment has a work potential in relation to it. In terrestrial applications, the environment consists of the atmosphere, the seas and the oceans, and the earth's crust. The environment can interact with an external system in three ways: i) through thermal interaction as a reservoir (source or sink) of thermal energy at the temperature T_0 , ii) through mechanical interaction as a reservoir of unusable work and, iii) through chemical interaction as a reservoir of a substance of low chemical potential in stable equilibrium. Through these types of interactions, the environment determines, for the purpose of evaluating exergy, the reference level of pressure, temperature and chemical potential. When there is a thermal and mechanical equilibrium between a system and the environment, the system is defined as in the environmental state. When in addition to the temperature and pressure, there

is also a chemical equilibrium, the system is in the dead state and so there is no possibility to produce further work. Exergy of a steady stream of matter is defined as the maximum amount of work obtainable when the stream is brought from its initial state to the dead state by processing during in which the stream may interact only with the environment [122].

Exergy can be divided into different components: kinetic exergy E_k , potential exergy E_p , physical exergy E_{ph} and chemical exergy E_{ch} .

$$E = E_k + E_p + E_{ph} + E_{ch} \quad (16)$$

In the presented work only the physical and chemical exergy are considered. The physical exergy is defined as the maximum work achievable from a system that from its initial state is brought to the environmental state with only thermal and mechanical interaction with the environment. While the chemical exergy is the maximum work obtainable from a system that is brought from the environmental state to the dead state, involving heat transfer and exchange of substances only with the environment. The two types of exergy are given by equation (17) and (18) [123]. In particular, for a mixture, the total chemical exergy $E_{ch,tot}$ is made by two contributes: the chemical exergy of the single i -th component $E_{0,i}$ and the work obtainable from a reversible isothermal expansion at T_0 from the partial pressure p_{00} of the i -th component and environment pressure p_0 .

$$E_{ph} = \sum_i x_i \cdot \left[(h_i - h_{0,i}) - T_0 \cdot (s_i - s_{0,i}) \right] \quad (17)$$

$$E_{ch,tot} = \sum_i x_i \cdot \left[E_{0,i} + \gamma \cdot R \cdot T_0 \ln \frac{p_0}{p_{00}} \right] \quad (18)$$

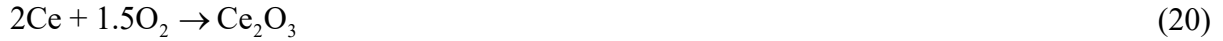
where: i) x_i is the mass fraction of the i -th component in the mixture, ii) h_i is the mass enthalpy of the i -th component, iii) $h_{0,i}$ is the mass enthalpy of the i -th component at the environment state, iv) T_0 is the temperature of the environment state, v) s_i is the mass entropy of the i -th component, vi) $s_{0,i}$ is the mass entropy of the i -th component at the environment state, vii) γ activity coefficient for the i -th component and viii) R is the ideal gas constant.

The advantage of an exergy analysis is that it is based on the second principle of thermodynamics, thus permits to evaluate the so-called ‘‘destroyed’’ exergy I_{dest} . Destroyed exergy represents the real loss in the quality of energy that cannot be identified by means of a simple energy balance because the conservation of energy will always apply. The following equation represents an exergy balance of a general device in steady state condition:

$$\sum_i (E_{out,i} - E_{in,i}) = \sum_i W_i + \sum_i Q_i \left(1 - \frac{T_0}{T_i} \right) + I_{dest} \quad (19)$$

Where: i) the members at the left side represents the exergy contribution of the $E_{in,i}$ inlet and $E_{out,i}$ outlet mass flows, ii) W_i represents the absorbed/produced work by the device, iii) the second member is the heat exchanged contribution, it represents the work obtainable from the heat flux Q_i operating with a Carnot machine and iv) I_{dest} is the irreversibility generated.

In order to perform an exergy analysis, it is important to establish an environment as a reference (Table 3). For the environmental state, a pressure (P_0) of 1 atm and a temperature (T_0) of 20°C were selected, while for the dead state the reference environment of Szargut [124] was chosen. Regarding Ce_2O_3 , there are no works in literature where it is a reference substance and so there are no data about its chemical exergy. In fact, in most of the works, Ce and CeO_2 are used as a reference substances, since they are the most abundant form of ceria in the heart. However, Ce_2O_3 chemical exergy can be calculated starting from the known exergy of Ce and O_2 (eq.20 and eq.21):



$$Ex_{Ce_2O_3}^0 = 2Ex_{Ce}^0 + 1.5Ex_{O_2}^0 + \Delta G_{Ce_2O_3}^0 \quad (21)$$

where: i) E_{Ce}^0 , $E_{Ce_2O_3}^0$, and $E_{O_2}^0$ are the standard chemical exergy of Ce, Ce_2O_3 and O_2 , respectively, ii) $\Delta G_{Ce_2O_3}^0$ represents the Gibbs free energy for the formation of Ce_2O_3 from the Ce- O_2 reaction (Eq.20).

Table 3: environment state and dead state data and assumptions

Environmental state: $P_0=1$ atm $T_0=20^\circ\text{C}$											
Dead State											
Chemical exergy E_{ch} [J/mol]											
H ₂	CO	CO ₂	H ₂ O _{va}	H ₂ O _{li}	N ₂	CH ₄	O ₂	CeO ₂	Ce ₂ O ₃	DME	MeOH
236,09	275,10	19,20	^p 9,181	^q 870	69	853,35	3,83	33,80	384,70	[24] 1,414,50	[24] 715,52
0	0	3			6	6	7	0	2	0	0

3.2.1. Exergy analysis indicators

In order to estimate the exergy efficiency (or efficiency of the second principle) of a system, it is necessary to define which are the material consumed during the process (Fuel) and which are the final products of the process (Products). The overall exergy efficiency or of a single system can be calculated by the following equation:

$$\eta_{ex} = \frac{E_p}{E_f} \quad (22)$$

Where E_p represents the exergy of the product streams and E_f the exergy of the resource streams. However, the only exergy efficiency does not give a complete framework of the plant or subsystem. For this reason, additional exergetic factor was adopted [125]:

$$- \text{Relative irreversibilities: } \chi_i = \frac{I_{i,destroyed}}{I_{tot,destroyed}} \quad (23)$$

$$- \text{Fuel depletion rate: } \mathcal{G}_i = \frac{I_{i,destroyed}}{E_{f,plant}} \quad (24)$$

$$- \text{ Productivity lack: } \xi_i = \frac{I_{i,destroyed}}{E_{p,plant}} \quad (25)$$

$$- \text{ Exergetic factor: } \psi_i = \frac{E_{f,i}}{E_{f,plant}} \quad (26)$$

3.3. Techno-economic and discounted cash flow analysis

An important aspect to be considered during process design is the economic performance of the modelled plant. An economic assessment can be performed to calculate the capital cost of investment for the construction of the proposed plant. The National Energy Technology Laboratory (NETL) guidelines for techno-economic analysis for power plants was adopted [126,127]. This methodology defines capital cost at five levels: bare erected cost (BEC), Engineering, Procurement, and Construction Cost (EPCC), total project cost (TPC), total overnight cost (TOC) and total as-spent cost (TASC). The first four items are “overnight cost” and are expressed in base year dollar that is the first year of capital expenditure. While, TASC is specified in mixed, current-year dollar over the all capital expenditure period. In the current study, the TOC was considered for the capital investment expenditure.

The first step in cost estimation is the evaluation of equipment expenditure. The best choice of cost calculation is using the exact cost of a vendor or a company database. However, it is not always possible to obtain these price, hence, the second best solution is to calculate the cost considering a similar known equipment [128]. In fact, it is possible to find out a good cost estimation (C_{equ}) considering a different size (A_0) equipment ($C_{equ,0}$) scaled to the desired size (A) through an exponent factor n [129]:

$$C_{equ} = C_{equ,0} (A/A_0)^\beta \quad (27)$$

Moreover, to take into account the fluctuating value of money due to inflation and deflation, all the estimated equipment costs were converted to the year 2017 dollar using the chemical engineering plant cost index (CEPCI, Table 4)

$$C_{equ,actual} = C_{equ} \frac{\text{CEPCI 2017}}{\text{CEPCI at the time of original cost}} \quad (28)$$

The Bare Erected Cost (BEC) comprises the cost of the equipment, facilities and infrastructure, and labour required for its installation. It was given summing to the equipment cost all the installation costs shown in Table 5:

$$\text{BEC} = C_{equ,actual} + \text{Installation Cost} \quad (29)$$

The engineering, Procurement, and Construction Cost (EPCC) comprises the BEC plus all the cost of all services provided by the engineering, procurement and construction contractor (eq. 30). These items include detailed design, contractor permitting and project management costs.

$$EPCC = BEC + \text{INDIRECT COST} \quad (30)$$

The total project cost (TPC) takes into account the EPCC plus the contingencies cost (eq. 31). Contingencies are added to account for unknown costs that are omitted or unheralded due to lack of complete project definition or uncertainties with the development status of a technology.

$$TPC = EPCC + \text{CONTINGENCIES} \quad (31)$$

The total overnight cost (TOC) comprises the TPC plus other overnight costs (*Table 5*), owner's cost included (i.e pre-production, inventory capital, land, financing), it was calculated as:

$$TOC = TPC + \text{OWNER'S COST} \quad (32)$$

Finally, to evaluate the profitability of the plant during its lifetime a discounted cash flow analysis (DCF) was adopted. DCF is based on the concept of the time value of money, all the future cash flows are estimated and discounted by a discounted factor (*i*) (*Table 7*), obtaining their present value [130]. The sum of the all discounted cash flows, both positive (revenues) and negative (operation cost, *Table 6*), gives the net present values (NPV).

$$NPV = -TASC + \sum_{n=1}^t \frac{(\text{net cash flows})_n}{(1+i)^n} \quad (33)$$

A project is acceptable only if the NPV is at least positive. In this particular case, TASC is used to evaluate the total project cost instead of TOC, in order to assess both escalation and interest during construction (*Table 7*) [126,127].

Another important factor used to take into account to assess the economic feasibility of a power plant is the payback time (PBT). PBT measures the time when negative cash flows equal the positive cash flows, or, in other words, evaluate the exact time when NPV is null. Hence, this factor allows the investor to have an idea of the required period of return on the investment. The smaller the payback time is the faster the return on the investment expenditure is and consequently, the more attractive the plant is.

3.3.1. Economic assumption

In the following table are shown the main assumption used in the economic performance of the plant. It is worth mentioning the assumption made for the contingencies. In the present case, since the proposed plant is based on a novel technologies arrangement a high contingency cost was selected (*Table 5*).

Table 4: CEPCI index

Year	CEPCI index
2017	572.7
2016	585.7
2008	575.4
2007	525
2006	499.6
2003	402

Table 5: main assumption in CAPEX estimation

Installation Cost [36]	
Accessory Electrical Plant	16,93 M\$
FO Supply System and Natural Gas Supply System	10,04 M\$
Erection, Steel Structures, and Painting	49% of equipment cost
Piping	9% of equipment cost
Indirect cost [36]	
Yard improvement	2% BEC
Services facilities	2% BEC
Engineering/consulting costs	5% BEC
Building	4% BEC
Miscellaneous	2% BEC
Owner's cost	5% EPC
Contingency [127]	30% EPC

Table 6: main assumption in OPEX estimation

Variable costs [36]	
Process Water	7.41 \$/m ³
Make-up water	0.41 \$/m ³
Fuel cost [131]	0.04 \$/kWh
Ceria oxide cost ([132])	49 \$/kg
Yearly Ceria oxide make-up	30% of the total
Fixed costs [36]	
Property, Taxes, and insurance	2% TOC
Maintenance cost	2.5% TOC
Labour cost	1% TOC

Table 7: economic assumptions

Life of the system (t)	30 years
Discount rate (i) [41]	10%
Capacity factor (CF)	85%
Debt	60%
Equity	40 %
Cost of debt	2.4 %
Inflation	1.5%
Project financing	10 years
TASC	7.8% TOC
Construction	3 years

3.4. Exergo-economic analysis

Exergo-economic rests on the concept that exergy is the only rational basis for assigning monetary costs to the interactions which a system experiences with the environment and to the sources of thermodynamics inefficiencies within it [133]. The exergo-economic analysis method was first introduced in 1990 by Tsatsaronis and Lin ([134]) and named SPECO (Specified Exergy Costing) in 1995 by Lazzaretto and Andreatta [135]. For analyzing the energy of the plant, this method provides an easy and straightforward scheme and it helps in time-saving by employing a compact matrix formulation [136]. So, the SPECO method was adopted in this work. The starting point of this methodology is the exergy analysis of the plant with all the exergy streams and irreversibilities produced during the process.

Secondly, the productive structure has to be defined i.e. which are the fuel (F), product (P) and loss (L) for each subsystem. Fuel is defined to be equal as i) all the exergy values to be considered at the inlet plus ii) all the exergy decreases between inlet and outlet (i.e. the exergy removals from the respective material streams) minus iii) all the exergy increases (between inlet and outlet) that are not in accord with the purpose of the component [137]. The product is defined to be equal to the sum of i) all the exergy values to be considered at the outlet (including the exergy of energy streams generated in the component) plus ii) all the exergy increases between inlet and outlet that are in accord with the purpose of the component [137]. While flows that leave the unit and the plant, are not subsequently used and do not require a special treatment are denominated as losses [138]. Based on the results of the exergy balance of the plant, an exergy cost E^* and unit exergy cost $k^*=E^*/E$ is assigned to each stream. The exergy cost of a physical flow is the exergy spent to produce it, irreversibilities comprised. Therefore, is completely connected to the production procedure efficiency, the highest the efficiency is the lowest is the irreversibilities produced, and the lowest the exergy cost of the stream is. In order to evaluate the exergy cost of each of the 'm' flows of a certain plant, it will be necessary to write 'm' independent equations. If the plant is sequential, that is all the subsystems are characterized by a single output, since the exergy cost is conservative, it is possible to write as many equations of exergy cost balance as the number of subsystems. Vice versa, if the subsystems are characterized by multiple outlets (bifurcations), additional equations must be written for each unit equations, equal in number to the outlet streams 'm' minus the fuel F and

losses streams L ($x=m-F-L$). Valero et al. [139] have formulated a rational procedure of exergy cost estimation based on four propositions:

- P1 rule: in the absence of an external assessment, the cost of the inlet flow to the plant is equal to the exergy of the stream:
 $E^*i=Ei$
- P2 rule: in absence of external assessment, the exergy cost of losses is null:
 $E^*i=0$
- P3 rule: if an output flow of a device is a part of the fuel, its exergy unit cost is the same as the input flow from which it comes.
- P4 rule: if a unit has as a product a multiple outlet flows, since the formation process is the same, an equal exergy cost is assigned to all the streams.

The exergy cost assessment can be formulated in a compacted matrix form as:

$$[A_c] \cdot C = Z_e \quad (34)$$

$$\begin{bmatrix} A \\ \alpha_e \\ \alpha_x \end{bmatrix} \cdot C = \begin{bmatrix} -Z \\ C_e \\ 0 \end{bmatrix} \quad (35)$$

$$C = [A_c]^{-1} \cdot Z_e \quad (36)$$

Where C_e is the cost of the external assessment.

After obtaining the cost C and relative specific cost ($c=C/E$), the exergo economic variables, such as the exergo economic factor (f_k) (equation 37) and relative cost difference (r_k) (equation 38), can be calculated. The exergo economic variable permits to evaluate the contribution of the investment cost on the product streams, the highest it is the bigger is the component investment cost contribution. While the relative cost difference allows locating the component with the highest difference between product and fuel.

$$f_k = \frac{Z_k}{Z_k + C_D} \quad (37)$$

$$r_k = \frac{c_{P,k} - c_{F,k}}{c_{F,k}} \quad (38)$$

where $c_{F,k}$ and $c_{P,k}$ represent the specific cost of the fuel and product of the the k -th component, while c_D is the cost of the destroyed exergy in the k -th component (equation 39):

$$c_{D,k} = c_{D,k} \cdot I_{dest,k} \quad (39)$$

In the current study, the cost rate (Z) was calculated using the annual capital cost ACC [140]:

$$ACC=TOC \times CRF \quad (40)$$

The annual capital cost is a combination of the total overnight cost and the recovery factor (CRF). CRF is defined as a ratio of constant annuity to the present value at a time (t) with a specified discount rate “i” as:

$$CRF = (i \cdot (1+i)^t) / ((1+i)^t - 1) \quad (41)$$

The cost rate Z comprises the total overnight cost plus the operational costs. It was given by the overall of this costs divided the annual operational time τ , based on the capacity factor CRF (Eq. 45).

$$Z = (ACC + \text{Fixed costs}) / \tau + \text{Variable cost} \quad [M\$/s] \quad (42)$$

When evaluating an equipment by an exergo-economic study, a general rule for reducing the final cost of the streams can be followed. The subsystems that have the priority for an intervention are the ones with the highest (Z+CD). Among these, the equipment with the highest relative difference cost r_k must be selected. The exergo-economic factor identifies the main causes of cost increase: a high value of this parameter (f) indicates a high influence of the cost of investment, a low value indicates a high incidence of the thermodynamic efficiency. In the first case a possible solution could be the use of cheaper components (generally characterized by lower efficiency), in the second case a higher efficiency component could be used with a consequent increase of the investment cost.

3.5. Water consumption estimation

An important parameter for an industrial and/or power plant is its water use. A generally accepted indicator of water use is the water footprint [141], it measures the volume of fresh water used to produce a product over the full supply chain [142]. In this specific case for water-footprint is intended the water exploited during the plant operation, i.e. for cooling and other processes. The following water withdrawal calculation is based on the model described in [143]. The water use can be expressed as a function of the heat rate HR (kJ/kWh) and three other adjustable parameters: A, B, and D:

$$I = A \times (HR - B) + D \quad (43)$$

The heat rate (HR) is defined as the amount of energy required to produce one kW of electricity:

$$HR = \frac{\text{Heat Input of Fuel}}{\text{Net Power Output}} \quad (44)$$

Not all the input heat is converted into electricity, but it is converted in waste heat that has to be dissipated to the environment. The greatest part is rejected through a cooling system, which usually uses water as a transfer medium. In general, water use in a polygeneration plant can be really complicated. However, a good estimation of it doesn't require a detailed analysis since, according to [144], the cooling process accounts for 73-99% of the water consumption. So that,

it is possible to have a good water need assessment by knowing only the heat rate and the type of cooling system used in the analysed plant. The energy going into the plant can leave it only in two ways, as a process heat losses or as a product stream, so the heat sent to the cooling system is given by $HR-B$. Where B (kJ/kWh) takes into account all the heat losses during the process, i.e steam turbine heat losses, generator heat losses, radiation losses, combustor losses etc. In general, depending on the technology, they ranged from 3% to 5% of the total energy input [143]. The parameter A (L/kJ) is the constant that takes into consideration the water need for the cooling system per unit of energy that has to be rejected. These parameters depend on many factors such as the type of cooling system (cooling tower, one-trough, dry cooling), the design of the cooling system, temperature and humidity of the air and water. Finally, the parameter D (L/kWh) includes water consumption for other processes like gas desulfurization, dust removal, WGS etc.

In the following are shown the main assumption used in the water consumption calculation.

Table 8: main assumption made in water consumption calculation

Heat Rate (HR)	11523,45 kJ/kWh _e
Heat losses	5%
B	4176,2 kJ/kWh _e
A [44]	0,001 L/kJ
D [44]	0,02 L/kWh _{e, gross}

4. Plant simulation and results

A polygeneration plant, producing, electricity, DME and Methanol have been proposed integrating chemical looping syngas production with methane reduction of Ceria as the oxygen carrier. In this chapter, the proposed plant has been analysed in detailed as a proof of concept and is documented as follows.

4.1. Process and plant description

The proposed plant is an Oxyfuel natural gas feed combined cycle power plant integrated with a chemical looping $\text{CO}_2/\text{H}_2\text{O}$ splitting unit for power and fuel generation (OXYF-CL-PFG). Figure 18. describes the general plant design concept. The supplied natural gas from the gas grid is sent to the chemical looping splitting unit (CL) where it is converted into a hydrogen-rich syngas by the simultaneous reduction of ceria. The produced syngas is sent to an oxyfuel unit where it is burnt with a pure stream of oxygen coming from an air separation unit (ASU). The hot exhaust gases composed mainly by H_2O and CO_2 are firstly expanded in a gas turbine and then sent in a heat recovery steam generation unit (HRSG). Here, the surplus heat is exploited to produce superheated steam for power production. Finally, the water and carbon monoxide are separated by a water condenser. The large part of the separated CO_2 is recirculated to the oxy-fuel combustor, while another fraction, together with steam is sent to the CL unit. In the CL unit, both H_2O and CO_2 are dissociated by the reduced ceria coming from the reduction reactor. The produced syngas is sent for the DME production process. Finally, the produced fuel is separated from the other diluted product in a distillation unit.

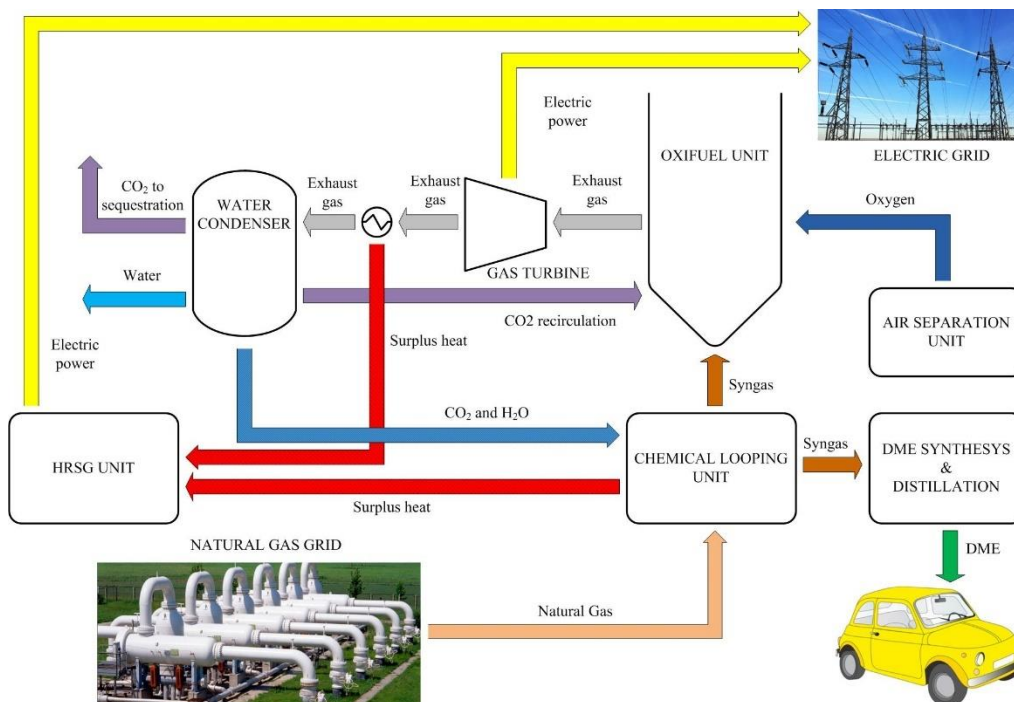
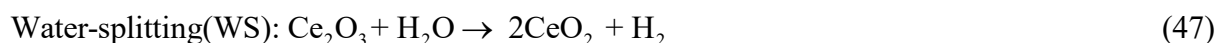
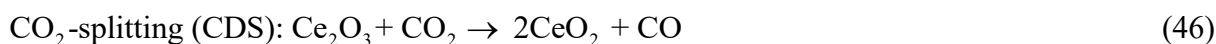


Figure 18: plant general concept

4.1.1. Simulation Assumption

The polygeneration gas to power and fuel plant integrated with a chemical looping CO₂/H₂O dissociation unit has been modelled by combining mass and energy balance equations. The hypothesis of chemical equilibrium has been applied to all the components of the layout with exception of the DME reactor, for which a kinetic approach has been used. To assess the performance of the chemical looping unit system a thermodynamic redox pair of CeO₂/Ce₂O₃ for stoichiometric reduction (eq. 45) and oxidation (eq. 46,47):



The material streams used in the model involve conventional and solid components. The Peng-Robinson-Boston-Mathias (PR-BM) property method was used for the conventional components [145,146] as this approach is recommended for hydrocarbon processing applications such as gas processing, refinery, and petrochemical processes [147]. This method uses the Peng-Robinson cubic equation of state combined with the Boston-Mathias alpha function for all the thermodynamic properties [145]. The oxygen carriers used for the chemical looping simulation were entered as conventional solid components. For this type of streams, the Barin equation was used [148,149]. The RGIBBS reactor blocks were used for modelling the oxidation reactor, the reduction reactor and the combustor of the oxyfuel unit. The distillation unit and the air separation unit were modelled using the RadFrac column. The DME reactor was simulated with an RPlug reactor combined with a Langmuir-Hinshelwood Hougen-Watson (LHHW) kinetic model. During the simulation of this component, the Soave-Redlich-Kwong (SRK) EOS was utilized. The Redlich Kwong (RK) EOS is usually applied to binary components [150]. Moreover, Graaf et al. [151] stated that the chemical equilibrium of the methanol reaction and WGS reaction can be well described at high-pressure by using the SRK-EOS. The main hypotheses used in the modelling phase are reported in Table 9. Figure 19 shows the layout of the plant.

Table 9: main assumptions and hypothesis used in the process simulation

Natural gas	Composition (std.vol%): 93.1% CH ₄ , 3.2% C ₂ H ₆ , 1.6% N ₂ , 1.1% C ₃ H ₈ , 1.0% CO ₂ LHV=47.1 MJ/kg	
Oxidation and reduction reactors	Model: RGIBBS, no heat losses	
Combustor	Model: RGIBBS $\Delta P=0.2$ bar, no heat losses	
Compressors, pumps and turbines	$\eta_{is,comp}=0.9$, $\eta_{mech,comp}=0.98$, $\eta_{is,pump}=0.9$, $\eta_{driver,pump}=0.90$, $\eta_{is,turb}=0.9$, $\eta_{mech,turb}=0.98$	
Oxygen carrier	Solid ceria: CeO ₂ /Ce ₂ O ₃ , diameter=100 μ m Temperature drop of 20°C during ceria recycling from OXI to RED	
DME reactor	Model: RPlug multitube reactor, Operation: T=250°C P=50 bar	
Heat exchangers	$\Delta T_{min}=10^\circ C$	
Distillation unit	Model: RadFrac, Reboiler type: Kettle	
CLN-CO ₂	CLN-DME	CLN-MeOH
P=10 bar	P=9 bar	P=2 bar

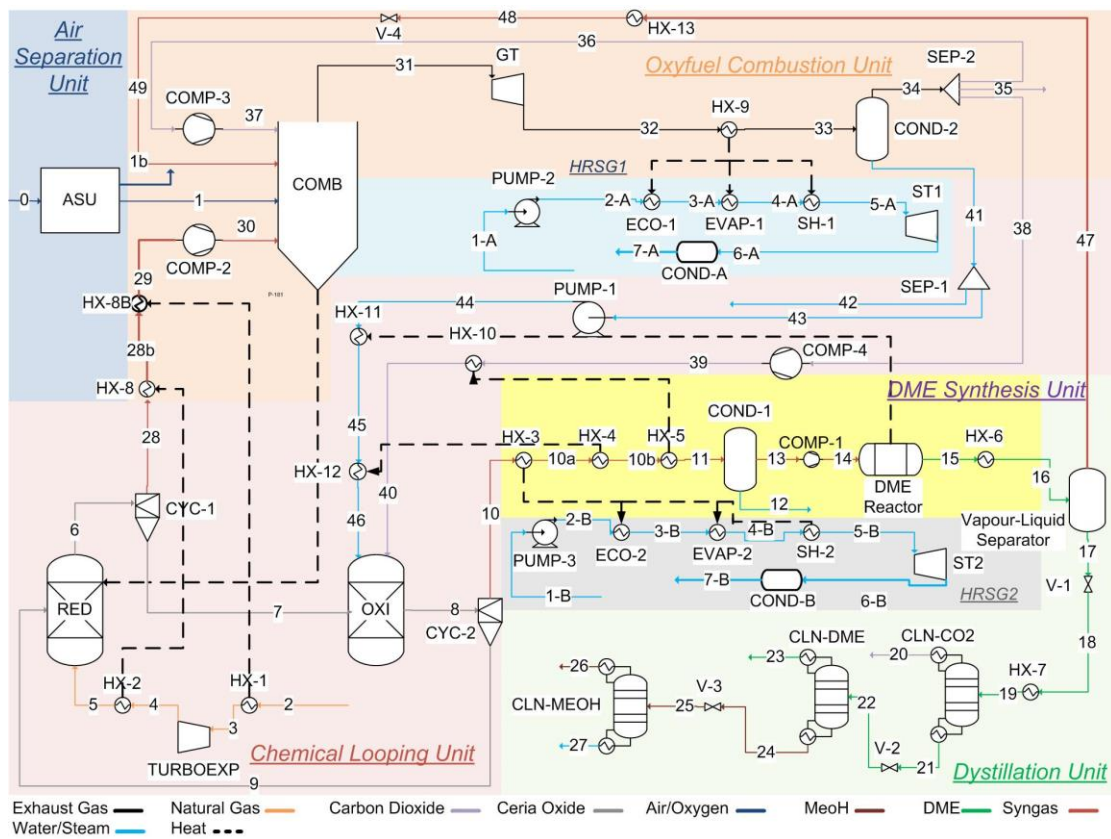


Figure 19: Detailed Plant Layout for Power and DME Production from Natural Gas Utilizing the CL Unit

4.1.2. Chemical looping syngas production Unit (CL unit)

The chemical looping unit is made by two interconnected reactors operating at 2 bar: the reduction reactor (RED) and oxidation reactor (OXI). The circulating oxygen carrier is ceria oxide ($\text{CeO}_2/\text{Ce}_2\text{O}_3$). The natural gas taken from the grid at 70 bars (stream 2) [152], is heated up at 290°C and expanded to 2 bar via the turbo-expander (TURBOEXP). The preheating is necessary to prevent an outlet temperature (stream 4) from the turbo-expander lower than 0°C . After the expansion, the natural gas is heated to 890°C (stream 5) and fed to the reduction reactor (RED). Here the ceria oxide CeO_2 (stream 9), with an inlet ratio $\text{CeO}_2:\text{NG}=1:0.7$, is completely reduced with natural gas, producing a syngas composed by H_2 and CO in a 2:1 ratio (eq. 45). The reaction is endothermic and so requires an external heat source. The high temperature from oxyfuel combustion is usually controlled by CO_2 recycling. A part of this heat has been proposed to be used for the endothermic reduction in RED. For this scope, a heat integrated combustion was proposed utilizing an annular combustion chamber [153]. The hot syngas (stream 6) exits the reduction reactor at 900°C and it is separated from the solid (stream 7) by a cyclone (CYC-1), cooled and sent to the oxyfuel unit. The reduced ceria is fed into oxidation reactor where it is then oxidized (reactions 2 and 3) by a mixture coming from the oxyfuel unit of 60% H_2O -40% CO_2 (stream 40 and 46) to have at the outlet the ideal $\text{H}_2:\text{CO}$ (1:1) for DME production as described in section 4.2.1. In order to achieve a full oxidation of Ce_2O_3 a 60% excess of water and carbon dioxide is required.

Before the oxidation, both water and carbon monoxide are compressed at the 2 bar chemical unit operation with a pump (PUMP-1) and a compressor (COMP-4) and heated up at 500°C . Since the reactions in the oxidation reactor are exothermic, the outlet temperature of the reactor goes to 1322°C . The hot syngas (Table 15 for the final composition) is separated from the oxidized ceria by the cyclone separator (CYC-2), cooled down (stream 10, 10a, 10b, 11) and sent to the DME unit, while the solid stream is re-circulated back for a new reduction cycle (stream 9).

4.1.3. Air separation unit (ASU)

The air separation unit consists of a cryogenic distillation unit able to 99.99% pure O_2 . The air is separated in two thermally interconnected distillation columns, HP-COL and LP-COL, which work at 5 and 1.2 bar respectively (Figure 20). The overall refrigeration is driven by the expansion from high pressure (30 bar) of the compressed air (stream 6-C and 7-C) through the VALVE-2 and the TURBOEXP.

The inlet air (1-C) is compressed at 6.3 bar by the compressor COMP-1C and separated in two streams (4-C and 8-C) by the splitter SPLIT-1C. The stream 8-C is cooled down in the exchanger HX-2C by the cold products of the LP-COL and is sent to the HP-COL. The HP-COL is a 40 stages distillation column which produces as a top product a gaseous rich-in N_2 (stream 12-C) and as a bottom product a liquid rich-in O_2 stream (stream 10-C). The latest stream is further cooled down through Joule-Thomson effect in the valve VALVE 1-C and fed in the 56 stages low-pressure column. The low-temperature air streams 15-C and 17-C, together with the rich-in O_2 liquid stream provides the necessary refrigeration in the LP-COL to obtain as a top product a pure N_2 stream (20-C) while as product from the bottom condenser the pure

4.1.4. Oxyfuel Combustion unit

In this unit, combustion is performed with oxygen instead of air. This eliminates the presence of nitrogen in the exhaust gases that affect the subsequent separation process. Another advantage is a substantial reduction in thermal NO_x since the absence of nitrogen [154]. Therefore, a highly pure stream of CO₂ can be obtained after water condensation from the flue gas.

The oxyfuel unit consists of a combustor (COMB), where the syngas from the reduction (stream 30) and the non-condensable gases from the clean-up unit (stream 49) are burnt with a 5% excess oxygen stream derived from the air separation unit (ASU) (stream 1). Stream 36 represents the part of the captured CO₂ which is re-circulated to the combustor. The recirculation ratio was set such as the total combustion heat was sufficient to have a combustor outlet syngas temperature of 1377°C and the required heat to carry on the reduction of the ceria in the reduction (RED) reactor. The CO₂ and syngas streams are compressed to 26 bars with two two-stage compressors (COMP-2 and COMP-3). The flue gas is firstly expanded in a two-stage gas turbine GT (26 bar to 5 bar and 5 bars to 1.05 bar) and then sent to heat recovery steam generator (HRSG1). Finally, the CO₂ is separated from the water in a condenser (COND-2) and split into three parts. One part is recirculated to the combustor (stream 36), one is sent for sequestration (stream 35) and the last part (stream 38) is sent to the oxidation reactor for dissociation (OXI).

4.1.5. Dimethyl ether production (DME) unit

The syngas produced in the oxidation reactor is used for DME synthesis within a catalytic reactor. Before the syngas is fed to the DME reactor, it undergoes water condensation (COND-1) and is compressed by a three-stage compressor at 50 bar (COMP-1). The DME reactor is a fixed bed reactor which is kept at the constant temperature of 250°C by a water-jacket cooler used for saturated steam generation at 2 bar (stream 44) for the oxidation (OXI) reactor.

4.1.6. DME distillation unit

Since a not pure in DME stream is generated at the outlet of the DME reactor, a separation unit is hence necessary to obtain pure dimethyl ether. The separation unit is composed of a cooling unit and a gas-liquid separation unit. A cooling unit, represented in the layout by a vapour-liquid separator is used to produce a chilled syngas at -40°C resulting in a liquid stream of DME with dissolved CO₂ and MeOH (stream 17) and a gas stream of incondensable gases, namely, H₂, CO, undissolved CO₂ and traces of other diluents (stream 47). The gas stream is re-circulated into the oxyfuel unit and burnt, while the liquid stream is further processed in the gas-liquid separation unit. The gas separation unit is composed of three different distillation columns: CO₂-CLN, DME-CLN and MEOH-CLN (Table 11). The first one is used to separate the dissolved CO₂, the second to produce a pure 99.99% DME and the last one to separate the methanol from the water. Before each column, it is placed a valve to adjust the pressure to the optimal value and a heat exchanger in order to have at the inlet a 50% vapour inlet stream [155].

The number of stages used in the distillation columns was estimated increasing them until a certain change in composition was detected [156].

Table 11: distillation unit operation parameters.

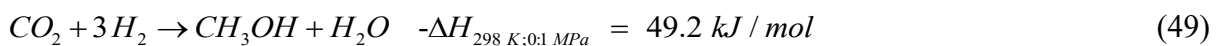
Column	T _{reb} [°C]	Q _{reb} [MW]	T _{cond} [°C]	Q _{cond} [MW]	Stages	Feed-in stage	Purity of the product [%]
CO ₂ -CLN	45.87	1.12	-40.83	-0.64	25	10	-
DME- CLN	150.99	0.93	42.57	-0.55	30	24	99.1
MeOH- CLN	101.53	0.03	66.36	-0.05	24	18	94.1

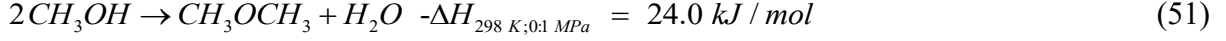
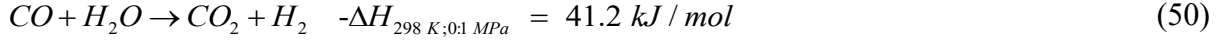
4.1.7. Steam cycle

A heat recovery steam generator unit has been utilized to recover the extra heat generated within the polygeneration system. The turbines and the HSRG were modelled as simple units, without reheating or multi-pressure systems. The primary objective of the present study being to understand the potential of the net benefits from polygeneration by the integration of a chemical looping unit in a conventional oxyfuel plant, the optimization of the system was not further considered. The presented layout is composed of two different HRSG units: HRSG1 and HRSG2. The HRSG1 uses the heat of the flue gases from the oxyfuel unit (stream 32) to produce 125582 kg/h of super-heated steam at 150 bar and 550°C (stream 5A). While the HRSG2 uses the extra heat from the chemical looping unit to produce 8305 kg/h of steam at the same condition of stream 5A (stream 5B). Each steam stream is respectively expanded in steam turbine ST1 and ST2. The reason for the choice of two HRSG connected to two different steam cycle is to ensure flexible operation by minimizing the impact of DME and power over each other.

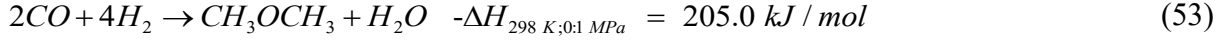
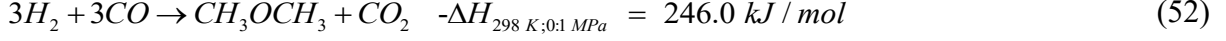
4.2. Synthesis of DME

Dimethyl ether (DME) is produced from methanol dehydration using a specific catalyst. The process can be realized in two steps (methanol and DME are produced in two different reactors) or in a single step adopting a dual catalyst. The disadvantage of the two-step process is that syngas conversion to methanol is significantly limited by equilibrium and thermodynamics constraints [157]. Consequently, the further conversion of methanol to DME in the single step process shifts the equilibrium toward more methanol production. For that reason, the direct DME synthesis is thermodynamically and economically preferable than the two steps process [158–160]. The overall process can be described by three main reactions: i) syngas conversion to methanol, ii) water gas shift and, iii) methanol dehydration.





A combination of either reaction (48), (50) and (51) or (49), (50) and (51) permits to fully describe the process thermodynamically. There are two overall reactions to synthesize the syngas to DME route, represented by equation (52) and (53):



The reaction (52) synthesizes the DME production in three steps (equation 48, 50, 51), while when WGS reaction doesn't take place, the overall DME formation is described by reaction (53) (reaction 48 plus reaction 51) [161]. Since both overall reactions are exothermic and generate two molecules of products from six molecules of reactants, according to the Le Châtelier principle, conversion is favoured working at high pressure and low temperature.

4.2.1. Kinetic Model

A kinetic model was implemented in order to simulate catalyst operation in Aspen Plus. The model well simulates the presence of the dual catalyst: Cu/ZnO/Al₂O₃ operates for the methanol synthesis while the acidic component γ -Al₂O₃ catalyse the methanol dehydration. It is reported [157] that the best loading catalyst ratio is 1:2 (Cu/ZnO/Al₂O₃: γ -Al₂O₃). Because DME synthesis is governed by catalytic reactions of syngas on the surface of the catalyst, Langmuir-Hinshelwood-Hougen-Watson (LHHW) kinetic model was used based on three simultaneous reactions (reaction 49-51). It was assumed that each CO, CO₂, H₂ and H₂O compounds are adsorbed at an active site on the catalyst surface [150]. The rate for each reaction is listed above [157,162,163]

$$r_{CO_2 \text{ hydrogenation}} = \frac{k_1 (p_{H_2} \cdot p_{CO_2}) \left[1 - \left(\frac{1}{K_{eq,1}} \right) \frac{p_{CH_3OH} \cdot p_{H_2O}}{p_{CO_2} p_{H_2}^3} \right]}{\left(1 + k_2 \frac{p_{H_2O}}{p_{H_2}} + \sqrt{k_3 \cdot p_{H_2}} + k_4 \cdot p_{H_2O} \right)^3} \quad (54)$$

$$r_{RWGS} = \frac{k_5 \cdot p_{CO_2} \left[1 - \frac{1}{K_{eq,2}} \frac{p_{CO} \cdot p_{H_2O}}{p_{CO_2} \cdot p_{H_2}} \right]}{1 + k_2 \frac{p_{H_2O}}{p_{H_2}} + \sqrt{k_3 \cdot p_{H_2}} + k_4 \cdot p_{H_2O}} \quad (55)$$

$$r_{MeOH \text{ dehydration}} = \frac{k_6 \cdot K_{CH_3OH}^2 \left[c_{CH_3OH}^2 - \left(C_{H_2O} \cdot \frac{C_{DME}}{K_{eq,3}} \right) \right]}{\left(1 + 2\sqrt{K_{CH_3OH} \cdot C_{CH_3OH}} + K_{H_2O} \cdot C_{H_2O} \right)^4} \quad (56)$$

Reaction rates (eqs. 54-56) are expressed in kmol/kg_{cat} s, p is the partial pressure of the gases in Pa and C the concentration expressed in kmol/m³. The equilibrium constant (K_i) and constant rate (k_i) values used to determine the reaction rates are shown in Table 12.

Table 12: kinetic parameters

	A	unit	B	unit
k ₁	1.07×10 ⁻¹³	(kmol/(kg-sPa ²))	36,696	(J/mol)
k ₂	3450	-	0	(J/mol)
k ₃ ^{0.5}	1.578×10 ⁻³	Pa ^{-0.5}	17,197	(J/mol)
k ₄	6.62×10 ⁻¹⁶	Pa ⁻¹	124,119	(J/mol)
k ₅	122	(kmol/(kg s Pa))	-94,765	(J/mol)
k ₆	1.486×10 ¹¹	(kmol/(kg s))	-143,666	(J/mol)
K _{CH₃OH}	5.39×10 ⁻⁴	m ³ /kmol	70,560.92	(J/mol)
K _{H₂O}	8.47×10 ⁻²	m ³ /kmol	42,151.98	(J/mol)

These parameters refer to the Arrhenius equation shown by equation (57):

$$k_i = A_i \exp\left(\frac{B_i}{RT}\right) \quad (57)$$

Where B represents either the activation energy or the reaction enthalpy or a combination of both [162]. This is because rate constant in LHHW kinetic mechanism is a combination of rate constants and equilibrium constants. Other equilibrium constant were obtained by the following equations [151,162,164]:

$$\log_{10} K_{eq,1} = \frac{3066}{T} - 10.592 \quad (58)$$

$$\log_{10}(1/K_{eq,2}) = -\frac{2073}{T} + 2.029 \quad (59)$$

$$\ln K_{eq,3} = \frac{3220}{T} - 1.7 \quad (60)$$

The described model was used to perform a sensitivity analysis of methanol and DME yield using the equations (61) and (62) varying the composition of the inlet stream, H₂:CO ratio, and the amount of the diluent H₂O and CO₂.

$$DME_{yield} = \frac{DME_{out}}{(CO + CO_2)_{in}} \quad (61)$$

$$MeOH_{yield} = \frac{MeOH_{out}}{(CO + CO_2)_{in}} \quad (62)$$

Where DME_{out} and $MeOH_{out}$ are the DME and methanol molar flow at the outlet of the reactor (stream 15) and CO and CO_2 the molar flow at the inlet (stream 14).

As shown in Figure 21 the highest DME yield is obtained sending a syngas with an $H_2:CO$ ratio equal to 1:1, this means that the overall reaction is the reaction 52. The main advantage of reaction 52 is that all the hydrogen is embedded in the DME production, while in reaction 53 one third is wasted in water production. Another positive effect of sending an equimolar $H_2:CO$ is that the main byproduct of the reaction is the CO_2 which can be easily separated from the DME and MeOH in the separation unit. With increasing the CO_2 content at the inlet feed, the DME yield decreases. This is attributed mainly due to two factors. As reported by [165], the methanol synthesis is retarded with the increase of CO_2 content. CO_2 molecules are absorbed by the methanol catalyst and occupy quicker than CO and H_2 the active sites, affecting the MeOH production and consequently also the DME synthesis as shown in Figure 22.a [166]. Moreover, with a high CO_2 the beneficial effect of the WGS is neglected. The water formed in reaction (49) and (51) is removed by WGS producing hydrogen which kinetically advances the methanol production. Therefore, the higher CO_2 favours the reverse-water gas shift that reduces the hydrogen content and produces more water. The effect of higher water content at the inlet is even worse than CO_2 and it can be seen in Figure 22.b. The high water percentage shifts towards the reactants the methanol dehydration, increasing the MeOH yield and reducing at the same time the DME yield. With a water percentage higher than 0.2, also methanol production is penalized. In addition, it is important to reduce the water content, since it tends to deposit near the catalyst enhancing the catalyst degradation [161]. Therefore, to increase the DME production it is necessary to have at the inlet of the DME reactor a syngas composed by an equimolar H_2 -CO mixture, reduce the CO_2 percentage (molar fraction) in the 0-5% range and remove as much as possible the water content.

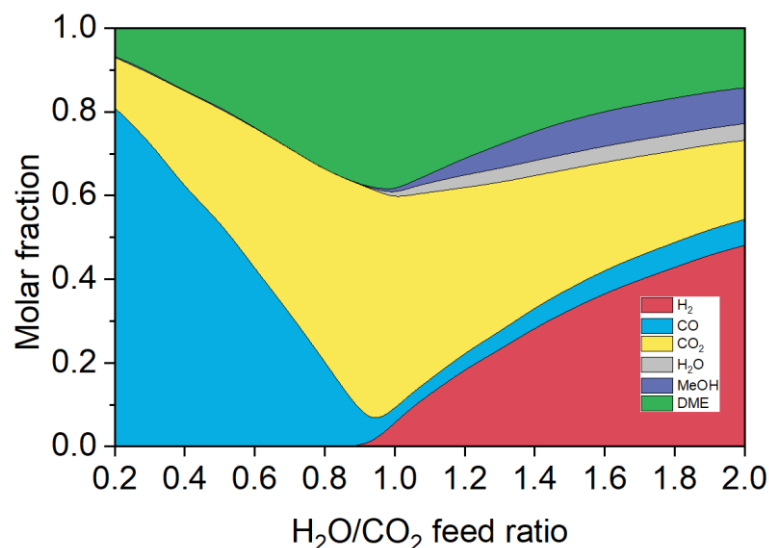


Figure 21: influence of the H_2/CO ratio on the equilibrium synthesis of DME at $T=250^\circ C$ and $p=50$ bar

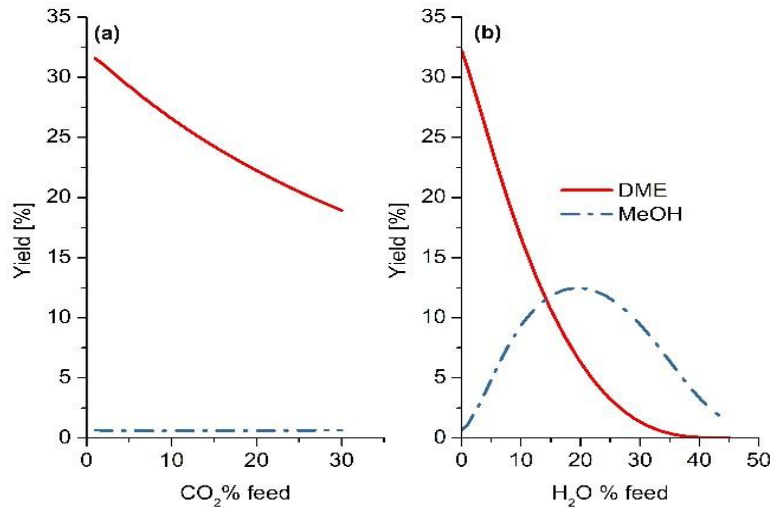


Figure 22: a) influence of the CO₂ on the equilibrium synthesis of DME at T=250°C and p=50 bar, b) influence of the H₂O on the equilibrium synthesis of DME at T=250°C and p=50 bar.

4.2.1. Reactor design

The DME reactor was designed as a multitube fixed bed reactor. Each tube contains the double catalyst with a bed voidage of 0.45. The total density of the catalyst particles is an average of the density of the two catalysts, Cu/ZnO/Al₂O₃ and γ -Al₂O₃, used in the 1:2 optimal ratio.

Table 13: fixed parameters for DME reactor design

N° tubes	Diameter [m]	Bed voidage	ρ Cu/ZnO/Al ₂ O ₃ [kg/m ³]	ρ γ -Al ₂ O ₃ [kg/m ³]	ρ average [kg/m ³]
5000	0.02	0.45	1200	1470	1380

The number of tubes and their diameter was fixed while the length was varied in order to maximize the DME yield. As shown in Figure 23 the maximum yield can be achieved with a reactor length of minimum 10 m, for this reason this value was selected in the design phase.

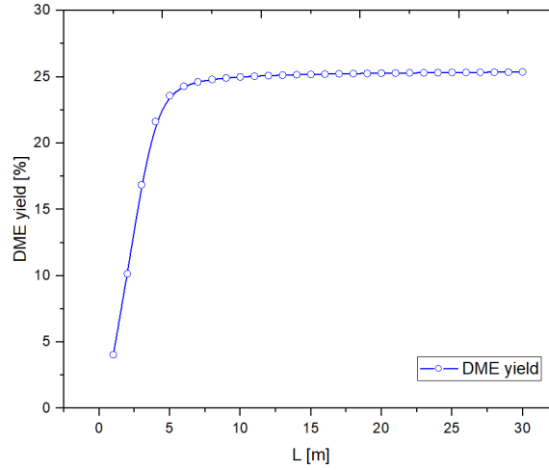


Figure 23: DME yield from DME reactor varying reactor length (L)

4.3. Performance results

4.3.1. Effect of operating conditions

A sensitivity analysis of the most influencing parameters (such as operating pressure of chemical looping CO₂/H₂O splitting unit, outlet temperature of reduction reactor, CO₂/H₂O composition in the oxidation reactor of the CL unit, turbine inlet temperature) was performed to maximize the global efficiency of the plant (Eq. 63) and the DME production.

$$\eta = \frac{\dot{m}_{DME} \cdot LHV_{DME} + \dot{m}_{MeOH} \cdot LHV_{MeOH} + W_{NET}}{\dot{m}_{NG} \cdot LHV_{NG}} \quad (63)$$

where: \dot{m}_{DME} , \dot{m}_{MeOH} represent the DME and MeOH produced (kg/s), LHV_{DME} and LHV_{MeOH} the lower heat value of DME, MeOH and natural gas (MJ/kg), W_{NET} the net power produced inside the plant (MW) and \dot{m}_{NG} the natural gas feed into the plant (kg/s)

Figure 24 shows the effect of varying the pressure of the chemical looping unit where both oxidation and reduction reactor works at the same pressure. An efficiency gain is obtained by increasing the pressure operation of the CL unit, from 49.35% at 1 bar to 51.11% at 5 bar. This can be attributed to the fact that a significant saving of the auxiliary power compression ($W_{COMP,tot}$) can be obtained by reducing the pressure ratio of syngas compression. However, with a further increment of the pressure, the efficiency drops down to 43.56%. Based on the Le Châtelier principle, it can be understood that the reaction in the RED reactor is not thermodynamically favoured at high pressure since the reduction reaction has three moles of reactants and four of products. In fact, as can be seen in Figure 24, after 6 bar the amount of reduced ceria at the outlet of the reactor decreases. This results in a drop in power production and overall efficiency.

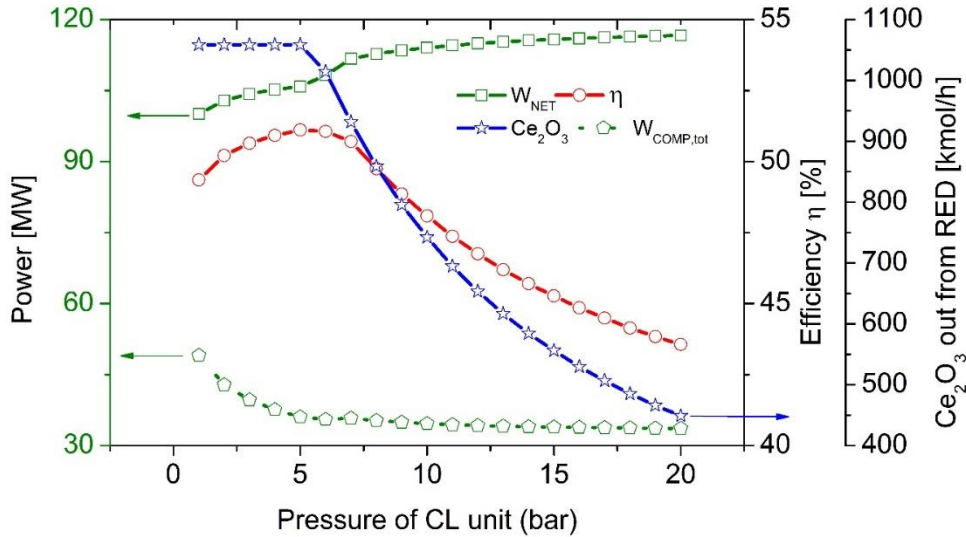


Figure 24: influence of chemical looping unit pressure on efficiency η , W_{NET} , Ce_2O_3 outlet from RED and $W_{COMP,tot}$ ($=W_{COMP-1}+ W_{COMP-2}+ W_{COMP-3}$).

Another fundamental parameter is the metal oxide outlet temperature from the reduction reactor. It is found that below $900^\circ C$ there is no complete metal oxide conversion. Since the analysis was performed considering the complete reduction of ceria, all the analysis was conducted above a reduction temperature of $900^\circ C$. A higher metal oxide temperature at the outlet of the reactor, inherently demands more heat supply. Since this heat is derived from the heat of combustion, to have more reduced metal oxide temperature, less CO_2 needs to be recirculated. This, even though results in a corresponding drop in the power spent for recycling CO_2 (W_{COMP-3}), also implies a lower mass flow through GT producing less power as shown in Figure 25. This is nevertheless partially counterbalanced by the increase in the power produced by the ST due to the higher temperature of the GT outlet. However, since the gas turbine generates more power than the steam turbine (about 2.5 times), the net power decreases.

Nevertheless, this also restricts the effective operation of the OXI. Since both the splitting reactions are exothermic, by principle this requires the reactions to take place at lower temperature. More so, for the water splitting reaction which shows a higher exothermicity than CO_2 with Ce_2O_3 , this would result in an even slower reaction. The effect of this is evident in Figure 25, in which a significant drop in the DME production can be seen beyond $1000^\circ C$ (from 2.14 kg/s for $900^\circ C$ to 2.13 kg/s at $1000^\circ C$ and to 1.99 at $1100^\circ C$) due to a deviation from the ideal H_2-CO ratio and an increase in CO_2 in the produced syngas (Figure 26).

Being a polygeneration power plant, the production of DME plays a key role in the overall plant effectiveness as well as significantly its efficiency. This is observed in Figure 25, where the higher drop in the DME production than the corresponding drop in the GT power output influences a sharp drop in the efficiency. To be more specific a relative 10.5% of efficiency drop is observed between $1000^\circ C$ and $1300^\circ C$, corresponding to a relative drop in DME production of 24% and a relative net power output drop of 2%.

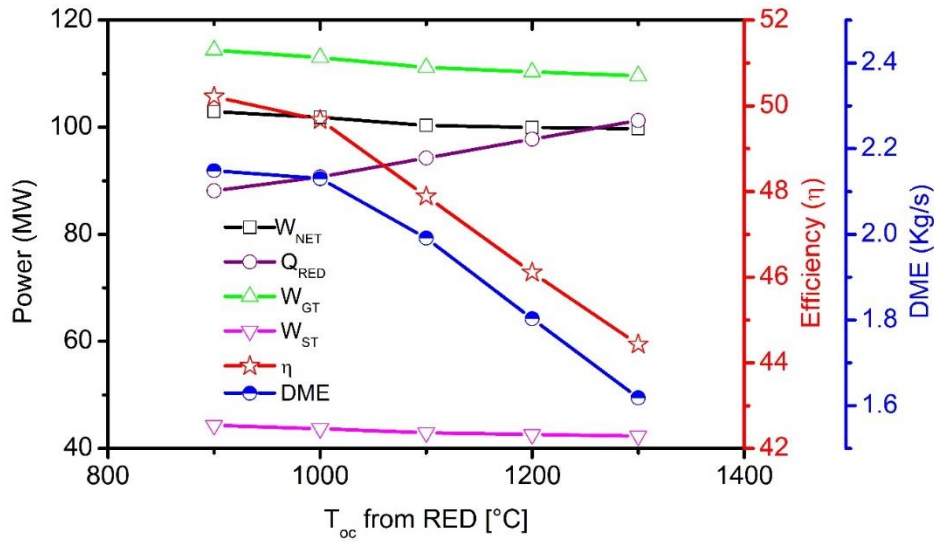


Figure 25: influence of the outlet temperature of RED on efficiency (η), net power (W_{NET}), gas turbine power (W_{GT}), heat need from RED (Q_{RED})

Figure 26.a-b shown the effect of the metal oxide inlet temperature to the OXI. As explained above, due to a higher exothermicity of the water splitting reaction, to have the ideal 1:1 CO-H₂ ratio for DME production a higher H₂O fraction in gas mixture inlet into the OXI is necessary. The amount of H₂O needed in the gas mixture inlet ranges from 60% to 74% with a metal oxide temperature inlet from 900°C to 1300°C to achieve the H₂-CO ratio of 1. In addition, as already explained in section 4.2, in order to enhance the DME production purity of H₂ and CO in the syngas from the OXI is to be maintained at a certain level. As shown in Figure 26.b, even if it might be possible to produce the ideal composition of syngas from the OXI, at higher metal oxide temperatures the CO₂ content increases. This is due to the fact that in order to have the complete splitting reaction, more gas mixture excess is needed, since as discussed, the exothermic reaction like CO₂-H₂O dissociation are penalized at higher temperatures. For this reason, it is suitable to work with low ceria inlet temperature (900-1000°C).

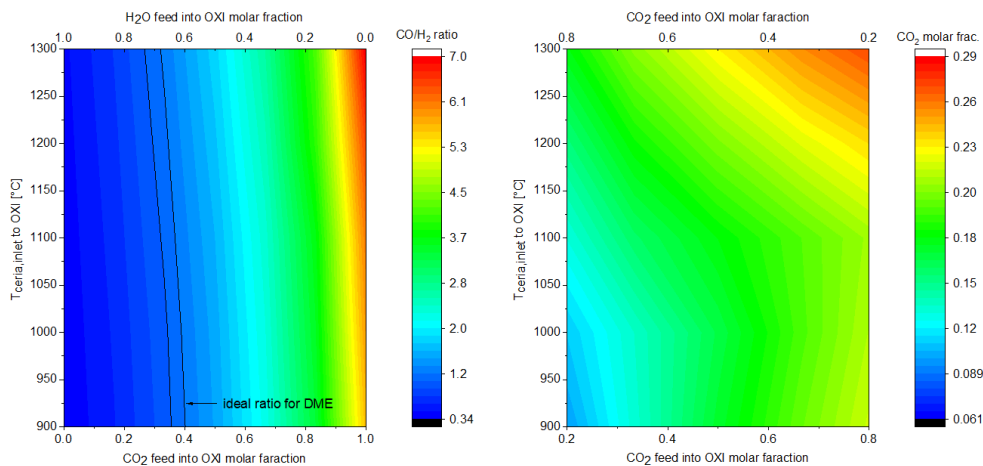


Figure 26: effect of the initial gas mixture composition fed into OXI on a) final syngas CO/H₂ ratio, b) CO₂ content in the syngas after water removal

Figure 27 describes the effect of the variation on the gas mixture composition at the inlet of the OXI on plant performance. The maximum efficiency of 50.2% is achieved with an OXI inlet mixture of 60% of H₂O, following the above discussion.

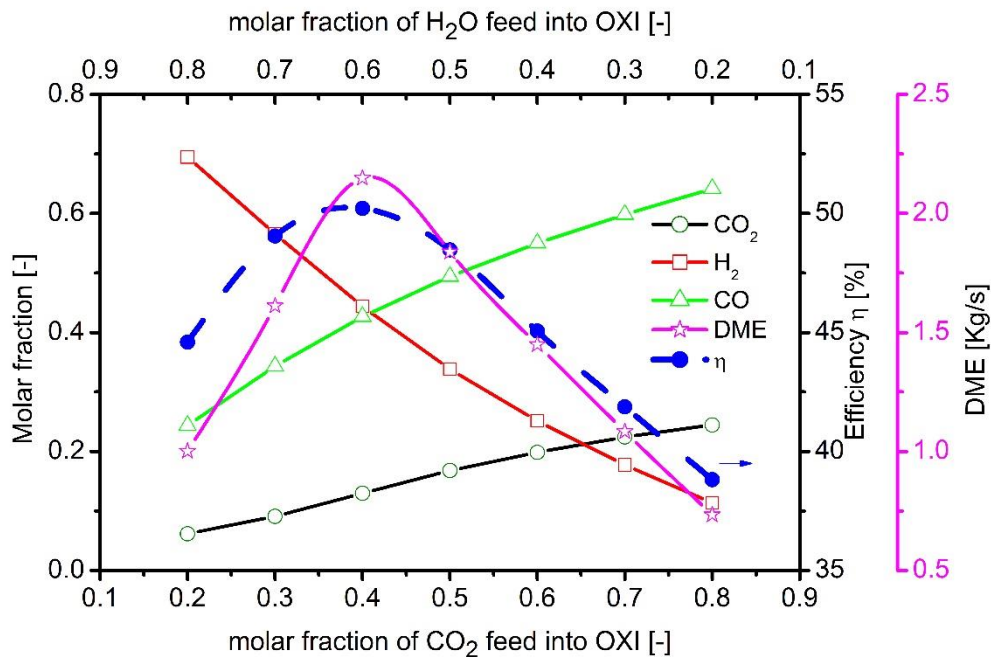


Figure 27: influence of the as mixture composition into the inlet of OXI on the plant performance b considering a metal outlet temperature from the RED equal to 900°C.

Following the above discussions, increasing the water content of the gas mixture feed into OXI, increases the temperature of the outlet metal oxide from the oxidation reactor (Figure 28.a). In the proposed OXYF-CL-PFG plant layout, the oxidized ceria is recirculated back to RED without intermediate heat recuperation. Hence, a higher ceria outlet temperature from OXI results in a higher metal oxide inlet temperature into the RED. This reduces the heat requirement for the reduction reaction. This, in term, increases the CO₂ recirculation into the GT and hence, the power output from the same. Thus, an increment in the net power production is achieved (Figure 28.d). However, in order to have a higher temperature, the inlet mixture to OXI has to diverge from the ideal to obtain the 1:1 ratio of CO-H₂. The drop in DME production due to the non-optimal syngas composition leads to an overall efficiency decrement (Figure 28.b-c). Furthermore, as can be seen from Figure 28.d working with the ideal gas mixture for DME production, the net power is reduced. As described in 4.2.1, to an inlet syngas to the DME reactor which diverges from the 1:1 H₂-CO ratio, correspond unreacted hydrogen and carbon monoxide. Since after distillation the unreacted species are recirculated in the combustor, more power is generated.

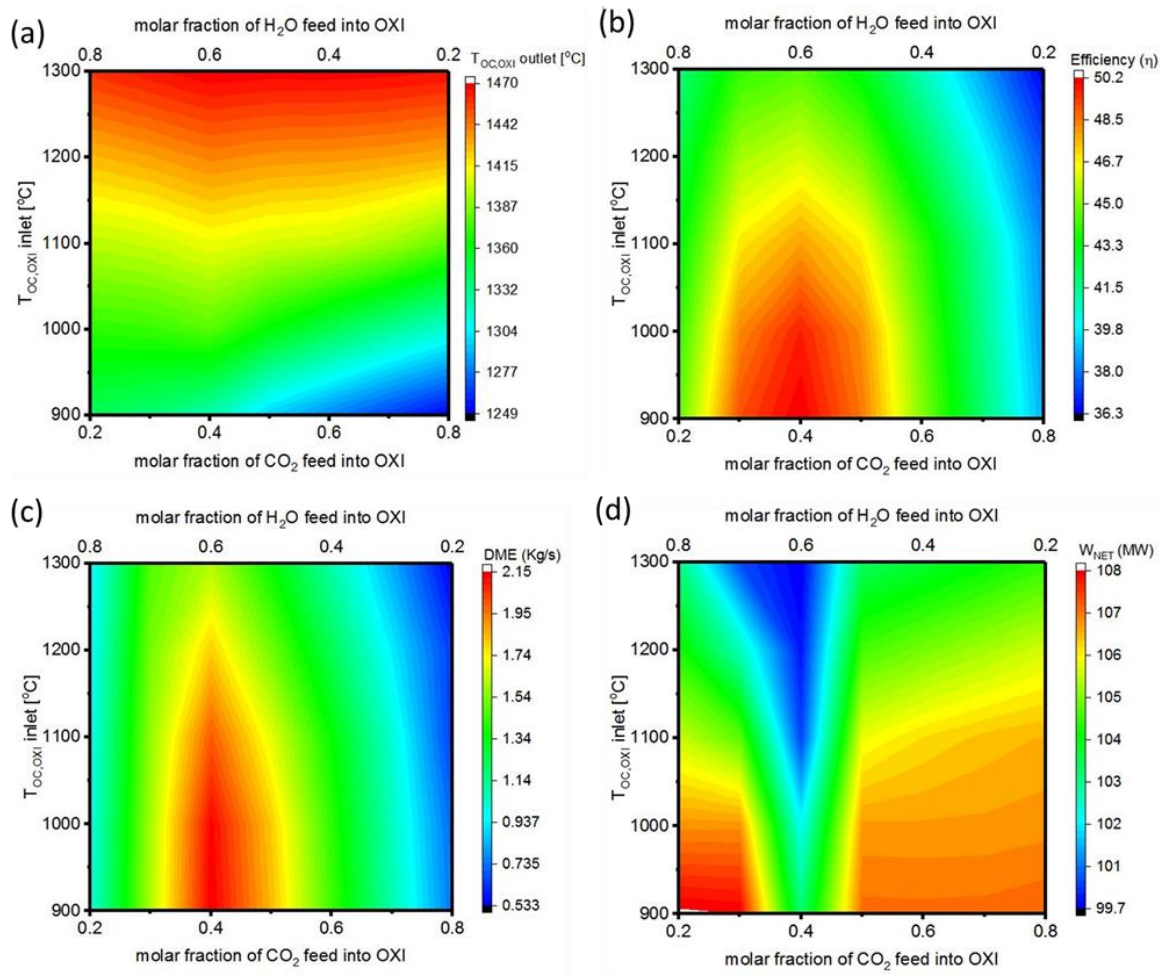


Figure 28: effect of the gas mixture inlet composition and metal oxide inlet temperature ($T_{OC,OXI}$ inlet) on the temperature of the metal oxide outlet

Finally, the impact of the gas turbine inlet temperature (TIT) was analysed. Efficiency and net power produced are positively influenced by TIT (Figure 29). Nevertheless, the output from the GT drops. This is due to the lower recirculation of CO_2 inside the combustor and so a lower gas volume being expanded within the GT. This loss is partially recovered by the lower compression work for the recirculated CO_2 in COMP-2. Also, the produced by the steam turbine ST_1 increases due to a higher exhaust temperature from the GT. Hence, corresponding to a TIT of $1100^\circ C$ and efficiency of 47.6% was obtained, which increases to 50.7% for a TIT of $1450^\circ C$.

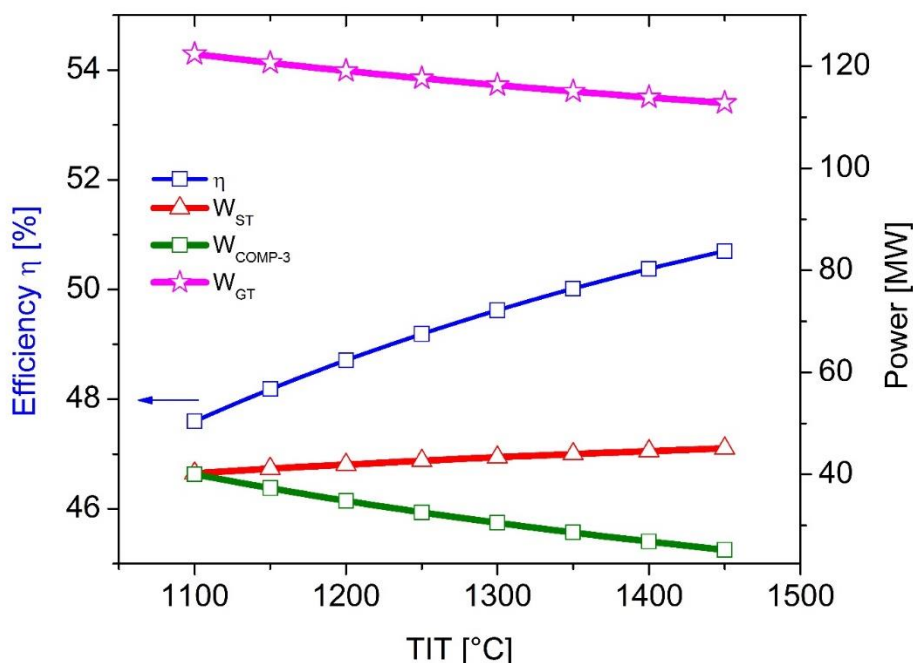


Figure 29: effect of the gas turbine inlet temperature TIT on the efficiency of the plant (η), power produced by the steam turbine (W_{ST}), by the gas turbine GT (W_{GT}) and the power absorbed by the COMP-3 (W_{COMP-3})

Based on the sensitivity analysis the following operating parameters were chosen:

- chemical looping pressure operation equal to 2 bar;
- 40% CO₂ and 60% H₂O feed in the oxidation reactor with an excess of 60% with respect to the stoichiometric value based on the Ce₂O₃ inlet to OXI;
- reduction reactor temperature outlet equal to 900°C;
- TIT of 1377°C.

The plant performance based on the listed parameters are summarized in Table 14. Table 15 gives the composition and main thermodynamics parameters of selected streams. The plant produces 102.90 MWe, 2.15 kg/s of DME and 0.03 kg/s of methanol with a total efficiency of 50.21%. The highest power consumption is represented by the COMP-3 for the recycle of the CO₂ followed by the compression work in the ASU, which account, respectively, for the 17% and 11.5% of the gross power generated.

The inlet stream to the DME reactor (stream 14) has the ideal CO:H₂ ratio, while the CO₂ content is 13%. However, it can be seen in Figure 26.b, that minimum CO₂ percentage which can be achieved from the oxidation reactor is near 6%, even though not producing the equimolar mixture of CO:H₂. So the actual plant configuration allows producing a syngas with a composition which diverges from the ideal one. A solution might be to propose two distinct oxidation reactors, one for the CO₂ dissociation and one for the water dissociation. However, this might lead to two different oxidized metal temperatures, complicating the system design and operations.

An encouraging result is that the proposed Oxyfuel-NGCC cycle with the chemical looping and DME units permits to cut the efficiency penalty of the carbon capture. In particular, compared with results from literature [41], it is possible to achieve a gain of 4 percentage points with respect to a stand-alone Oxyfuel-NGCC process¹.

The total CO₂ produced and captured is equal to 3.34 million tons per year out of which 3.4% is embedded in the DME (CO_{2,DME}). The recirculation streams of CO₂ (CO_{2,REC}) in the combustor accounts for the 85% of the mole per second of CO₂ while the one sent into OXI for dissociation is 7%.

Table 14: Plant results

NG feed	25.2 ton/h
W _{GROSS}	167.61 MW
W _{NET}	102.90 MW
η _{TOT}	50.21%
W _{COMP-1}	3.76 MW
W _{COMP-2}	10.67 MW
W _{COMP-3}	28.29 MW
W _{ASU}	19.34 MW
W _{GT}	114.42 MW
W _{ST1}	44.30 MW
W _{ST2}	2.96 MW
W _{TURBEXP}	4.37 MW
ṁ _{DME}	2.15 kg/s
ṁ _{MeOH}	0.03 kg/s
CO _{2,REC}	0.85
CO _{2,DME}	0.034

¹ considering 0.09 kWh/Nm³ energy requirement for CO₂ compression [183].

Table 15: thermodynamics properties and composition of selected streams.

stream	28	10	15	16	17	20	31	37	38	43	47	7	9
T (°C)	900	1322	200	250	46	40	1377	80	40	40	46	900	1322
P (bar)	2	2	5	5	1	9	26	2		1	10	2	2
Mole flow (kmol/h)	1	0.47	0.34	0.15	0.05	0.04	3.7	2.44	0.19	0.28	0.09	0.59	0.29
Molar fraction													
O ₂	0	0	0	0	0	0	0	0	0	0	0	0	0
H ₂	0.57	0.32	0.44	0.06	0	0	0	0	0	0	0.01	0	0
H ₂ O	0	0.28	0	0.01	0.03	0	0.22	0	0	0.99	0	0	0
CO ₂	0	0.09	0.13	0.57	0	0	0.77	0.99	0.99	0	0.93	0	0
CO	0.3	0.31	0.43	0.05	0	0	0	0.01	0	0	0.03	0	0
CH ₄	0.12	0	0	0	0	0	0	0	0	0	0	0	0
MeOH	0	0	0	0.01	0.02	0	0	0	0	0	0	0	0
DME	0	0	0	0.3	0.94	1	0	0	0	0	0.02	0	0
CeO ₂	0	0	0	0	0	0	0	0	0	0	0	1	0
Ce ₂ O ₃	0	0	0	0	0	0	0	0	0	0	0	0	1

4.3.2. Heat integration in the plant

A pinch analysis was adopted to assess the heat integration within the proposed plant and hence, strategies to increase the overall efficiency.

As can be seen from Figure 30 three distinct regions can be identified:

- a high-temperature zone for the preheating of the natural gas by the hot syngas from the reduction reactor;
- the intermediate temperature zone which comprises the steam generation from saturated water between 343°C to 550°C and the preheating of the gas mixture to the OXI;
- the low-temperature zone which comprises the heating of the water in the economizer and the other preheating for the operation of the plant;

The last part of the hot utilities corresponds to the distillation of DME.

As can be observed a good heat integration among hot and cold utilities has been achieved as per the current model. Therefore, the scope for a further increment in the efficiency of the power plant through optimized heat integration is limited.

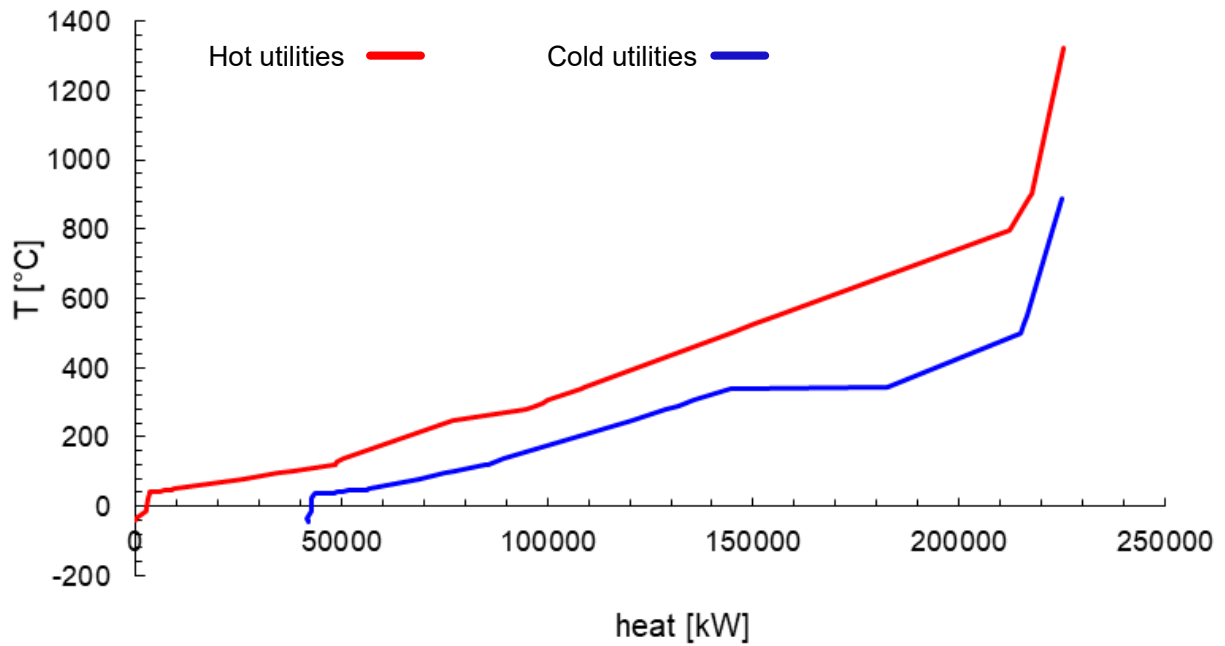


Figure 30: pinch point analysis, hot and cold composite curve

4.4. Exergy analysis

An exergy analysis was performed following the methodology described in section 3.2. Since in the proposed layout there are several chemical reactions, which change the composition of the gaseous streams, the first step was to evaluate the reference chemical exergy of the multiple mixture streams using the dead state of the reference elements (eq. 18). The results are shown in Table 16.

Table 16: specific chemical exergy of the gas mixture streams

Stream	31	28	10	15	13	47
$e_{ch,i}$ [kJ/kg]	388.68	27,109.72	7,391.26	11,287.08	11,919.06	6,225.07

A similar sensitivity analysis to the one previously reported has been performed to assess the exergetic performance of the plant (eq. 64) and the irreversibilities generated during the process (eq. 65). As can be clearly observed, due to both electricity and heat self-sufficiency of the system, the input fuel, namely natural gas contributes entirely (100% of the total exergy input)

to the net exergy input to the system. The product instead is the total DME, MeOH and the net power produced by the plant.

$$\eta_{ex} = \frac{\dot{m}_{DME} \cdot E_{DME} + \dot{m}_{MEOH} \cdot E_{MEOH} + W_{NET}}{\dot{m}_{CH_4} \cdot E_{NG}} \quad (64)$$

$$I_{tot, dest} = \dot{m}_{CH_4} \cdot E_{NG} - \dot{m}_{DME} \cdot E_{DME} - \dot{m}_{MEOH} \cdot E_{MEOH} - W_{NET} \quad (65)$$

As expected, since the efficiency is related to only natural gas, DME, MeOH and net power production, the exergy efficiency trend is reflective of the thermodynamics efficiency previously described. For this reasons, the same explanation of the plot in section 4.3.1 can be adopted for the following Figure 31 and Figure 32.

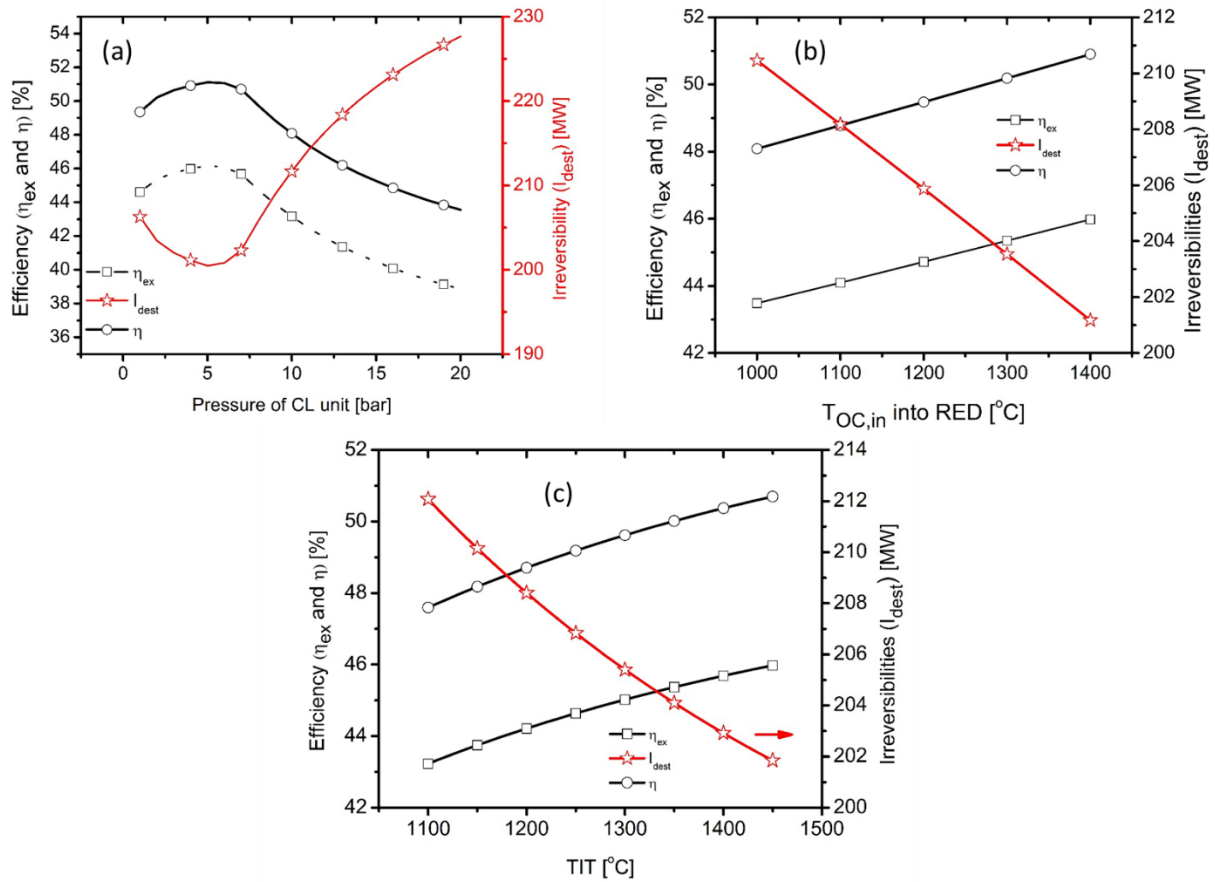


Figure 31: exergetic efficiency and total irreversibilities generated varying a) the operating pressure of the CL unit, b) the temperature of the inlet metal into the reduction reactor ($T_{MET,in}$) c) the temperature inlet into the gas turbine (TIT)

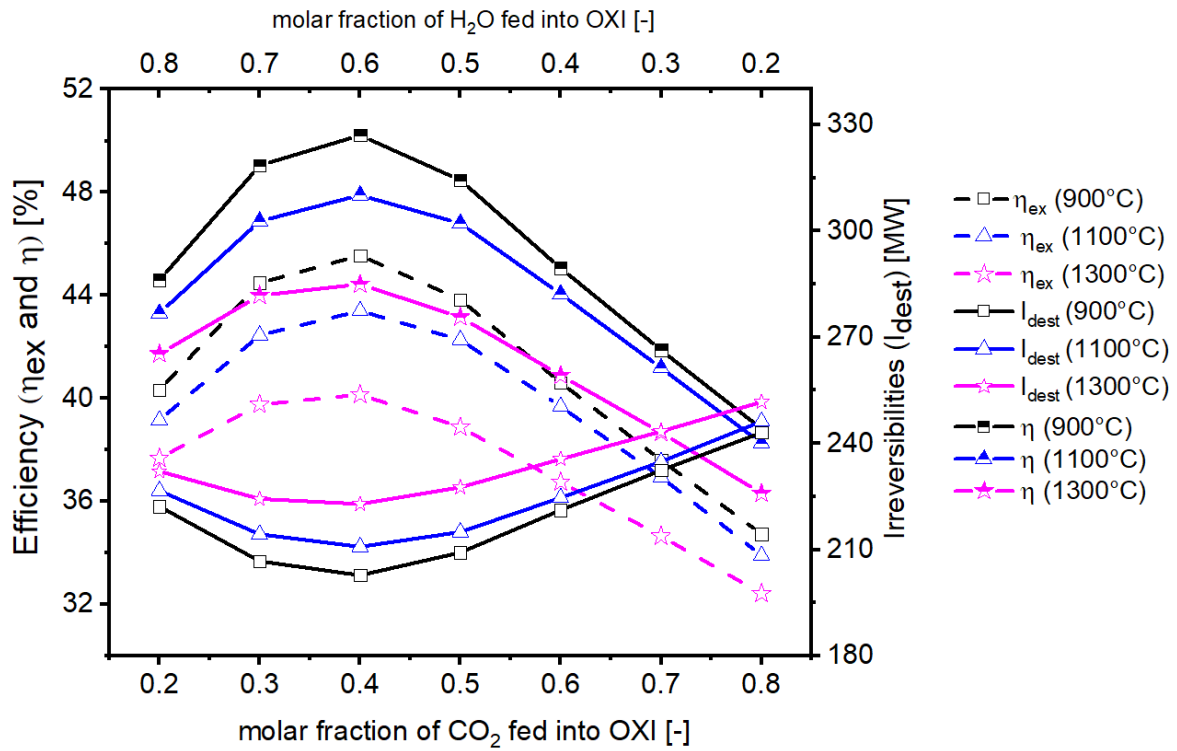


Figure 32: effect of the gas mixture composition feed into the OXI on the exergetic efficiency η_{ex} and irreversibilities I_{dest}

Finally, a detailed exergy analysis of the main components of the layout operating at the conditions described in section 4.3.1 was performed. Table 17 reports the exergy values of the main streams.

Table 17: chemical, physical and total exergy of the plant's streams.

State	Specific Physical Exergy [kJ/kg]	Specific Chemical Exergy [kJ/kg]	Specific Exergy [kJ/kg]	Exergy Flow [MW]	State	Specific Physical Exergy [kJ/kg]	Specific Chemical Exergy [kJ/kg]	Specific Exergy [kJ/kg]	Exergy Flow [MW]
0	-	-	-	-	31	1.375,23	387,84	1.763,06	246,88
1	247,15	119,91	367,05	7,98	32	515,30	387,84	903,14	126,47
1a	14,72	24,86	39,58	2,83	33	37,04	387,84	424,87	59,50
2	584,21	53.201,75	53.785,96	376,50	34	49,60	436,43	486,04	57,23
3	806,40	53.201,75	54.008,14	378,06	35	49,60	436,43	486,04	4,84
4	97,86	53.201,75	53.299,61	373,10	36	40,96	436,43	477,40	47,78
5	1.851,99	53.201,75	55.053,73	385,38	37	218,95	436,43	655,38	69,78
6	1.542,39	27.109,67	28.652,06	335,37	38	49,60	436,43	486,04	4,02
7	718,95	1.172,02	1.890,97	182,52	39	94,68	436,43	531,11	4,39
9	599,54	195,24	794,78	80,45	40	294,88	436,43	731,31	6,04
10	1.772,70	7.416,35	9.189,05	79,42	41	3,18	48,33	51,52	0,76
10a	1.063,98	7.416,35	8.480,33	73,29	42	3,18	48,33	51,52	0,50
10b	546,08	7.416,35	7.962,43	68,81	43	3,18	48,33	51,52	0,12
11	313,68	7.416,35	7.730,03	66,81	44	3,11	48,33	51,44	0,12
12	3,21	48,33	51,54	0,12	45	497,88	48,33	546,21	1,27
13	90,35	11.914,03	12.004,38	74,87	46	1.022,64	48,33	1.070,97	2,48
14	579,24	11.914,03	12.493,27	77,92	47	621,44	6.044,21	6.665,65	0,75
15	291,85	11.273,25	11.565,10	72,13	48	607,94	6.044,21	6.652,15	0,75
16	198,40	11.273,25	11.471,65	71,55	49	505,90	6.044,21	6.550,11	0,74
17	171,76	11.246,12	11.417,87	69,93	1-A	19,82	48,33	68,15	2,36
18	164,88	11.246,12	11.411,00	69,89	2-A	19,45	48,33	67,78	2,35
19	127,61	11.246,12	11.373,73	69,66	3-A	630,56	48,33	678,89	23,51
20	133,68	436,43	570,11	2,23	4-A	1.161,85	48,33	1.210,18	41,90
21	81,93	30.292,33	30.374,25	67,05	5-A	1.552,72	48,33	1.601,06	55,43
22	95,62	30.292,33	30.387,95	67,08	6-A	109,18	48,33	157,51	5,45
23	109,35	30.750,00	30.859,35	66,67	7-A	2,06	48,33	50,40	1,74
24	100,82	9.216,04	9.316,86	0,44	1-B	19,82	48,33	68,15	0,16
25	66,65	9.216,04	9.282,69	0,44	2-B	20,74	48,33	69,07	0,16
26	4.638,21	21.603,97	26.242,18	0,53	3-B	630,56	48,33	678,89	1,57
27	43,82	48,33	92,15	0,00	4-B	1.161,85	48,33	1.210,18	2,80
28	357,80	27.109,67	27.467,47	321,51	5-B	1.552,72	48,33	1.601,06	3,71
28b	189,96	27.109,67	27.299,62	319,54	6-B	109,18	48,33	157,51	0,36
29	145,98	27.109,67	27.255,65	319,03	7-B	2,06	48,33	50,40	0,12
30	868,38	27.109,67	27.978,05	327,48					

The global exergy efficiency of the plant is 45.03%, five points lower than the calculated thermal efficiency. The total irreversibilities generated are 202.72 MW with an overall fuel depletion rate (θ) of 53.84%.

All the components present an exergetic efficiency of over 80%, with the exception of the air separation unit (55.9%) and the two condensers for the steam cycle (32%). However, the

contribution of COND-A, COND-B and ASU to the overall efficiency is marginal since their relative irreversibilities χ_i don't exceed the 3.9%

Table 18).

The exergy efficiency of the RED+COMB results in 88.07%. Although this value is not extremely low, more than half of the 202.72 MW total irreversibilities are located in this component. As shown in

Table 18, the COMB+RED exergetic factor ψ results in 231.29%, so the irreversibilities are not due to the efficiency but are mainly proportionally correlated to the high exergy of the inlet streams. In fact, the exergy inlet of the COMB+RED ranks first among the components (870 MW), the second is the turbo-expander inlet (378 MW). Moreover, it is worth mentioning that, thanks to the hypothesis of no heat losses inside the combustor and reduction reactor, the main contributor to the exergy losses are of chemical form. In fact, the exergy efficiency of the COMB+RED, considering only the chemical exergy of the inlet and outlet streams, results in 70%.

The oxidation reactor is the second-ranked component for the relative irreversibilities parameter (14.43%) even if the exergy efficiency (83.44%) results in to be lower than the one of the RED+COMB. This is due to the lower exergy factor (50.74%).

The other irreversibilities are mostly located in the HRSG1 (13.99 MW) and in the compression process (9.34 MW). The DME reactor jacketing for saturated steam production allows increasing the exergy efficiency of the component of 2.2%.

Table 18: results from the exergetic analysis of the main components

Componet	Exergy balance eq. ¹	I _{rr} [MW]	$\eta_{ex,i}$ [%]	θ_i [%]	ψ_i [%]	ξ_i [%]
ASU	$E_0 + W_{ASU} = E_1 + E_{1b} + I_{ASU}$	85.3	55.91	2.26	5.14	5.03
TURBOEXP	$E_3 = W_{TURBOEXP} + I_{TURBOEXP}$	0.59	99.84	0.16	100.41	0.35
RED + COMB	$E_{9a} + E_5 + E_{30} + E_1 + E_{49} + E_{37} =$ $E_{31} + E_{28} + E_7 + I_{RED+COMB}$	103.83	88.08	27.58	231.29	61.23
OXI	$E_7 + E_{46} + E_{40} = E_{10} + E_{9b} + I_{OXI}$	29.47	84.57	7.83	50.74	17.38
HRSG2	$E_{10} + E_{2-B} = E_{10a} + E_{5-B} + I_{HRSG-2}$	3.68	97.49	0.98	38.88	2.17
ST2	$E_{5-B} = E_{6-B} + W_{ST2} + I_{ST2}$	0.38	89.77	0.10	0.99	0.22
COND-B	$E_{6-B} = E_{7-B} + I_{COND-B}$	0.25	32.00	0.07	0.10	0.15

COMP-4	$E_{38} + W_{COMP-4} = E_{39} + I_{COMP-4}$	0.08	98.262	0.021	1.186	0.046
COMP-3	$E_{49} + W_{COMP-3} = E_{37} + I_{COMP-3}$	6.29	91.73	1.67	20.21	3.71
COMP-2	$E_{29} + W_{COMP-2} = E_{30} + I_{COMP-2}$	2.21	99.33	0.59	87.57	1.30
GT	$E_{31} = W_{GT} + E_{32} + I_{GT}$	6.00	97.57	1.59	65.57	3.54
HRSG1	$E_{32} + E_{2-A} = E_{33} + E_{5-A} + I_{HRSG-1}$	12.88	90.00	3.42	34.21	7.60
ST	$E_{5-A} = E_{6-A} + W_{ST} + I_{ST}$	5.68	89.75	1.51	14.72	3.35
COND-2	$E_{33} = E_{34} + E_{41} + I_{COND-2}$	0.88	98.51	0.23	15.80	0.52
COND-A	$E_{6-A} = E_{7-A} + I_{COND-A}$	3.71	32.00	0.99	1.45	2.19
COMP-1	$E_{13} + W_{COMP-1} = E_{14} + I_{COMP-1}$	0.71	99.10	0.19	20.88	0.42
DME Reactor	$E_{14} + E_{44} = E_{15} + E_{45} + I_{DME reactor}$	4.64	94.05	1.23	20.73	2.74
VLS	$E_{15} = E_{47} + E_{17} + I_{VLS}$	1.45	97.99	0.39	19.16	0.86
CLN-CO2	$E_{19} + Q_{COND,CLN-CO2}^* + Q_{REB,CLN-CO2}^* = E_{20} + E_{21} + I_{CLN-CO2}$	0.60	99.15	0.16	18.56	0.35
CLN-DME	$E_{22} + Q_{CON,CLN-DME}^* + Q_{REB,CLN-DME}^* = E_{22} + E_{23} + I_{REB-DME}$	0.30	99.56	0.08	17.90	0.18
CLN-MeOH	$E_{25} + Q_{CON,CLN-MeO}^* + Q_{REB,CLN-MeOH}^* = E_{22} + E_{23} + I_{REB-MeOH}$	0.15	77.39	0.04	0.18	0.09
NG _{PHX1}	$E_2 + E_{28} = E_3 + E_{28b} + I_{NGPHX1}$	0.41	99.94	0.11	185.39	0.24
NG _{PHX2}	$E_4 + E_{28b} = E_5 + E_{29} + I_{NGPHX2}$	1.59	99.78	0.42	188.17	0.94
CO2 _{PHX}	$E_{10a} + E_{39} = E_{10b} + E_{40} + I_{CO2PHX}$	0.38	99.48	0.10	19.34	0.23
H ₂ O _{PHX}	$E_{10b} + E_{45} = E_{11} + E_{46} + I_{H2OPHX}$	3.26	95.63	0.87	19.80	1.92

¹ The left-side of the equation represents the fuel of the component, while the right-side represent the product and the irreversibilities of the component,

² Q^* represents the exergy obtainable using the heat of the selected stream

$$Q_{COND,CLN-CO2}^* = Q_{COND,CLN-CO2} \times \left(1 - \frac{T_{COND,CLN-CO2}}{T_0}\right), \quad Q_{REB,CLN-CO2}^* = Q_{REB,CLN-CO2} \times \left(1 - \frac{T_0}{T_{REB,CLN-CO2}}\right)$$

$$Q_{COND,CLN-DME}^* = Q_{COND,CLN-DME} \times \left(1 - \frac{T_0}{T_{COND,CLN-DME}}\right), \quad Q_{REB,CLN-DME}^* = Q_{REB,CLN-DME} \times \left(1 - \frac{T_0}{T_{REB,CLN-DME}}\right)$$

$$Q_{COND,CLN-MeOH}^* = Q_{COND,CLN-MeOH} \times \left(1 - \frac{T_0}{T_{COND,CLN-MeOH}}\right),$$

$$Q_{REB,CLN-MeOH}^* = Q_{REB,CLN-MeOH} \times \left(1 - \frac{T_0}{T_{REB,CLN-MeOH}}\right)$$

4.5. Economic analysis

An economic assessment was performed using the guideline and assumptions described in section 3.3. The equipment cost of the main components is reported in Table 19. The total overnight cost of the plant resulted in 537.45 M\$.

Table 19: equipment cost

Equipment	Scaling Parameter A	Cost Year	$C_{equ,0}$ [M\$]	$C_{equ,actual}$ [M\$]
GT [152]	GT Net Power [MW]	2008	\$60.99	\$25.70
HRSG, ducting and stack [167]	ST Net Power [MW]	2003	\$6.10	\$4.55
ST and ST2, generator and auxiliaries [152]	ST Gross Power [MW]	2008	\$41.60	\$15.82
Cooling Water System and Balance of Plant [152]	Q rejected [MW]	2008	\$61.23	\$24.84
COMP-3 [152]	Compressor Power [MW]	2008	\$9.95	\$16.77
COMP-2 [168]	Compressor Power [MW]	2003	\$4.83	\$5.02
COMP-1 [168]	Compressor Power [MW]	2003	\$4.83	\$2.50
ASU [169]	Oxygen Production [ktO ₂ /day]	2008	\$62.96	\$117.65
CLC and Oxy Reactor [170]	Sized According to CLC Plant, 150MW	2016	\$48.72	\$14.55
TURBEXP [171]	MW Power Produced	2008	\$0.73	\$1.32

DME reactor and BOP [168]	Inlet gas [kmol/s]	2007	\$21.00	\$5.16
DME cooling system [168]	Electrical power [MW]	2007	\$1.70	\$0.73
Clean-Up unit [168]	inlet DME [kg/s]	2007	\$28.40	\$13.33
HRSG2, ducting and stack [167]	ST Net Power [MW]	2003	\$6.10	\$13.23
COMP-4 [152]	Compressor Power [MW]	2008	\$9.95	\$0.74
Exchangers [168]	Heat exchanged [MWth]	2007	\$52.00	\$1.32

The cost of the cooling tower system was included in the cost of the four condensers (COND-1, COND-2, HRSG1 and HRSG2 condenser). The overall cost was subdivided between the four components proportionally to the calculated rejected heat. The cost of the two condensers (COND-A and COND-B) of the two HRSG were included in the HRSG investment cost. The most expensive equipment is the ASU, followed by the GT. The RED+COMB unit accounts for 5.2% of the total expenditure. The individual contribution of the respective equipment to the total overnight cost is shown in Figure 33.

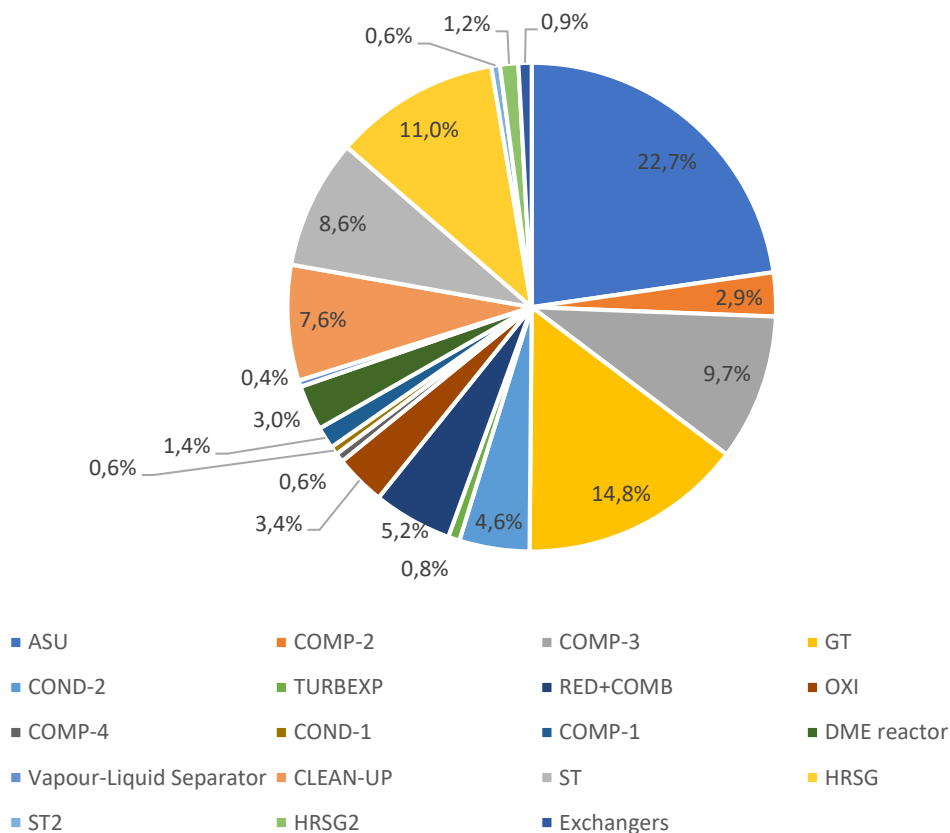


Figure 33: contribution of the components to the TOC

4.5.1. Discounted Cash Flow analysis

To evaluate the profitability of the plant during its lifetime a discounted cash flow analysis was adopted using the assumptions reported in section 3.3.1.

A sensitivity analysis was performed to evaluate the effect of the selling price of power and DME on the economic performance of the plant. The results are shown in Figure 34.a-b.

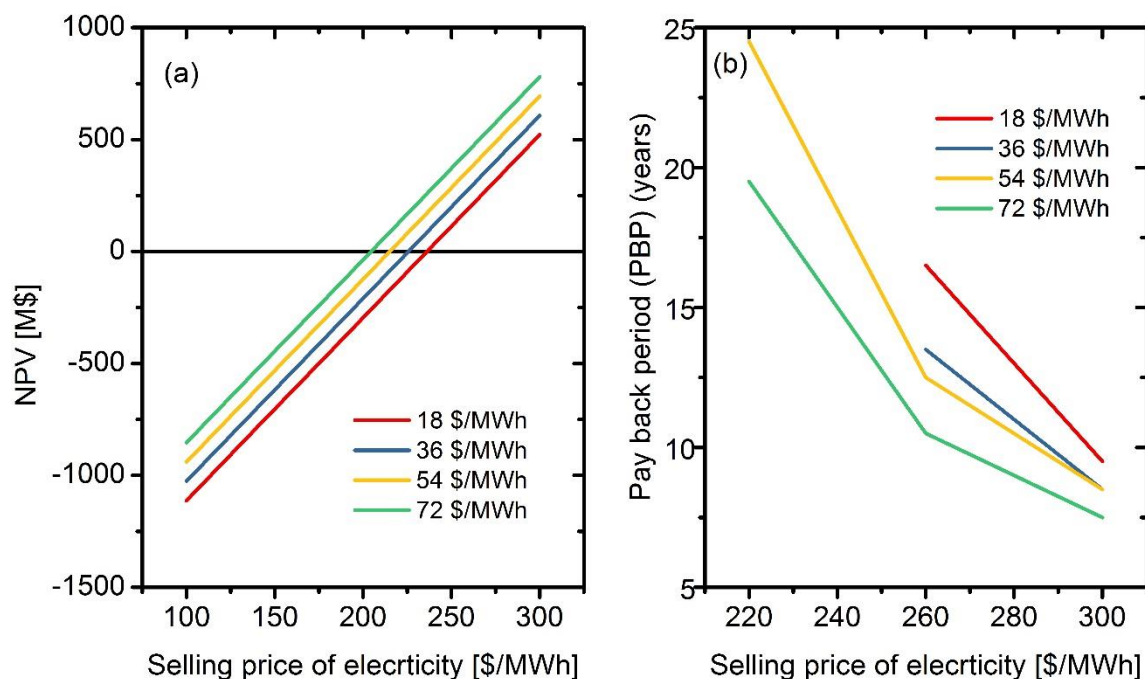


Figure 34: (a) Economic performance varying DME and electricity price. (b) Payback period (PBP) varying DME and electricity price

A positive NVP corresponds to a high selling cost of the products. The breakeven point was obtained for an electricity and DME price of at least 190 \$/MWh and 72 \$/MWh respectively (Figure 34.a), which are higher than the current market price [172,173]. Moreover, a payback period of 20 years was obtained with a selling price of DME and electricity equal to 72 \$/MWh and 220 \$/MWh (Figure 34.b). However, a more lenient carbon credits and a further development of technologies such as Oxyfuel combustion, air separation and chemical looping will make the proposed polygeneration plant more competitive. More specifically, with the adoption of the ion transport membrane technology for oxygen separation for a particular of the plant the cost would be 31% less compared to the ASU would decrease the cost of DME and power production by tremendously [174].

4.5.2. Exergo-economic analysis

An exergo-economic analysis was performed to understand which components are the main contributors to the high costs. The analysis was performed considering 64 streams (49 physical streams and 15 energy streams) and 23 components. Hence, 41 auxiliary equations were formulated (Table 20). The operational cost of the process water was attributed to the four condensers proportionally to the heat rejected.

Table 20: productive structure of the plant and auxiliary equations

COMPONENT	FUEL	PRODUCTS	WASTE	AUX.EQS
ASU	$0+W_{ASU}$	$1+1_b$	-	$P_1: E_1 = E_1^*$ $P_1: E_{ASU} = E_{ASU}^*$ $P_3: k_{1b}^* = k_1^*$
COMP-2	$29+W_{COMP-2}$	30	-	$P_1: E_{WCOMP1} = E_{WCOMP1}^*$
COMP-3	$36+W_{COMP-3}$	37	-	$P_1: E_{WCOMP2} = E_{WCOMP2}^*$
GT	31-32	W_{GT}	-	$P_3: k_{31}^* = k_{32}^*$
COND-2	33	$35+36+38+43$	42	$P_2: k_{42}^* = 0$ $P_4: k_{35}^* = k_{36}^*$ $P_4: k_{36}^* = k_{38}^*$ $P_4: k_{38}^* = k_{43}^*$
HX-1	28b-29	3-2	-	$P_1: E_2 = E_2^*$ $P_3: k_{28}^* = k_{29}^*$
TURBOEXP	3-4	$W_{TURBEXP}$	-	$P_3: k_3^* = k_4^*$
HX-2	28-28b	5-4	-	$P_3: k_{28}^* = k_{28b}^*$
RED+COMB	$9+5+30+1+37+49$	$7+28+31$	-	$P_4: k_7^* = k_{28}^*$ $P_4: k_{28}^* = k_{31}^*$
OXY	$7+46+40$	$10+9$	-	$P_4: k_{10}^* = k_9^*$
LIQPUMP1	$43+W_{PUMP-1}$	44	-	$P_1: E_{WPUMP1} = E_{WPUMP1}^*$
HX-12	10a-10b	46-45	-	$P_3: k_{10a}^* = k_{10b}^*$
CO2COMP	$38+W_{COMP-4}$	39	-	$P_1: E_{WCOMP4} = E_{WCOMP4}^*$
HX-10	10b-11	40-39	-	$P_3: k_{10b}^* = k_{11}^*$
COND-1	11	13	12	$P_2: k_{12}^* = 0$
COMP-1	$13+W_{COMP-1}$	14	-	$P_1: E_{WCOMP1} = E_{WCOMP1}^*$
DME Reactor	$14+44$	$15+45$	-	$P_4: k_{15}^* = k_{45}^*$
VLS	15	$17+49$	-	$P_4: k_{17}^* = k_{49}^*$
Distillation Unit (only columns)	$16+Q_{cond,CO2-COL}$ $Q_{cond,DME-COL}$ $+Q_{reb,CO2-COL}$ $+Q_{reb,DME-COL}$ $+Q_{reb,MeOH-COL}$	$26+23+20$	27	$P_1: E_{QC1} = E_{QC1}^*$ $P_1: E_{QC2} = E_{QC2}^*$ $P_1: E_{QRB1} = E_{QRB1}^*$ $P_1: E_{QRB2} = E_{QRB2}^*$ $P_1: E_{QRB3} = E_{QRB3}^*$ $P_2: k_{27}^* = 0$ $P_4: k_{20}^* = k_{23}^*$ $P_4: k_{23}^* = k_{26}^*$
ST	5-A - 6-A	W_{ST}	-	$P_3: k_{5-A}^* = k_{6-A}^*$
HRSG1	32-33	5-A - 1-A	-	$P_1: E_{1-A} = E_{1-A}^*$ $P_3: k_{32}^* = k_{33}^*$
ST2	5-B - 6-B	W_{ST2}	-	$P_3: k_{5-B}^* = k_{6-B}^*$
HRSG2	10-10a	5-B - 1-B	-	$P_1: E_{1-B} = E_{1-B}^*$ $P_3: k_{10}^* = k_{10a}^*$
LOOP FOR CERIA			-	$k_{9a}^* = k_{9b}^*$
			-	$k_{28b}^* = k_{28c}^*$

Details about the water consumption calculation are contained in section 4.5.3.

Table 21: main results of exergo-economic analysis

COMPONENT	c_f [\$/MWh]	c_{pr} [\$/MWh]	r_k	C_d [\$/\$]	Z [\$/\$]	$Z+C_d$	f_k
ASU	0.00	163.55	0.00	0.00	0.49	0.49	1.00
COMP-2	78.16	79.37	0.02	0.05	0.06	0.11	0.57
COMP-3	35.32	49.22	0.39	0.06	0.21	0.27	0.77
GT	43.96	56.29	0.28	0.07	0.32	0.39	0.81
COND-2	43.96	56.23	0.28	0.06	0.12	0.18	0.66
HX-1	80.77	123.66	0.53	0.01	0.01	0.02	0.50
TURBEXP	32.66	50.61	0.55	0.08	0.02	0.10	0.16
HX-2	80.77	565.56	6.00	0.04	0.04	0.07	0.52
RED+COMB	60.19	80.77	0.34	1.71	0.11	1.82	0.06
OXY	80.77	102.00	0.26	0.71	0.11	0.82	0.13
HX-12	102.00	396.19	2.88	0.09	0.01	0.10	0.06
COMP-4	59.35	62.20	0.05	0.00	0.01	0.01	0.91
HX-10	102.00	149.22	0.46	0.01	0.01	0.02	0.52
COND-1	102.00	102.00	0.00	0.13	0.01	0.14	0.10
COMP-1	86.69	88.91	0.03	0.02	0.03	0.05	0.65
DME Reactor	88.86	97.49	0.10	0.11	0.06	0.18	0.37
Vapour-Liquid Separator	98.70	98.70	0.00	0.02	0.01	0.02	0.38
Distillation Unit (only columns)	97.44	114.38	0.17	0.15	0.17	0.32	0.52
ST	69.38	93.23	0.34	0.11	0.19	0.30	0.63
HRS1	43.96	121.79	1.77	0.17	0.25	0.42	0.60
ST2	196.28	236.39	0.20	0.02	0.01	0.03	0.37
HRS2	102.00	205.12	1.01	0.10	0.03	0.13	0.22

Table 21 details the main results of the exergo-economic analysis. The exergo-economic factor (f) ranged from 1 to 0.06. The highest exergo-economic factor was observed for the ASU since the power absorbed is self-produced inside the plant. The component COMB+RED represents the equipment with the highest $Z+C_D$ factor. Hence, as discussed in section 3.4, it is the equipment that has the priority to be improved. According to its exergo-economic factor f , which results in the lowest among all components, an improvement in efficiency is required. In fact, as denoted by the exergy analysis, the 51.2% of the total irreversibilities are located in the RED+COMB.

A similar consideration for the OXI can be assumed, since it has the second highest ($Z + C_D$) factor and a factor (f) equal to 0.09. The HRS1 has the fourth highest $Z+C_D$, the relative cost difference of 1.77, so the product cost of this unit is bigger than the fuel cost of about 170%.

The exergo-economic factor is equal to 0.6 so the capital cost is the main contributor. The compressors and turbines exergo-economic factor ranged from 0.37 to 0.8 which are common values in literature. Finally, the overall plant presents a relative cost of 1.5 and an exergo-economic factor of 0.37, so a general efficiency improvement is required.

4.5.3. Water consumption

The water consumption has been calculated following the procedure described in section 4.5.3 and reported in Table 22. Based on the calculation it is found that 73.3 kg/kg_{DME} of water are consumed for cooling application. It has been observed that for DME polygeneration plants with CSP the water consumption for cooling is 103 kg/kg_{DME}, 26.8 kg/kg_{DME} with PV solar and 1561 kg/kg_{DME} with biomass driven cycle [175]. Hence, the water consumption is lower than the renewable technology driven polygeneration DME plant, except PV solar.

Table 22: results of water consumption calculation

$W_{cooling}$	2834374,4 m ³ /year
$W_{process}$	24893,7 m ³ /year

5. Chemical looping unit analysis

With reference to the analysis performed with respect to the reactor system for chemical looping syngas production, many reactor systems have been proposed such as packed bed, fluidized bed and moving bed reactor concept. The analysis performed [176] with packed bed reactor is not suitable for non-catalytic heterogeneous gas-solid reaction system as the solid interact and need regeneration, which leads to a non-continuous operation plus the pressure loss in the bed which is not favourable to the process. Fluidized bed reactor has been used in the chemical looping combustion, reforming and gasification in recent times due to its huge industrial use and experience with solid handling in boilers, furnaces and combustors. Therefore, in some studies [177] it was proposed to use the fluidized bed reactor system for reduction and oxidation. Therefore, few studies reported to have used fluidized bed reactor concept of oxidation reactor but not reduction reactor as the study was conducted for solar thermochemical fuel production. However, it was reported that the huge volume of fuel would require to fluidize the reduction reactor and CO_2 and H_2O for oxidation reactor. Since the primary objective is to produce a syngas of H_2/CO ratio of close to 1 to produce DME. It is essential to have high selectivity and very minimal impurity in the product. This would limit the usage of fluidized bed reactor system for the present study. Fan et al. [178] studied and reported the relative advantages of a moving bed reactor over a fluidized bed reactor for reduction of oxygen carriers with methane reduction. Besides a more homogeneous reduction of the OCs, reactions in a moving bed reactor result closer to thermodynamic states, rather than fluidized bed reactors. In fluidized bed reactor, due to the requirement of desired flows for fluidization, this often results in a low gas or metal oxide conversion (transport reactors for smaller configurations) or would require sufficiently large reactors with a very high oxygen carrier inventory (bubbling bed reactors). Additionally, for transport reactors, the relative gas conversion is very low. This would then require downstream purification before the use of the generated product for the subsequent industrial application. However, the effectiveness of the cycle decreases thus. Alternatively, moving bed reactor system is industrially used which gives more flexibility and control of the reactants in the reactor as the solids (here metal oxide) would feed at the top section of the reactor and gas is fed from the bottom. This counter-current motion of the gas and solid reactant gives the sufficient residence time which would essentially increase the selectivity of the product. The analysis comprised a study based on theoretical thermodynamics considerations. However, from practical considerations, the analysis was further extended by adopting a kinetic model based on experimental data for both ceria redox steps.

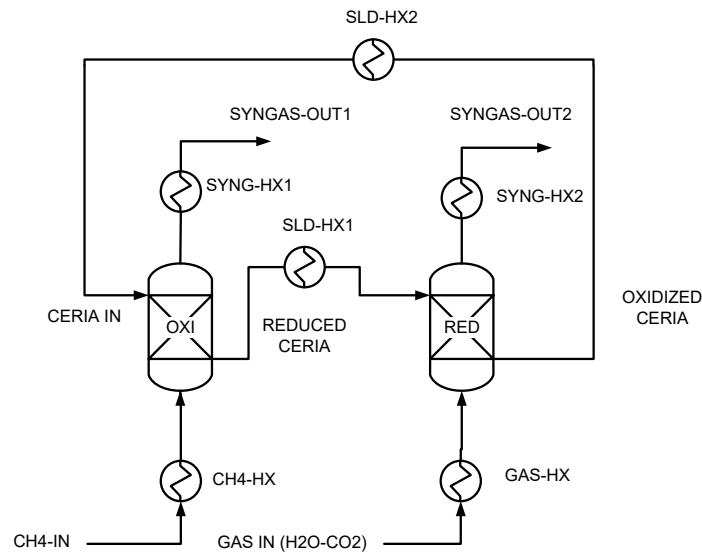


Figure 35: Schematic of Interconnected CL unit for ceria reduction with methane and subsequent oxidation with CO_2 and H_2O splitting using moving bed reactors.

The system was modelled as a series of two sets of reactors, one each for the reduction and the oxidation reactor. Each reactor set comprises of more than one reactor so as to simulate the performance of an updraft moving the bed. It was assumed that each reactor work in counter-flow operation: the gas enters from the bottom part of the reactor and came out from the upper part while the solid ceria is fed at the top and collected in the bottom. The reduction reactor was set as isothermal, while the oxidation reactor as an adiabatic one. The layout of the CL unit (Figure 35) is completed by six exchangers: CH4-HX for the methane preheating, GAS-HX for the preheating of the gas inlet to the OXI, SYNG-HX1 and SYNG-HX2 for the cooling of the syngas produced from the RED and OXI respectively, SLD-HX1 and SLD-HX2 for the cooling of the reduced and oxidized ceria respectively.

5.1. Analysis of the thermodynamic model of the CL unit

5.1.1. Reactor model design

The thermodynamic study of the chemical looping unit was performed considering the equilibrium conditions among the species involved in both reduction and oxidation. For this scope, the Aspen Plus[®] RGIBBS reactor model was adopted using the Peng Robinson equation of state. Considering all the possible reactions within the thermodynamics field that might be involved among selected species, the RGIBBS reactor evaluates the equilibrium composition. For this scope, it calculates the final products which minimize the Gibbs free energy at the operation condition of the system.

Both reactors were simulated as a series of multiple RGIBBS. In order to select the number of reactors, a sensitivity study was performed varying their numbers while checking the solid

conversion. A good conversion was found using a series of four RGIBBS for the oxidation reaction, while, being the reduction reactor set as isothermal one RGIBBS was chosen.

5.1.2. Reduction reactor results

The equilibrium of the considered species (CH_4 , H_2O , CO_2 , CO , O_2 , C , CeO_2 , Ce_2O_3) was studied varying the main operating parameters of the reduction reactor:

- CH_4/CeO_2 ratio from 0.25 to 1 (two times the stoichiometric value);
- the isothermal temperature of the reduction reactor T_{RED} from 600°C to 1100°C ;

The temperature range was fixed based on the need of studying the evolution of the thermodynamics of reduction over a wide temperature range. The analysis was performed by considering a fixed inlet of 200 mol/s metal oxide of pure CeO_2 .

Figure 36 reports the effect of both the CH_4/CeO_2 ratio and the isothermal temperature of the reduction reactor over the equilibrium of the main species. As can be seen from Figure 36.a at 600°C the reduction by methane is not favoured, since a Ce_2O_3 molar flow of only 0.75 mol/s and 2.99 mol/s with a CH_4/CeO_2 ratio equal to 0.25 and 1 respectively is achieved. As expected, by increasing the temperature of the reactor and the CH_4/CeO_2 ratio the equilibrium is shifted towards the products. However, an excess of methane would result in a higher unreacted methane at the outlet of the reactor (Figure 36.b), hence diminishing the effectiveness of the CL unit. The full conversion of CeO_2 can be achieved starting from a temperature of 850°C and a CH_4/CeO_2 ratio equal to 0.675. By further increasing the temperature till 950°C it is possible to achieve the full conversion of the ceria with a stoichiometric feed of methane (CH_4/CeO_2 ratio equal to 0.5) producing 95.83 mol/s of CO and 190.92 mol/s of H_2 .

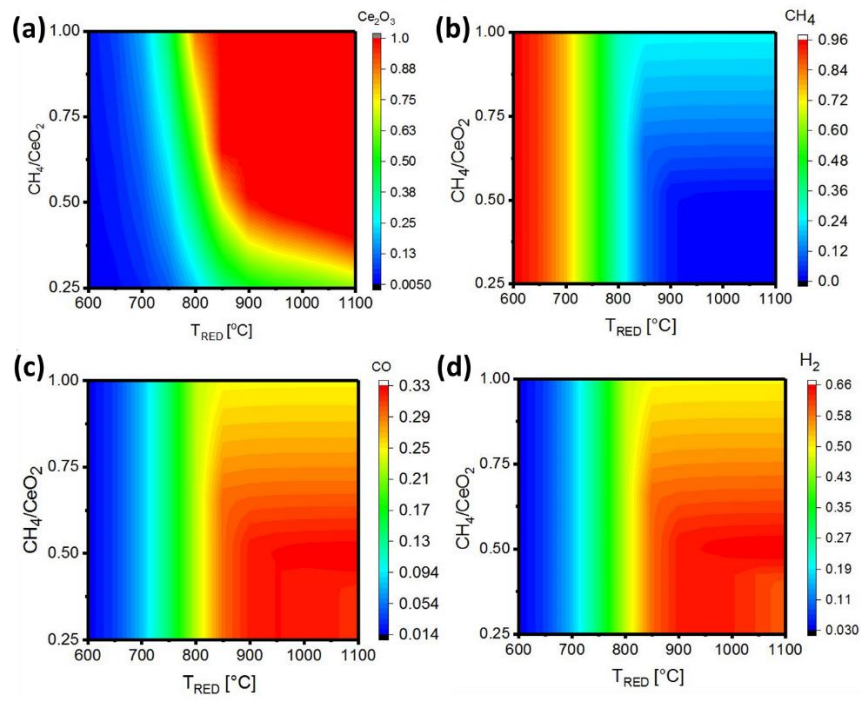
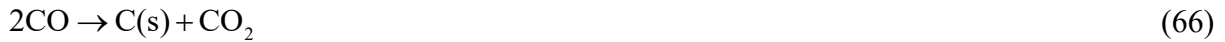


Figure 36: Effect of the CH_4/CeO_2 ratio and the isothermal temperature of the reduction reactor over the equilibrium of the main species, a) Ce_2O_3 , b) CH_4 , c) CO , d) H_2

The increment in temperature of the reactor enhances the reduction of ceria and hence the syngas production. However, as shown in Figure 37.a-c, starting from 900°C there is the formation of not desired by-product named CO₂, H₂O and C. So that, since the goal of the chemical unit is the syngas production, the formation of CO₂ and H₂O would reduce the efficiency of the system. The production of the first two by-products can be connected to the methane scarcity (CH₄/CeO₂ ratio lower than 1). The released oxygen by the metal structure of the ceria instead to react with methane, oxidizes the produced CO and H₂. In addition to the CO₂ formation, it might be related also to the water gas shift (eq. 50). However, based on the thermodynamics, the selected operating conditions are not favourable for it. At 900°C with a CH₄/CeO₂ ratio equal to 0.5 the CO₂ and H₂O production account for the 1.3% in a molar fraction of the outlet syngas, while at a higher temperature, 1100°C, the fraction rises to 8.9% with a CH₄/CeO₂ ratio equal to 0.75.

As shown in Figure 37.c, starting from a CH₄/CeO₂ ratio equal to 1.25 and at a reactor temperature of 1100°C, there is the carbon formation. This phenomenon is mainly related to the Boudouard and methane decomposition reactions (eqs. 66,67), which are favoured at high temperature.



Even though the carbon produced is low (5.3e^{-19} - 4.2e^{-18} mol/s), it would affect the system in efficiencies by recombination. For this reason, it can be strongly recommended to not work at a temperature higher than 1050°C.

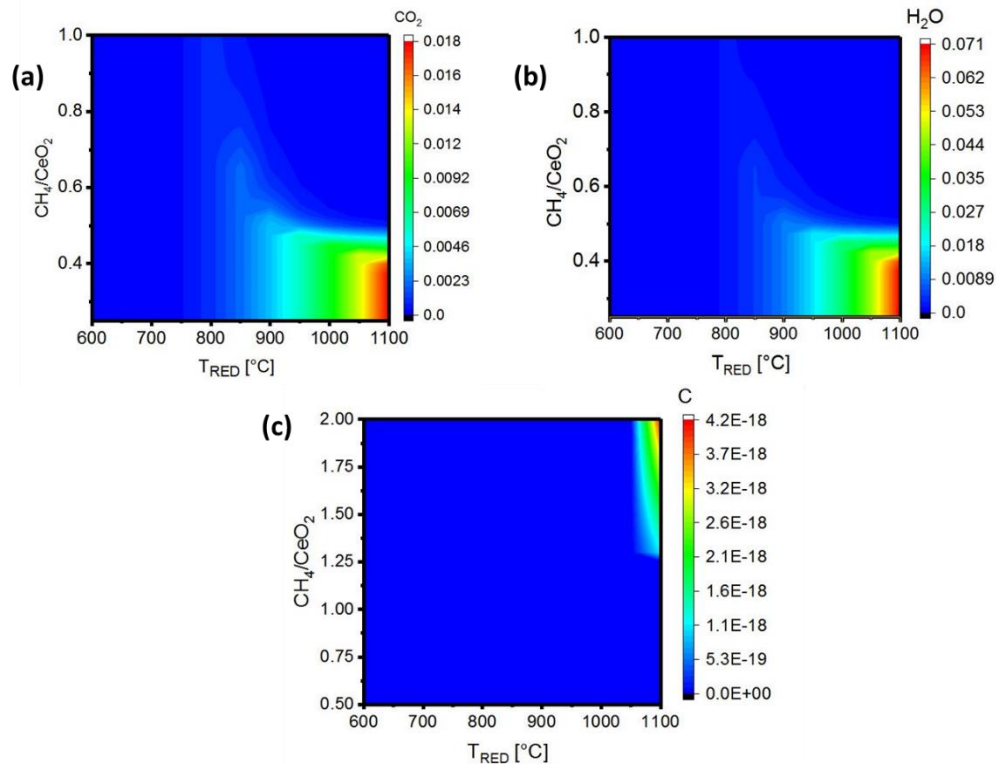


Figure 37: effect of the CH₄/CeO₂ ratio and the isothermal temperature of the reduction reactor over the equilibrium of the sub-products, a) CO₂, b) H₂O, c) C

In conclusion, the results of the model agree with the literature reported in section 2.3.2. The advantage of using methane to drive the chemical looping unit is demonstrated, since it allows to reduce the operating temperature of the reduction reaction at 850-900°C obtaining, at the same time, a good conversion of CeO₂ into Ce₂O₃.

5.1.3. Oxidation reactor results

The equilibrium analysis of CO and H₂ produced by CO₂ and H₂O dissociation over Ce₂O₃ in the reduction reactor is reported in the following. As done for the reduction reactor, the equilibrium of the listed species was analysed considering different operation parameters:

- Inlet gas mixture molar composition (80% CO₂-20% H₂O, 60% CO₂-40% H₂O, 50% CO₂-50% H₂O, 40% CO₂-60% H₂O, CO₂ 20%-80% H₂O);
- Gas-mixture/Ce₂O₃ ratio from 1 (stoichiometric value) to 2 with a step of 0.05;
- The temperature of the metal inlet from 600°C to 1000°C;
- The temperature of the gas mixture inlet from 500°C to 1000°C;

All the study was performed considering a full reduction of the 200 mol/s of CeO₂ in the reduction reactor, hence a molar flow equal to 100 mol/s of Ce₂O₃ was fixed. All the sensitivity results are related to an operating condition of 2 bar.

Figure 38.a-d shows the effect of the inlet temperature of the fed Ce₂O₃ and of an equimolar (50% H₂-50% H₂O) inlet gas mixture on the ceria oxidation reaction and the products outlet. Both the water and carbon dioxide dissociation being exothermic reactions, by increasing the temperature of the inlet streams the equilibrium of the reaction is shifted towards the reactants. In fact, as can be seen from Figure 38.a starting from a gas inlet temperature of 850°C, the complete conversion of Ce₂O₃ into CeO₂ (100 mol/s of CeO₂) is not achieved anymore. The lowest amount of CeO₂ produced, 193.87 mol/s, corresponding to a temperature of both streams equal to 1000°C. As a consequence of the unreacted water and carbon dioxide, there is the higher fraction of CO₂ and H₂O in the produced syngas (Figure 38.c-d).

Furthermore, the increment of the temperature influences the composition of the outlet syngas. Based on thermodynamics, since H₂O dissociation is more exothermic than CO₂ splitting, it is more penalized by a rise in temperature. This can be easily found in Figure 38.b-d. In fact, moving from the lowest metal oxide and gas-mixture inlet temperature ($T_{\text{metal,inlet}}=600^{\circ}\text{C}$ and $T_{\text{gas-mixture,inlet}}=500^{\circ}\text{C}$) towards the highest ($T_{\text{OC,inlet}}=1000^{\circ}\text{C}$ and $T_{\text{gas-mixture,inlet}}=1000^{\circ}\text{C}$), the CO/H₂ ratio ranges from 1.025 to 1.156. Moreover, as illustrated by Figure 38.c-d, moving towards the highest temperature conditions, the water content at the outlet of the reactor increases faster than the one of CO₂.

Figure 39 shows the effect of increasing the ratio between the gas flow and the solid inlet. As expected, by increasing the flow of the gaseous stream beyond the stoichiometric value allows reaching a full conversion. This is due to the higher partial pressure of the reactants which shifts the reaction towards the products. However, as can be clearly understood, the increment of the gaseous stream by taking constant the metal inlet flow decreases the purity of the syngas at the outlet of the reactor.

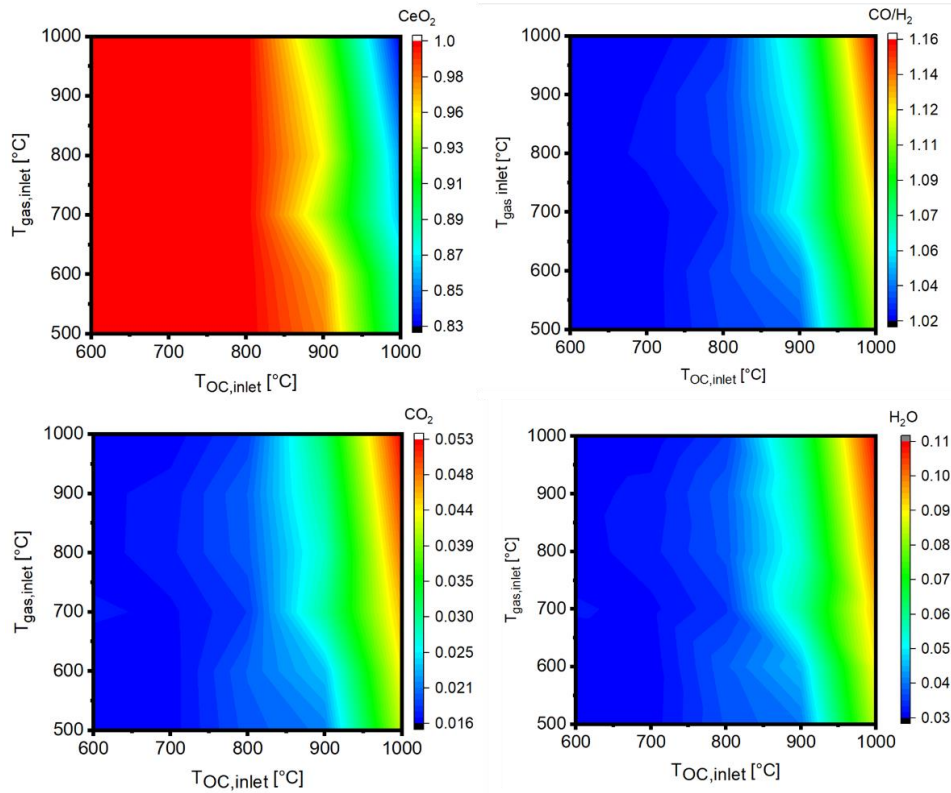


Figure 38: the effect of the inlet temperature of the fed Ce_2O_3 and of an equimolar (50% H_2 -50% H_2O , with a gas-mixture/ Ce_2O_3 ratio fixed to 1.05) inlet gas mixture on a) CeO_2 production, b) CO/H_2 ratio, c) CO_2 dilution, d) H_2O dilution

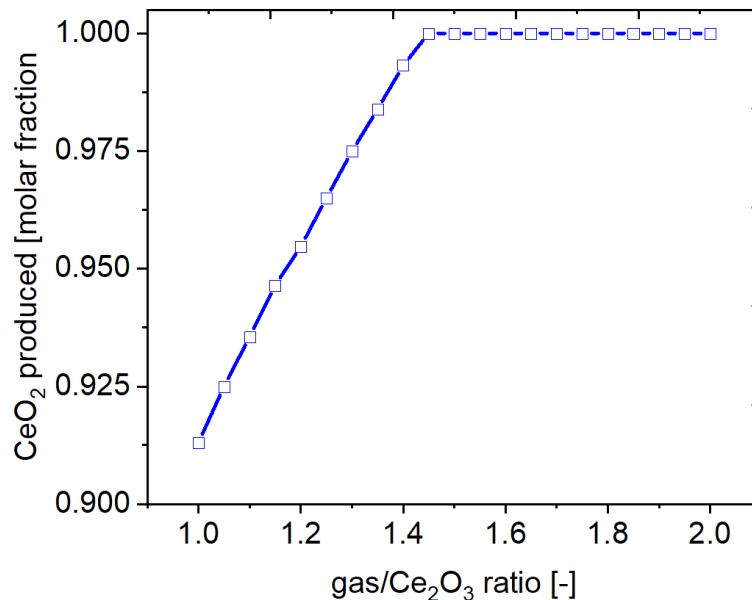


Figure 39: effect of the gas-mixture/ Ce_2O_3 ratio on the production of CeO_2 by an equimolar gas inlet with a temperature inlet of 1000°C and a metal inlet temperature of 1000°C

Finally, Figure 40.a-b illustrates the effect of the metal inlet temperature and the composition of the inlet gas mixture on the final syngas composition and the CO_2 content (after water condensation). The proposed chemical looping unit has a great flexibility. In fact, by varying the CO_2 - H_2O ratio in the gas inlet is it possible to obtain different syngas mixture composition

(CO/H₂ ratio), hence it can be integrated to different fuel/chemical production unit. However, as discussed before, increasing the temperature of the metal inlet (as well the gas inlet temperature), the dissociation reaction is penalized, which results in a higher dilution by CO₂ (Figure 40.b) (and water).

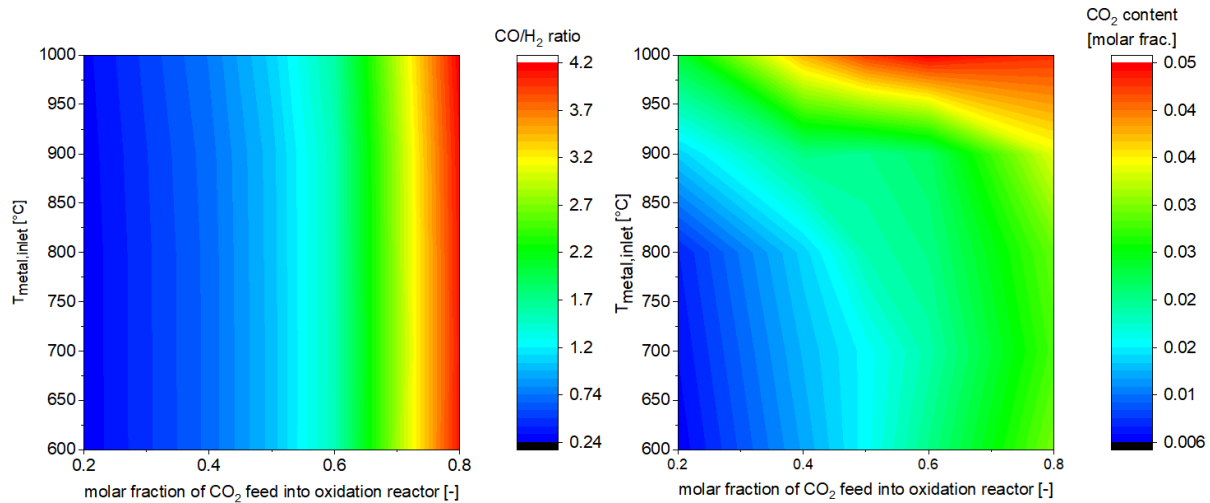


Figure 40: effect of varying the metal inlet temperature $T_{\text{metal,inlet}}$ and the composition of the inlet gas stream (the remaining part of the gas mixture is composed by water) on a) CO/H₂ ratio of the outlet syngas, b) CO₂ content after syngas dehydration (gas-mixture/Ce₂O₃ ratio equal to 1.05 and $T_{\text{gas,inlet}}$ equal to 500°C)

5.1.4. Heat Requirement results

In this section the effect of varying the operation conditions of the chemical looping unit to the heat balance of the system is reported. While the reduction reactor is endothermic, the oxidation reactor is usually exothermic. Figure 41.a-b illustrate the effects of varying the CH₄/CeO₂ ratio and the isothermal temperature of the reduction reactor (T_{RED}) on the heat need by the reactor and effect of both inlet temperature of the methane ($T_{\text{in,methane}}$) and CeO₂ ($T_{\text{in,CeO}_2}$) respectively. As can be seen in the Figure 41.a, by increasing either the temperature of the reactor or the ratio between the methane and the ceria, the heat need increases. This is due to two factors: firstly to keep a reactor at higher temperature the heat need is higher; secondly moving towards higher temperature and methane flows, as reported in section 5.1.2, the ceria reduction is enhanced. Hence, being an endothermic reaction, more heat is required. Figure 41.b describes the effect of varying the inlet temperature of the two reactants. As can be clearly understood, by increasing the temperature of the inlet feeds, the heat need is lowered.

Figure 42.a-b illustrates the effect of the metal inlet temperature, gas composition and gas-mixture/Ce₂O₃ ratio on the heat released by the oxidation reaction. As can be seen from the Figure 42.a, by increasing the water content in the inlet gaseous streams, the heat released increases. This is due to the higher exothermicity of the water splitting with respect to the carbon dioxide dissociation. With the rise of the metal temperature, it is possible to achieve more heat. However, this phenomena doesn't improve the performance of the CL unit, since a higher metal inlet temperature results from a higher metal exit temperature from the reduction reactor. This has already been reported to increase the Q_{RED} . In addition, by increasing the metal

temperature, according to section 5.1.2, the metal conversion by $\text{H}_2\text{O}-\text{CO}_2$ dissociation is decreased, hence the temperature of the outlet gas is lowered.

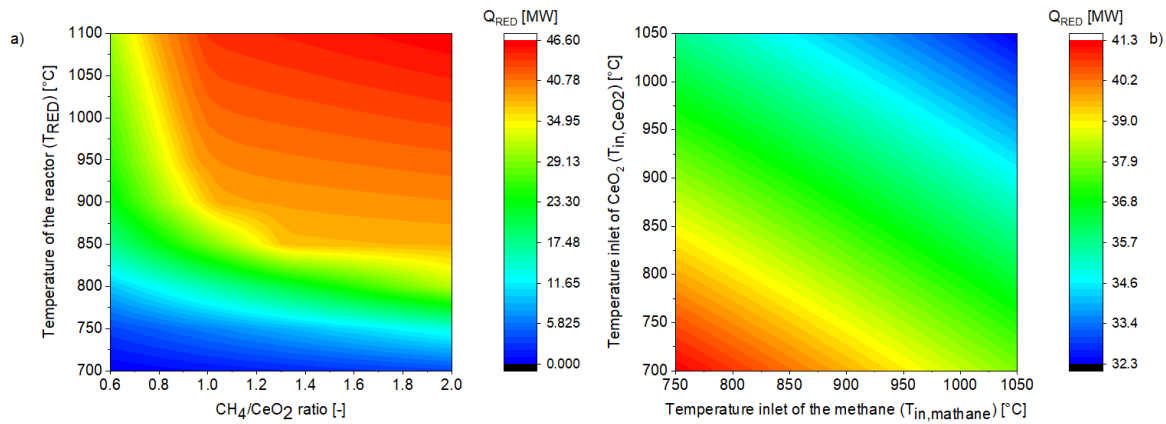


Figure 41: effect of the CH_4/CeO_2 ratio and isothermal temperature of the reduction reactor (T_{RED}) on the heat need by the reactor (Q_{RED}) (a) and effect of both inlet temperature of the methane ($T_{\text{in, methane}}$) and CeO_2 ($T_{\text{in, CeO}_2}$) on the heat need by the reactor (Q_{RED}) (b)

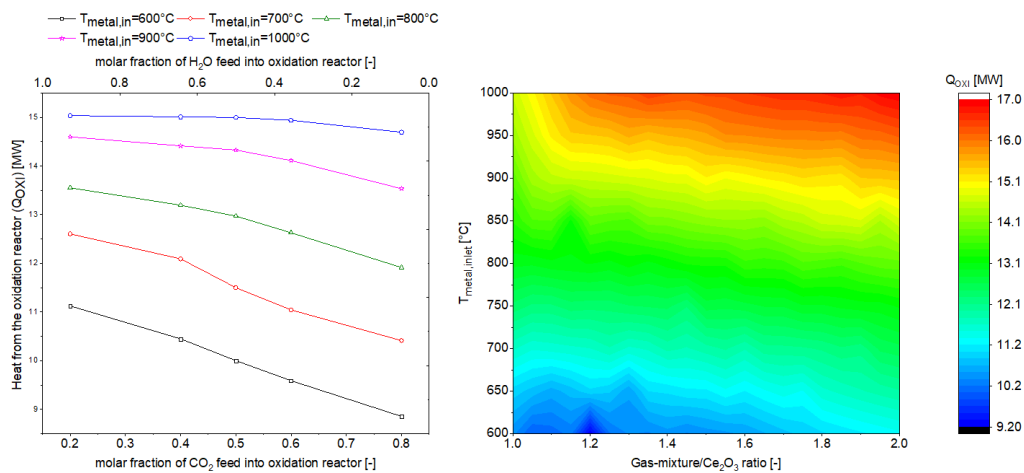


Figure 42: a) effect of the composition of the inlet gas and metal temperature inlet ($T_{\text{metal, in}}$) on the heat from oxidation reactor (Q_{OXI}), b) effect of the metal inlet temperature ($T_{\text{metal, in}}$) and Gas.mixture/ Ce_2O_3 ratio on the heat from the oxidation reactor (Q_{OXI})

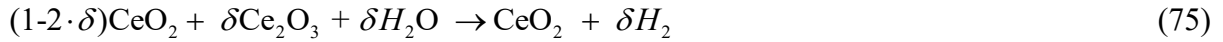
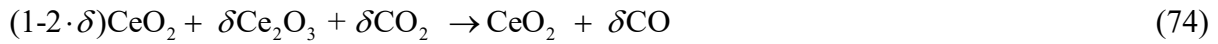
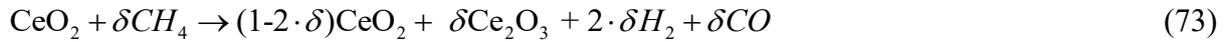
Concluding, by comparing Figure 41.a and Figure 42.b it can be seen that for whatever operating conditions, the heat released by the oxidation reaction is always not sufficient to counterbalance the heat need by the reduction reactor. For this reason, as already reported in section 2.3.1, the chemical looping unit is usually integrated with a concentrated solar plant. However, thanks to the adoption of the methane, it is possible to enhance the ceria reduction at a lower temperature, hence it is possible to use different heat source from solar, or at least it is possible to adopt a concentrated solar system that can work with lower concentration ratio.

5.2. Kinetic model of CL unit

As previously reported in section 2.3 the non-stoichiometric reaction (δ) of ceria during the methane reduction and oxidation steps follow the below equations:



However, due to limited thermodynamic data available in literature about non-stoichiometric form of ceria ($CeO_{2-\delta}$), a different approach was adopted using the fully reduced form of ceria Ce_2O_3 , which is completely investigated in literature. Consequently, the above equations were rearranged in a different form:



In this case the non-stoichiometric factor was used as indicator of the ratio between the reduced ceria (Ce_2O_3) and the maximum amount of Ce_2O_3 achievable :

$$\delta = \frac{\dot{n}_{Ce_2O_3}}{2\cdot\dot{n}_{Ce_2O_3} + \dot{n}_{CeO_2}} \quad (76)$$

Consequently, to a full reduced CeO_2 correspond a δ equal to 0.5. However, since the proposed kinetic is based on the non-stoichiometric reduction of ceria, in order to guarantee the stability of the lattice structure of the metal, a limit to the δ equal to 0.35 (δ_{max}) was selected. Hence, according to the model proposed by Bulfin et al. [179], the degree of advancement of the reduction reaction, X_{RED} , was calculated as follow:

$$X_{RED} = \frac{\delta}{\delta_{max}} \quad (77)$$

So the reduction reaction is considered fully completed ($X_{RED}=1$) when the non-stoichiometric factor reaches the δ_{max} . While the degree of advancement of the oxidation reactor (X_{OXI}), which occurs in the opposite direction of reduction, was calculated as the complementary of X_{RED} :

$$X_{OXI} = 1 - X_{RED} = 1 - \frac{\delta}{\delta_{max}} \quad (78)$$

More details about kinetic model of reduction and oxidation reactions are contained in next sections.

5.2.1. Ceria oxidation kinetic

The ceria oxidation kinetics is based on the experimental work conducted by Arifin [180,181]. He investigated the reaction mechanism of thermal reduced CeO₂ with both water and carbon monoxide. The general equation proposed for the kinetics of oxidation is based on the Arrhenius equation:

$$\frac{dX_{OXI}}{dx} = A_0 \cdot \exp\left(-\frac{E_0}{RT}\right) y_i^\gamma (1 - X_{OXI})^n \quad (79)$$

Where: R is the universal gas constant and y_i the oxidant molar fraction.

The coefficients values to be used are reported in Table 23.

Table 23: kinetic parameters of Ce₂O₃ oxidation with H₂O and CO₂ [181]

Oxidant	Temp [°C]	A ₀ [1/s]	E ₀ [kJ/mol]	γ [-]	n[-]
CO ₂	750-950	1.0	29	0.89	1.0
	650-725	4.2	47	0.53	1.0
H ₂ O	750-800	3.4	45	0.65	1.2
	825-875	2.5	41	0.7	1.7

As reported by Arifin [180], the oxidation with water behaves similarly to a homogeneous reaction. Therefore, its rate decreases proportionally to the depletion of the reactant (1-X_{OXI}). In addition, water dissociation has a lower energy of activation, which helps its kinetic.

The same analysis done for CO₂ dissociation revealed a temperature dependence of the rate of reaction. Arifin stated that as temperature increases carbon site blocking and related surface recombination stops. At 875°C the only reaction pathway is direct desorption of CO from the surface. As a consequence of these phenomena, there is a change of γ and n with the temperature (Table 23) which influences the depletion of the reactants.

Based on reaction 71 and reaction 72 in section 5.2, for each mole of Ce₂O₃ oxidized by one mole of CO₂/H₂O, correspond to the production of two moles of CeO₂ and one mole of CO/H₂. Hence, following this logic and using the time-dependent equation (79) it is possible to define the reaction rate for each species during the oxidation step:

$$k_{OXI,CeO_2} = 2 \cdot \dot{n}_{Ce_2O_3} \left\{ \frac{dX_{OXI}}{dt} \right\} \Delta t \quad (80)$$

$$k_{OXI,Ce_2O_3} = -1 \cdot \dot{n}_{Ce_2O_3} \left\{ \frac{dX_{OXI}}{dt} \right\} \Delta t \quad (81)$$

$$k_{OXI,H_2O} = -1 \cdot \dot{n}_{Ce_2O_3} \left\{ \frac{dX_{OXI}}{dt} \right\} \Delta t \quad (82)$$

$$k_{OXI,H_2} = 1 \cdot \dot{n}_{Ce_2O_3} \left\{ \frac{dX_{OXI}}{dt} \right\} \Delta t \quad (83)$$

$$k_{\text{OXI,CO}_2} = -1 \cdot \dot{n}_{\text{Ce}_2\text{O}_3} \left\{ \frac{dX_{\text{OXI}}}{dt} \right\} \Delta t \quad (84)$$

$$k_{\text{OXI,CO}} = 1 \cdot \dot{n}_{\text{Ce}_2\text{O}_3} \left\{ \frac{dX_{\text{OXI}}}{dt} \right\} \Delta t \quad (85)$$

Where Δt represent the reaction step time, calculated using the inlet volume flow (V_{OC}) of the ceria in the reactor:

$$\Delta t = \frac{\dot{V}_{\text{OC,in}}}{\Delta V_{\text{reactor}}} \quad (86)$$

5.2.2. Ceria reduction kinetic

No solid-state kinetic model exists for ceria reduction by methane. Correspondingly, a set of experiments were performed at the DENERG, Politecnico di Torino to develop the same, however, as a part of a separate thesis. The experiments were performed in a packed bed reactor with 250 mg of commercial CeO_2 (99% pure) and 120 Nml/min of gas flow, where, the fraction of methane was varied between 20 and 50%, the balance being Argon. The temperature range was selected to be between 900 to 1100°C to obtain the desired kinetics. The results from the experiments have nonetheless been used herein to perform the necessary kinetic assessment of the reduction reactor. Indeed, beyond 1100°C, considerable carbon deposition was obtained, and hence was decided as the limiting temperature to perform the desired reduction of ceria.

Following a similar approach to the previously performed oxidation reaction, the sensitivity of the ceria reduction of methane has been subsequently performed between the temperature range 900°C and 1100°C

The same approach reported in the previous section was adopted for the reduction kinetic. Hence, considering the reduction reaction (eq. 70) and the time-dependent equation for the degree of advancement of the reduction reaction, the reaction rates of the species involved are:

$$k_{\text{RED,CeO}_2} = -2 \cdot \dot{n}_{\text{CeO}_2} \left\{ \frac{dX_{\text{RED}}}{dt} \right\} \Delta t \quad (87)$$

$$k_{\text{RED,CH}_4} = \dot{n}_{\text{CeO}_2} \left\{ \frac{dX_{\text{RED}}}{dt} \right\} \Delta t \quad (88)$$

$$k_{\text{RED,CO}} = \dot{n}_{\text{CeO}_2} \left\{ \frac{dX_{\text{RED}}}{dt} \right\} \Delta t \quad (89)$$

$$k_{\text{RED,H}_2} = \dot{n}_{\text{CeO}_2} \left\{ \frac{dX_{\text{RED}}}{dt} \right\} \Delta t \quad (90)$$

5.2.3. Reactor model

Both reduction and oxidation reactors were modelled as a vertical updraft moved bed reactor. The reactors were modelled using a series of 10 built-in Aspen RCSTR blocks (Figure 43) [182] with the assumption that each RCSTR is characterized by an equal temperature in all the phases. The heat required to kept the RED reactor isothermal was calculated in a dedicated Aspen calculation block (C-HEATNEED, Figure 44). Both reduction and oxidation reaction described in section 5.2 was written in external subroutines (REDKIN.f and OXIKIN.f) using FORTRAN77 language connected to each RCSTR (Figure 44). All code files were compiled with the use of Intel Fortran Compiler contained in the Intel Cluster Studio XE 2013 SP1 package and linked with Microsoft Visual Studio 12/2013 package. Broyden method was selected for the unit mass balance convergence setting a maximum number of iteration equal to 1000.

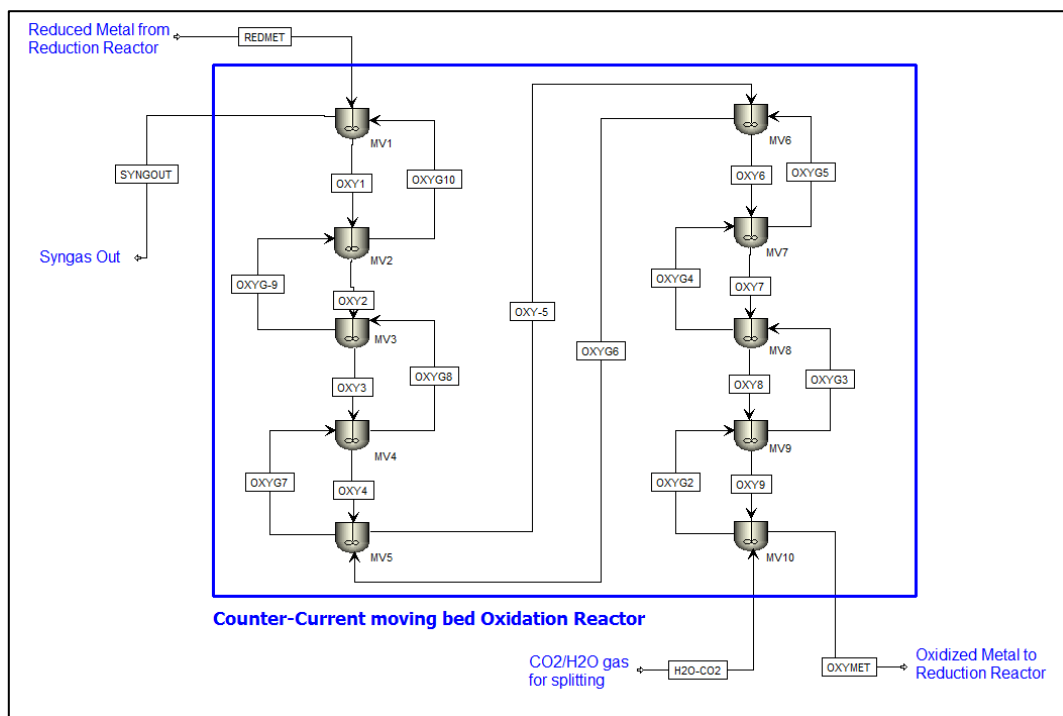


Figure 43: ASPEN Plus model for moving bed reactor with 10 RCSTRs (only oxidation reactor shown), where with OXYG it is intended the gas flow and OXY the metal oxide flow

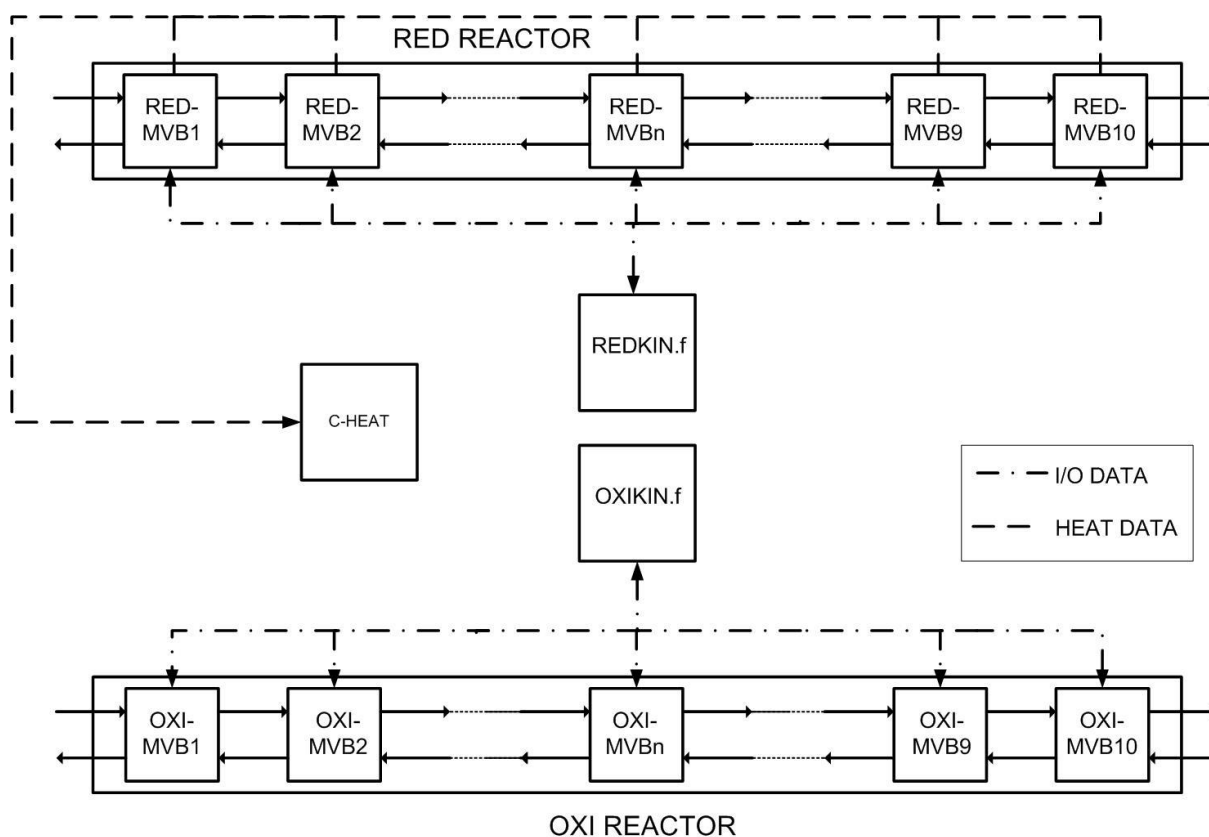


Figure 44: Logic diagram of moving bed reactor model in ASPEN Plus hooked with user kinetics written in an external FORTRAN Code

5.2.4. Simulation Assumption

Since the kinetic reported in section 5.2.2 is based on the non-stoichiometric reduction of ceria (eq. 70), it was assumed a maximum achievable δ equal to 0.35 in order to preserve the lattice structure of the oxygen carrier. Since reduction experiments were not performed varying pressure, it is assumed that the chemical looping unit works at the same pressure used in the past section (2 bar).

5.2.5. Reactor sizing and performance sensitivity

5.2.5.1 Reduction Reactor

A sensitivity analysis was performed to assess the influence of the reactor size and operating conditions on the performance of the reduction reactor. During the analysis, a fixed CeO_2 molar flow of 285.7 mol/s was assumed. This specific value was chosen in order to have a comparison with the results of the thermodynamic analysis. As already explained, the main goal of the chemical looping unit is to produce syngas by CO_2 - H_2O dissociation over reduced ceria. In the previous section (section 5.1) an inlet CeO_2 equal to 200 mol/s was assumed, to which, in case of full reaction correspond 100 mol/s of Ce_2O_3 in the oxidation reactor. So that, in case of favouring condition for ceria oxidation, it is possible to produce a maximum syngas flow of 100 mol/s. However, since the kinetic model is based on the non-stoichiometric reduction of

CeO₂, in order to have at the inlet of the oxidation reactor an equivalent of 100 mol/s of Ce₂O₃, 285.7 mol/s of CeO₂ are needed.

In Figure 45 the advancement of the reduction reaction (X_{RED}) varying the reactor volume from 1 to 20 m³ is reported. From the thermodynamics perspective, it was reported that starting from 900°C-950°C it is possible to obtain a full CeO₂ conversion by methane. On the contrary, from a kinetic point of view the reduction reaction is way slower, hence big volumes are required in order to guarantee a sufficient residence time to the solid. However, it is important to underline, that, since the reduction reactor is set as isothermal, one of the most important parameter in the design phase is the volume. In fact, in order to keep the isothermal condition, it is really important to minimize it. Moreover, as previously described, with the integration of the CL unit in the polygeneration plant, the reduction reactor would be connected to the combustor in the annular set-up. Hence, again, it is important to lower the volume of the reactor. For this reason, a solution is to work at higher temperatures (1000-1050°C). In fact as shown in Figure 45, at these conditions, the reaction is significantly faster. So that, the volume set for the rest of the analysis is 4 m³ which allow to achieve a reduction extent of 98.7% and 99.2% at 1000°C and 1050°C respectively. The choice of this values results in a trade-off between volume and advancement of the reaction. Even though it is possible to achieve a higher advancement of the reaction, the more the reaction moves towards the full conversion, the slower it becomes. Hence, at higher advancement of the reaction, even to achieve a small increase in conversion (X_{RED}) a relatively high increment in volume is required.

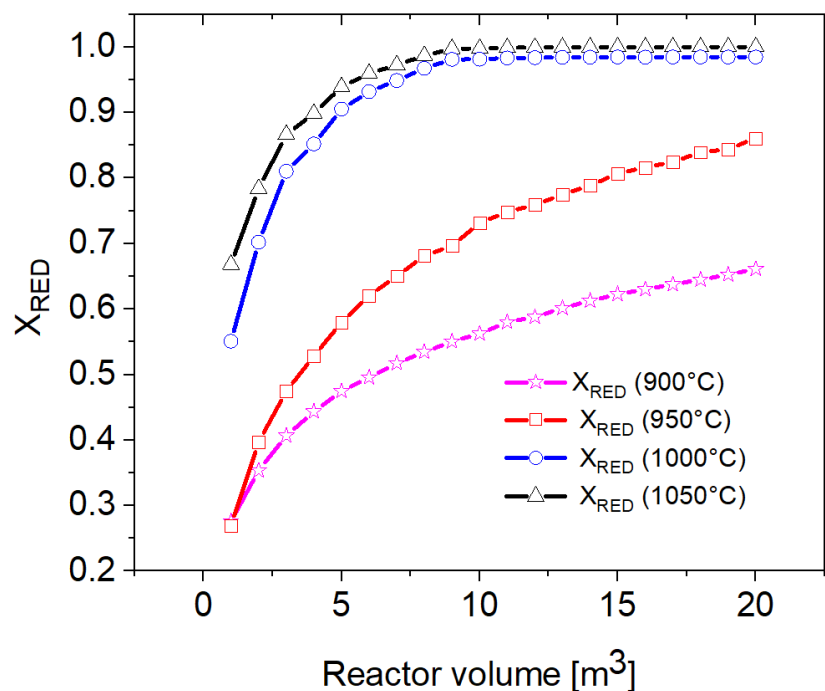


Figure 45: effect of the reactor volume on the degree of advancement of the reduction reaction (X_{RED})

Similarly to the study for the thermodynamic analysis of the reduction reactor, a sensitivity analysis by varying the CH₄/CeO₂ ratio was performed. However, since the trends are similar to the one of the thermodynamic model (section 5.1.2), they are not discussed again.

5.2.5.2 Oxidation reactor

A sensitivity analysis was performed in order to assess the effect of the size and the operating conditions on the performance of the reactor. During the study it was assumed a full reduction ($\delta=0.35$) of the circulating ceria, hence as a metal inlet to the oxidation reactor was assumed a mixture of 85.7 mol/s of CeO₂ and 100 mol/s of Ce₂O₃.

Similarly to the reduction reactor, the first analysis performed was the one to assess the effect of the reactor size. As illustrated in Figure 46, the solid conversion ranged from a minimum of 78.1% to a maximum of 99.5% with a pure stream of CO₂ and a pure stream of H₂O respectively. This is due to the fact that water dissociation results kinetically faster than carbon monoxide splitting, so that, by increasing the water content in the gas mixture, the degree of advancement of the oxidation reaction is enhanced.

Based on the logic described in section 5.2.5.2, a volume equal to 6 m³ was selected as optimal for the oxidation reactor, since this value resulted in a good compromise between size and solid conversion. In fact, with the selected volume it is possible to achieve a solid conversion of 94.1% with a pure CO₂ stream while, by increasing the water content, the conversion reaches the 97.3% and 98.8% with an equimolar H₂O-CO₂ and a pure water stream. The further increase in size of the reactor till 20 m³ would bring the solid conversion to a maximum of 96.4%, 99.1 and 99.5% with respectively a pure in CO₂, equimolar and pure H₂O inlet gas. Hence it is considered not favourable to increase the reactor volume by a ratio higher than two to obtain few percentage points in conversion.

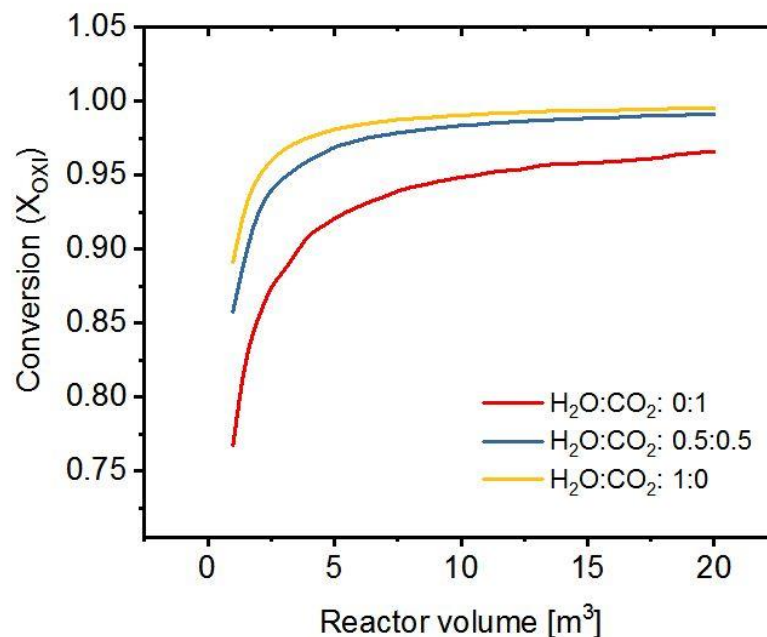


Figure 46: effect of the reactor volume on the degree of advancement of the oxidation reaction (X_{Oxi}) with different gas mixture (with a 5% excess from the stoichiometric value) at the inlet of the reactor considering a gas temperature inlet of 500°C and a metal inlet temperature of 800°C

Figure 47.a-d shows the effect of the inlet temperatures on the degree of the advancement of the oxidation reaction and on the product composition. Differently from the results of the thermodynamics, due to the selected size of the reactor and the slowdowns of the reaction

towards the complete conversion, it is not possible to achieve a full oxidised ceria. However, by increasing the temperatures, the conversion of the oxygen carrier is enhanced. This means that at higher temperature the water and carbon monoxide dissociation are kinetically faster. This results in the opposite of what found by the thermodynamics investigation. Nevertheless, as predicted by the thermodynamics, the H₂O dissociation results penalized with respect to the CO₂ dissociation with the increment of the temperature inlet. In fact, as can be seen in Figure 47.b, the H₂/CO ratio ranges from 1.073 to 1.033 by increasing the temperature inlet of the oxygen carrier from 600°C to 1000°C. This trend is confirmed by Figure 47.c-d where according to an increment in the metal oxide temperature the water content in the syngas outlet is increased, while at the same time, the CO₂ content is reduced.

In addition, it can be seen that the effect of the temperature inlet of the gas mixture into the OXI is negligible for all the temperatures range considered.

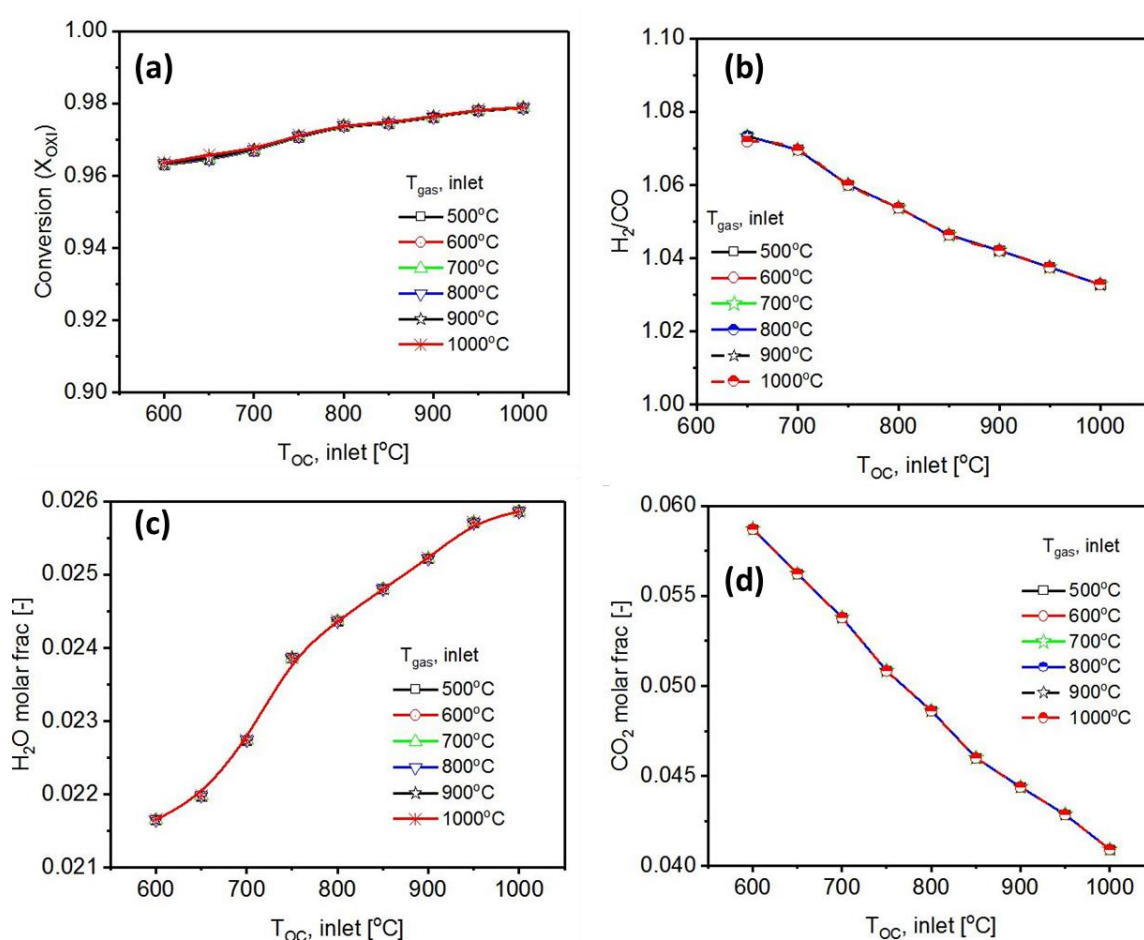


Figure 47: effect of the inlet temperature of the fed Ce₂O₃ ($T_{OC,inlet}$) and of the equimolar (50% H₂-50% H₂O, with an excess of 5% with respect to the stoichiometric) inlet gas mixture ($T_{gas,inlet}$) on a) CeO₂ production, b) CO/H₂ ratio, c) H₂O molar fraction, d) CO₂ molar fraction at the outlet

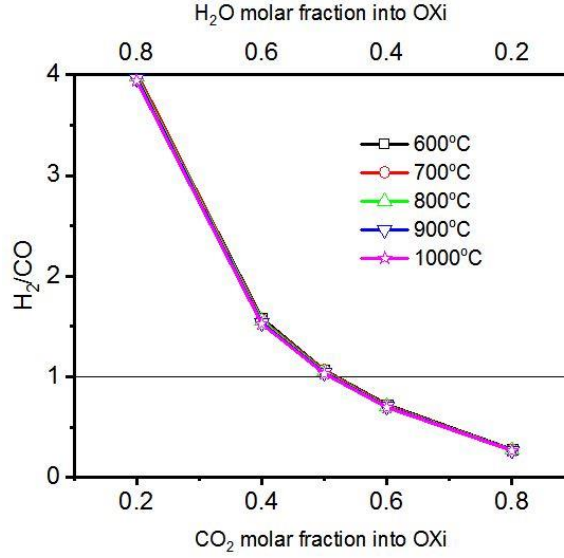


Figure 48: effect of the gas mixture inlet composition into OXI (with an excess of 5%) and the metal oxide inlet temperature on the H₂/CO ratio of the syngas outlet from OXI, considering a gas temperature inlet into OXI equal to 500°C

Figure 48 shows the effect of both the composition of the gas into the OXI and the temperature of the metal oxide inlet on the H₂/CO ratio of the outlet syngas. As expected by increasing the CO₂ content the H₂/CO ratio decreases. In addition, due to the purpose of the proposed plant, in the same figure, is highlighted the gas composition of the inlet gas for the ideal 1:1 H₂/CO ratio for DME production which results in 52%-48% CO₂-H₂O.

5.3. CL unit performance results - thermodynamic and kinetic model comparison

In order to assess the performance of the chemical unit, two different efficiency definitions were proposed. The reason for this choice is the following. The aim of the described chemical looping unit is to produce syngas by dissociating H₂O and CO₂ over Ce₂O₃ oxidation. In order to have a dissociation reaction in the oxidation reactor, it is required that CeO₂ is reduced. As already described, the reduction of ceria is driven by methane partial oxidation which produces syngas. This syngas can be used for either power production by combustion or it can be further treated for chemical/fuel production. With the first option, however, the conversion of methane in the syngas is unnecessary since in any case it would have been burned. While in the case of fuel/chemical production using both syngas streams, the methane conversion is a useful reaction. For these reasons, the first efficiency (eq. 68) takes into account both the syngas streams while the second (eq. 69) just the second one.

$$\eta_1 = \frac{(\dot{m}_{H_2} LHV_{H_2} + \dot{m}_{CO} LHV_{CO})_{red} + (\dot{m}_{H_2} LHV_{H_2} + \dot{m}_{CO} LHV_{CO})_{oxy}}{(\dot{m}_{CH_4} LHV_{CH_4} + (\dot{Q}_{red} - \dot{Q}_{oxd}) + \dot{Q}_{need, net}) + (\dot{Q}_{spht} - \dot{Q}_{sld})} \quad (68)$$

$$\eta_2 = \frac{(\dot{m}_{H_2} LHV_{H_2} + \dot{m}_{CO} LHV_{CO})_{oxy}}{(\dot{m}_{CH_4} LHV_{CH_4} + (\dot{Q}_{red} - \dot{Q}_{oxd}) + \dot{Q}_{need, net}) + (\dot{Q}_{spht} - \dot{Q}_{sld})} \quad (69)$$

Where \dot{Q}_{red} is the heat requirement for the reduction reaction, \dot{Q}_{oxd} is the heat released from the endothermic reaction in the oxidation reactor, $\dot{Q}_{need, net} = (\dot{Q}_{need, CH_4} + \dot{Q}_{need, waste\ gas}) - (\dot{Q}_{syngas, red} + \dot{Q}_{syngas, oxd})$ is the net heat needed for the system operations, including the heat needed for methane and waste gas heat-up and the heat recovered from the syngas product streams, that are directly used to pre-heat the inlet gases, and hence included in the defined manner. $(\dot{Q}_{spht} - \dot{Q}_{sld})$ represents the net heat required to preheat the solids in case of the operation of the two reactors at different temperatures, with the reduction reactor at higher temperature due to thermodynamic considerations. \dot{Q}_{sld} represents the heat recovered from the solids from the reduction reactor before it enters oxidation, while \dot{Q}_{spht} is the heat delivered to the solids for preheating. Heat losses from system components were neglected in the efficiency assessment.

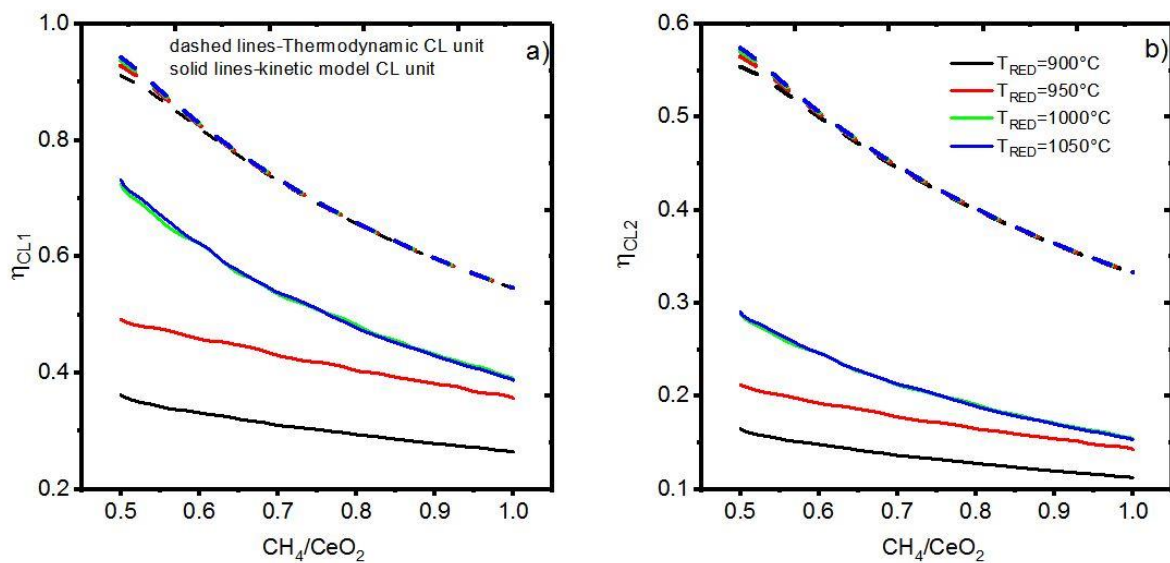


Figure 49: effect of the CH₄/CeO₂ ratio and isothermal temperature of the reduction reactor (T_{RED}) on a) first efficiency parameter (η_{CL}), b) second efficiency parameter (η_{CL2}), with an equimolar gas feed in the oxidation reactor (excess of 5%) for thermodynamic and kinetic model

Figure 49.a-b represent the effect of both methane and reduction temperature on the efficiencies of the CL unit. Due to the explanation given before, the first efficiency (η_{CL}) results always higher than the second efficiency (η_{CL2}) (by an approximate 30%). With a higher methane flow, both efficiencies drop. This is due to the fact that once the CeO₂ is fully converted, no further increase in the syngas production occurs. As can be observed from the thermodynamic efficiency beyond a CH₄/CeO₂ ratio of 0.68 a complete reaction is obtained irrespective of reduction temperature. Hence a coincident efficiency trend is obtained with temperature variation. On the other hand for kinetics, due to the constant volume and a superior kinetics at a higher temperature, the syngas production increases considerably above 1000°C. Furthermore, this implies a higher non-stoichiometric ceria at the inlet of the oxidation reaction, producing more syngas from the CL unit as a whole. The subsequent effect is observed on both efficiency (Figure 49).

6. Integration of the kinetic model in the polygeneration plant

In this section, the integration of the proposed polygeneration plant with the moving bed connected to the kinetic model is discussed.

6.1. Reactors sizing

With the same approach described in sections 5.2.5.1 and 0 reactor size selection was performed for the reduction and the oxidation reactor. The size chosen were 6 m³ for both the reactors, resulting in a solid conversion of 95.8% for the oxidation reactor. While for the reduction reactor the conversion ranges from 54% to 100 % with an increment in temperature (Figure 50.a-b).

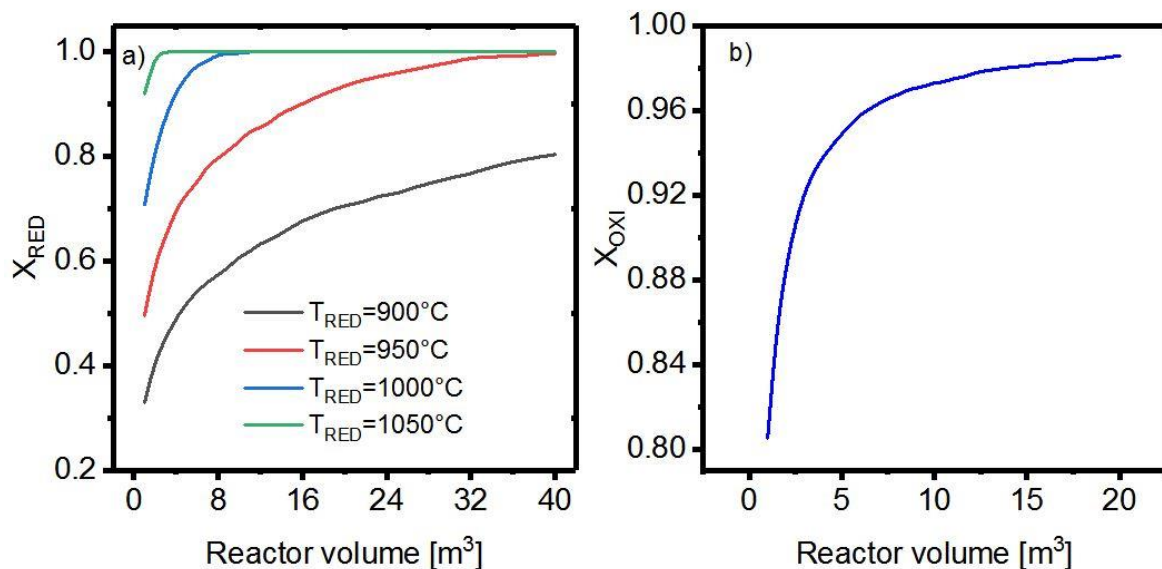


Figure 50: effect of the size on the degree of the advancement of a) oxidation reactor (X_{OXI}) b) reduction reactor (X_{RED}), with a gas mixture into OXI composed by 52%-48% CO₂-H₂O with an excess of 5%.

6.2. Performance results

A sensitivity analysis was performed to assess the performance of the layout integrated with the counterflow moving bed model. The circulating flow of ceria used in section 4.1 was retained (588 mol/s of CeO₂ to RED). Moreover, since the main goal of this section is to assess the influence of the moving bed integrated within the polygeneration plant, all the operation parameters outside of the CL unit used in section 4.1 are retained (gas inlet temperature, pressure of the steam in the steam cycle, pressure inlet to the combustor). The effect of the inlet mixture on the CO:H₂ fraction of the syngas from the OXI and subsequently its effect on the DME yield has already been discussed in section 4.1. Following thus, in the present analysis a 52% CO₂-48%H₂O inlet stream mixture to OXI was fixed to have the ideal 1:1 H₂:CO syngas composition for DME production.

For this reason, the only parameters that are varied are the following:

- Temperature of the reduction reactor from 900°C to 1050°C;
- Methane flow from 140 mol/s to 580 mol/s.

All the study was conducted fixing an inlet oxygen carrier temperature equal to 800°C and a gas inlet temperature of 500°C to the OXI. The pressure of the CL unit was fixed at 2 bar.

Figure 51.a-c shows the effect of varying the methane flow and the isothermal temperature (T_{RED}) on the plant performance. As already discussed, at lower reduction temperature, the methane reduction kinetics is considerably slow, hence the advancement of the reduction is lower (Figure 51.a). This results in a higher molar fraction of methane at the outlet of the reduction, hence for low temperature since the less methane is reduced in syngas, more power can be generated in the oxyfuel unit. This trend is confirmed by the 1000°C W_{NET} curve (Figure 51.b), that starts to coincide with the 1050°C curve once the full reaction is achieved (with a CH_4 flow of 490 mol/s). Furthermore, the same figure it can be seen that, since with 900°C and 950°C there is no possibility of a complete reaction, the net power results always higher.

Also, the trend in DME yield is interesting to note. With a lower reduction corresponding to a lower non-stoichiometry of ceria to the oxidation reactor, the syngas produced drops. This results in a subsequent drop in the DME production (Figure 51.c). Being a polygeneration plant, this results in a lower effectiveness of the overall plant output and hence should be avoided as much as possible.

Combining all the individual effects, the overall trend in the efficiency of the power plant can be discussed henceforth. Elaborating, as can be visualized from Figure 51.c, the recirculation fraction of CO_2 in the oxidation reactor drops with an increase in methane input to the plant. This indicates a lower recirculation fraction of CO_2 , which in turn results in a decrease in the DME production with respect to the methane fed to the power plant. To simplify, with an increase in the methane flow, the plant tends more towards a simple oxyfuel power plant, whereby the effectiveness of polygeneration decreases. Thus, with the increment of the methane flow, even if the power generation results higher, the relative drop in the DME production results in a drop in the efficiency.

In addition, the effect of temperature of the reduction reactor on the overall efficiency of the power plant can also be obtained from Figure 51.c. For a lower temperature of the reduction reactor, the degree of advancement of the reduction reaction is decreased. Consequently, a lower non-stoichiometric ceria results, which leads to less syngas being produced and hence, a lower DME. This results in a lower overall efficiency as discussed before about the effect of DME drop.

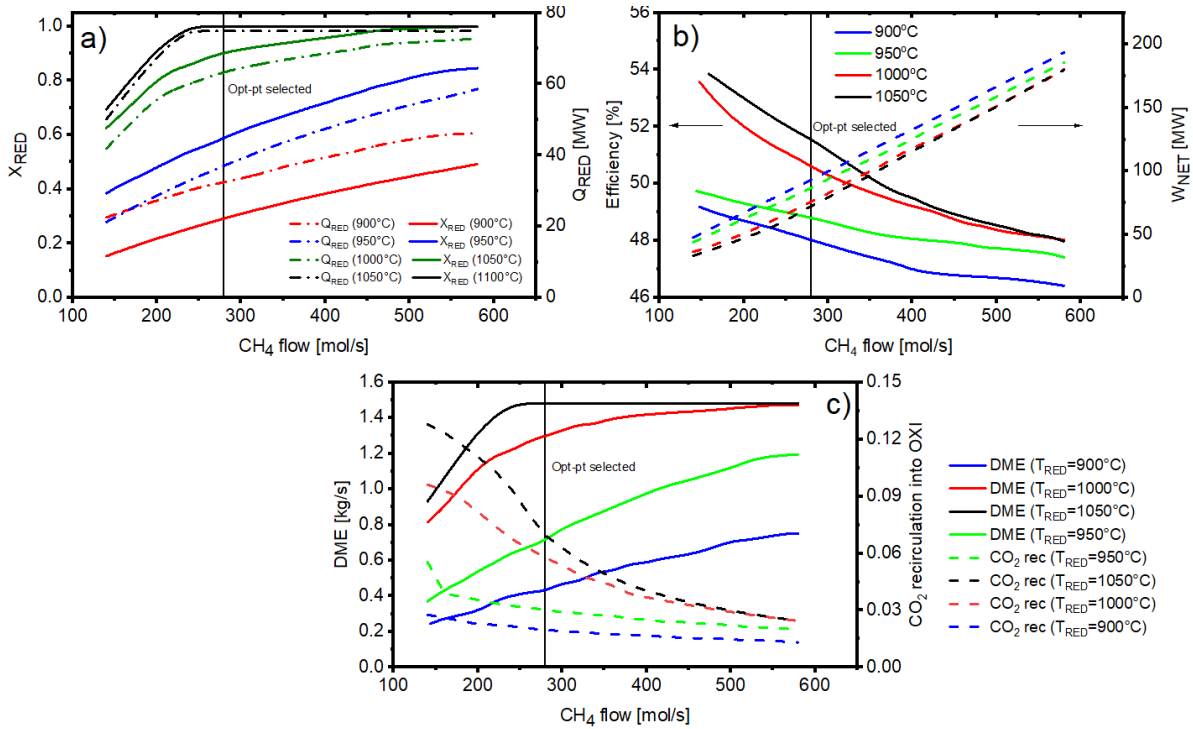


Figure 51: effect of the operation condition T_{RED} and inlet methane flow on a) advancement of the reduction reaction (X_{RED}) and heat needed Q_{RED} , b) efficiency and total power produced W_{NET} , c) DME production and CO_2 recirculation into OXI.

Considering the sensitivity analysis, the best point of operation (Opt-point selected) was set coincident to reduction reactor temperature of 1050°C and a methane flow of 280 mol/s. With these parameters, the total efficiency results in 51.8% with a power production of 72.2 MW and 1.48 kg/s of DME. For the kinetic model based layout, it is also evident that due to less conversion of the ceria in the reduction reactor it leads to lower production of syngas in the oxidation reactor which in turns reduces the DME production by ~30% compared to thermodynamic study. Similarly, the power production from the plant is ~30% less. As the basic assumptions for the two layouts are a bit different except the ceria flow by which it is wise to completely compare each parameter rather to just see how the kinetics and reactor selection could influence the overall system performance. Therefore, from the above results, it is found that for heterogenous non-catalytic gas-solid chemical looping cycles thermodynamic results are overestimated and do not represent a clear picture and a detailed kinetic model inclusion and reactor selection is necessary with optimization. The present study reports an inclusive moving bed model for chemical looping syngas production which is well integrated for the DME production as well as power production with 100% capture.

Table 24: final results of the best point of operation of the polygeneration plant integrated with the moving bed CL unit (KM-LAYOUT) compared with the results of the layout with the thermodynamic CL unit (TM-LAYOUT)

Parameters	KM-LAYOUT	TM-LAYOUT
Circulating ceria	588 mol/s	588 mol/s
Excess (CO ₂ /H ₂ O) in OXI	5%	60%
CH ₄ /NG	16.17 ton/h	25.2 ton/h
W _{GROSS}	110.92 MW	167.61 MW
W _{NET}	72.17 MW	102.90 MW
η _{TOT}	51.80%	50.21%
W _{COMP-1}	2.41 MW	3.76 MW
W _{COMP-2}	6.18 MW	10.67 MW
W _{COMP-3}	15.61 MW	28.29 MW
W _{ASU}	13.89 MW	19.34 MW
W _{GT}	68.45 MW	114.42 MW
W _{ST1}	26.14 MW	44.30 MW
W _{ST2}	13.36 MW	2.96 MW
W _{TURBEXP}	2.96 MW	4.37 MW
\dot{m}_{DME}	1.48 kg/s	2.15 kg/s
\dot{m}_{MeOH}	0.01 kg/s	0.03 kg/s

7. Conclusion

In this work, the methane driven Chemical-looping (CL) syngas production as an innovative fuel production technology based on splitting CO₂ and H₂O, for production of syngas (CO and H₂) has been studied in detail. The primary focus was to assess the feasibility of a novel polygeneration plant integrated with the syngas chemical looping unit for DME and power production. For this reason, an Aspen Plus[®] model was developed in order to simulate the performance of the system. The thermodynamic equilibrium model has been considered for CL unit and kinetics has been implemented in DME synthesis. A detailed sensitivity was performed to evaluate the optimal conditions for the system layout. The system efficiency could reach a maximum of 50.2% with 2.14 kg/s DME and 102 MWe production. The corresponding exergetic efficiency resulted equal to 45%. The economic analysis resulted in a total investment cost equal to 532.45 M\$. The equipment with the highest investment cost is the ASU, which account for the 22% of the total investment. A payback period of 20 years was achieved with electricity and DME selling price of 220 \$/MWh and 72 \$/MWh respectively.

The type of reactors play a crucial role in the overall performance of the CL unit, which in turn, affects the entire plant to which it is integrated. Based on the assessment it was found that moving bed reactors would yield good conversion of gases and metal oxide in each reduction and oxidation reactor due to its ability to control the residence time within the reactor. Moving bed reactor was developed considered number of RCSTRs in series in ASPEN PLUS and reaction kinetics of the ceria with methane (reduction reactor) and CO₂ and H₂O splitting (oxidation reactor) was written as user kinetic subroutine in FORTRAN and compiled and hooked to ASPEN PLUS. Based on the model developed for a redox cycle, the performance of the CL unit was assessed with a thermodynamic equilibrium model which was developed considered RGIBBS reactors. It was found that the CL unit based on the kinetics has 20% less efficiency compared to CL unit based on the thermodynamic model. Based on the results it was found that kinetics has a strong effect on the CL unit performance. Subsequently, the CL unit with the thermodynamic model was replaced with moving bed interconnected model CL unit and overall system performance was re-evaluated. It was found that the DME production drops to 1.48 Kg/s when kinetics has been considered for the CL unit. Similarly the power production has also dropped to 71 MW. The efficiency of the whole layout is 51.8% as in this case methane feed reduces due to lower demand in the CL unit due to its kinetics.

Further work

Even though the amount of work done, an optimization of the plant can be considered an interesting future work. However, the integration of the proposed plant with different fuel unit can be seen as a clear continuation of the presented study.

References

- [1] UNFCCC, Paris Agreement, Conf. Parties Its Twenty-First Sess. (2015) 32. doi:FCCC/CP/2015/L.9/Rev.1.
- [2] J.G.J. (PBL) Olivier, G. (EC-J. Janssens-Maenhout, M. (EC-J. Muntean, J.A.H.W. (PBL) Peters, Trends in Global CO₂ Emissions: 2016 Report, PBL Netherlands Environ. Assess. Agency Eur. Comm. Jt. Res. Cent. (2016) 86. http://edgar.jrc.ec.europa.eu/news_docs/jrc-2016-trends-in-global-co2-emissions-2016-report-103425.pdf.
- [3] United States Environmental Protection Agency (EPA), Greenhouse Gas Emissions, (2016). <https://www.epa.gov/ghgemissions/overview-greenhouse-gases> (accessed May 29, 2018).
- [4] J. Rogelj, M. Schaeffer, P. Friedlingstein, N.P. Gillett, D.P. Van Vuuren, K. Riahi, M. Allen, R. Knutti, Differences between carbon budget estimates unravelled, *Nat. Clim. Chang.* 6 (2016) 245–252. doi:10.1038/nclimate2868.
- [5] IPCC, Climate Change 2014: Synthesis Report. Contribution of Working Groups I, II and III to the Fifth Assessment Report of the Intergovernmental Panel on Climate Change, 2014. doi:10.1017/CBO9781107415324.004.
- [6] K.L. Ricke, R.J. Millar, D.G. MacMartin, Constraints on global temperature target overshoot, *Sci. Rep.* 7 (2017) 1–7. doi:10.1038/s41598-017-14503-9.
- [7] P. Viebahn, D. Vallentin, S. Höller, Prospects of carbon capture and storage (CCS) in China's power sector - An integrated assessment, *Appl. Energy.* 157 (2015) 229–244. doi:10.1016/j.apenergy.2015.07.023.
- [8] M.E. Boot-Handford, J.C. Abanades, E.J. Anthony, M.J. Blunt, S. Brandani, N. Mac Dowell, J.R. Fernández, M.-C. Ferrari, R. Gross, J.P. Hallett, R.S. Haszeldine, P. Heptonstall, A. Lyngfelt, Z. Makuch, E. Mangano, R.T.J. Porter, M. Pourkashanian, G.T. Rochelle, N. Shah, J.G. Yao, P.S. Fennell, Carbon capture and storage update, *Energy Environ. Sci.* 7 (2014) 130–189. doi:10.1039/C3EE42350F.
- [9] R.P. Cabral, N. Mac Dowell, A novel methodological approach for achieving £/MWh cost reduction of CO₂ capture and storage (CCS) processes, *Appl. Energy.* 205 (2017) 529–539. doi:10.1016/j.apenergy.2017.08.003.
- [10] International Energy Agency, 20 years of carbon capture and storage, 2016.
- [11] D.Y.C. Leung, G. Caramanna, M.M. Maroto-Valer, An overview of current status of carbon dioxide capture and storage technologies, *Renew. Sustain. Energy Rev.* 39 (2014) 426–443. doi:10.1016/j.rser.2014.07.093.
- [12] R.M. Cuéllar-Franca, A. Azapagic, Carbon capture, storage and utilisation technologies: A critical analysis and comparison of their life cycle environmental impacts, *J. CO₂ Util.* 9 (2015) 82–102. doi:10.1016/j.jcou.2014.12.001.
- [13] C.M. Quintella, S.A. Hatimondi, A.P.S. Musse, S.F. Miyazaki, G.S. Cerqueira, A. De Araujo Moreira, CO₂ capture technologies: An overview with technology assessment based on patents and articles, *Energy Procedia.* 4 (2011) 2050–2057.

doi:10.1016/j.egypro.2011.02.087.

- [14] A. Bose, K. Jana, D. Mitra, S. De, Co-production of power and urea from coal with CO₂ capture: Performance assessment, *Clean Technol. Environ. Policy*. 17 (2015). doi:10.1007/s10098-015-0960-7.
- [15] Q. Zhang, Nurhayati, C.L. Cheng, D. Nagarajan, J.S. Chang, J. Hu, D.J. Lee, Carbon capture and utilization of fermentation CO₂: Integrated ethanol fermentation and succinic acid production as an efficient platform, *Appl. Energy*. 206 (2017) 364–371. doi:10.1016/j.apenergy.2017.08.193.
- [16] C. Graves, S.D. Ebbesen, M. Mogensen, K.S. Lackner, Sustainable hydrocarbon fuels by recycling CO₂ and H₂O with renewable or nuclear energy, *Renew. Sustain. Energy Rev.* 15 (2011) 1–23. doi:10.1016/j.rser.2010.07.014.
- [17] C.H. Huang, C.S. Tan, A review: CO₂ utilization, *Aerosol Air Qual. Res.* 14 (2014) 480–499. doi:10.4209/aaqr.2013.10.0326.
- [18] K. Jana, S. De, Polygeneration performance assessments: Multi-dimensional viewpoint, *Clean Technol. Environ. Policy*. 17 (2015) 1547–1561. doi:10.1007/s10098-014-0885-6.
- [19] S.C. Bayham, A. Tong, M. Kathe, L.-S. Fan, Chemical looping technology for energy and chemical production, *Wiley Interdiscip. Rev. Energy Environ.* 5 (2016) 216–241. doi:10.1002/wene.173.
- [20] V. Spallina, A. Shams, A. Battistella, F. Gallucci, M.V.S. Annaland, Chemical Looping Technologies for H₂ Production with CO₂ Capture: Thermodynamic Assessment and Economic Comparison, *Energy Procedia*. 114 (2017) 419–428. doi:10.1016/j.egypro.2017.03.1184.
- [21] A.E. Farooqui, A.M. Pica, P. Marocco, D. Ferrero, A. Lanzini, S. Fiorilli, J. Llorca, M. Santarelli, Assessment of kinetic model for ceria oxidation for chemical-looping CO₂ dissociation, *Chem. Eng. J.* 346 (2018) 171–181. doi:10.1016/j.cej.2018.04.041.
- [22] P.T. Krenzke, J.H. Davidson, Thermodynamic analysis of syngas production via the solar thermochemical cerium oxide redox cycle with methane-driven reduction, *Energy and Fuels*. 28 (2014) 4088–4095. doi:10.1021/ef500610n.
- [23] M. Welte, K. Warren, J.R. Scheffe, A. Steinfeld, Combined Ceria Reduction and Methane Reforming in a Solar-Driven Particle-Transport Reactor, *Ind. Eng. Chem. Res.* 56 (2017) 10300–10308. doi:10.1021/acs.iecr.7b02738.
- [24] T.A. Semelsberger, R.L. Borup, H.L. Greene, Dimethyl ether (DME) as an alternative fuel, *J. Power Sources*. 156 (2006) 497–511. doi:10.1016/j.jpowsour.2005.05.082.
- [25] M. Samavati, M. Santarelli, A. Martin, V. Nemanova, Production of Synthetic Fischer-Tropsch Diesel from Renewables: Thermo-economic and Environmental Analysis, *Energy and Fuels*. 32 (2018) 1744–1753. doi:10.1021/acs.energyfuels.7b02465.
- [26] Global CCS Institute, *The Global Status of CCS: 2017*, (2017) 43. doi:978-0-9944115-2-5.
- [27] T.C. Merkel, H. Lin, X. Wei, R. Baker, Power plant post-combustion carbon dioxide capture: An opportunity for membranes, *J. Memb. Sci.* 359 (2010) 126–139. doi:10.1016/j.memsci.2009.10.041.

- [28] P. Chiesa, G. Lozza, A. Malandrino, M. Romano, V. Piccolo, Three-reactors chemical looping process for hydrogen production, *Int. J. Hydrogen Energy*. 33 (2008) 2233–2245. doi:10.1016/j.ijhydene.2008.02.032.
- [29] IEA, *Energy Technology Analysis: Prospects for CO₂ Capture and Storage*, (2004) 249. doi:10.1016/B978-1-85617-710-8.00010-8.
- [30] M. Wang, A. Lawal, P. Stephenson, J. Sidders, C. Ramshaw, Post-combustion CO₂ capture with chemical absorption: A state-of-the-art review, *Chem. Eng. Res. Des.* 89 (2011) 1609–1624. doi:10.1016/j.cherd.2010.11.005.
- [31] B.J.P. Buhre, L.K. Elliott, C.D. Sheng, R.P. Gupta, T.F. Wall, Oxy-fuel combustion technology for coal-fired power generation, *Prog. Energy Combust. Sci.* 31 (2005) 283–307. doi:10.1016/j.pecs.2005.07.001.
- [32] M.A. Habib, M. Nemitallah, R. Ben-Mansour, Recent development in oxy-combustion technology and its applications to gas turbine combustors and ITM reactors, *Energy and Fuels*. 27 (2013) 2–19. doi:10.1021/ef301266j.
- [33] I. Pfaff, A. Kather, Comparative thermodynamic analysis and integration issues of CCS steam power plants based on oxy-combustion with cryogenic or membrane based air separation, *Energy Procedia*. 1 (2009) 495–502. doi:10.1016/j.egypro.2009.01.066.
- [34] T. Lockwood, *Developments in oxyfuel combustion of coal*, IEA Clean Coal Centre, CCC/240, London, United Kingdom. (2014) 1–122.
- [35] M. Chorowski, W. Gizicki, Technical and economic aspects of oxygen separation for oxy-fuel purposes, *Arch. Thermodyn.* 36 (2015) 157–170. doi:10.1515/aoter-2015-0011.
- [36] N.M. A., H.M. A., B.H. M., S.S. A., J. Aqil, B. Rached, M.E.M. A., M. K., Oxy-fuel combustion technology: current status, applications, and trends, *Int. J. Energy Res.* 41 (2017) 1670–1708. doi:10.1002/er.3722.
- [37] White Rose project, (n.d.). <http://www.zeroco2.no/projects/developers/alstom>.
- [38] W. Xiuzhang, Shenhua Group's carbon capture and storage (CCS) demonstration, *Min. Rep.* 150 (2014) 81–84. doi:10.1002/mire.201400006.
- [39] R.J. Allam, M.R. Palmer, G.W. Brown, J. Fetvedt, D. Freed, H. Nomoto, M. Itoh, N. Okita, C. Jones, High efficiency and low cost of electricity generation from fossil fuels while eliminating atmospheric emissions, including carbon dioxide, *Energy Procedia*. 37 (2013) 1135–1149. doi:10.1016/j.egypro.2013.05.211.
- [40] R. Anderson, H. Brandt, S. Doyle, F. Viteri, A demonstrated 20 MWt gas generator for a clean steam power plant, 28th Int. Tech. Conf. Coal Util. Fuel Syst. . (2003).
- [41] D.Y.C. Leung, G. Caramanna, M.M. Maroto-Valer, An overview of current status of carbon dioxide capture and storage technologies, *Renew. Sustain. Energy Rev.* 39 (2014) 426–443. doi:10.1016/j.rser.2014.07.093.
- [42] R. Stanger, T. Wall, R. Spörl, M. Paneru, S. Grathwohl, M. Weidmann, G. Scheffknecht, D. McDonald, K. Myöhänen, J. Ritvanen, Oxyfuel combustion for CO₂ capture in power plants, *Int. J. Greenh. Gas Control*. 40 (2015) 55–125.
- [43] N. MacDowell, N. Florin, A. Buchard, J. Hallett, A. Galindo, G. Jackson, C.S.

- Adjiman, C.K. Williams, N. Shah, P. Fennell, An overview of CO₂ capture technologies, *Energy Environ. Sci.* 3 (2010) 1645. doi:10.1039/c004106h.
- [44] O. Dr. Bolland, Carbon dioxide capture, 2009.
- [45] B. Van Der Zwaan, K. Smekens, CO₂ capture and storage with leakage in an energy-climate model, *Environ. Model. Assess.* 14 (2009) 135–148. doi:10.1007/s10666-007-9125-3.
- [46] C. Doughty, B.M. Freifeld, R.C. Trautz, Site characterization for CO₂ geologic storage and vice versa: The Frio brine pilot, Texas, USA as a case study, *Environ. Geol.* 54 (2008) 1635–1656. doi:10.1007/s00254-007-0942-0.
- [47] K.Z. House, D.P. Schrag, C.F. Harvey, K.S. Lackner, Permanent carbon dioxide storage in deep-sea sediments, *Proc. Natl. Acad. Sci.* 103 (2006) 12291–12295. doi:10.1073/pnas.0605318103.
- [48] D.Y.C. Leung, G. Caramanna, M.M. Maroto-Valer, An overview of current status of carbon dioxide capture and storage technologies, *Renew. Sustain. Energy Rev.* 39 (2014) 426–443. doi:10.1016/j.rser.2014.07.093.
- [49] C.R. Jenkins, P.J. Cook, J. Ennis-King, J. Undershultz, C. Boreham, T. Dance, P. de Caritat, D.M. Etheridge, B.M. Freifeld, A. Hortle, D. Kirste, L. Paterson, R. Pevzner, U. Schacht, S. Sharma, L. Stalker, M. Urosevic, Safe storage and effective monitoring of CO₂ in depleted gas fields, *Proc. Natl. Acad. Sci.* 109 (2012) E35–E41. doi:10.1073/pnas.1107255108.
- [50] M.D. Zoback, S.M. Gorelick, Earthquake triggering and large-scale geologic storage of carbon dioxide, *Proc. Natl. Acad. Sci.* 109 (2012) 10164–10168. doi:10.1073/pnas.1202473109.
- [51] Z. Yuan, M.R. Eden, R. Gani, Toward the Development and Deployment of Large-Scale Carbon Dioxide Capture and Conversion Processes, *Ind. Eng. Chem. Res.* 55 (2016) 3383–3419. doi:10.1021/acs.iecr.5b03277.
- [52] Q.E. Alessandra, C. Gabriele, D. Jean-Luc, P. Siglinda, Carbon Dioxide Recycling: Emerging Large-Scale Technologies with Industrial Potential, *ChemSusChem.* 4 (2011) 1194–1215. doi:10.1002/cssc.201100473.
- [53] J.M. Tour, C. Kittrell, V.L. Colvin, Green carbon as a bridge to renewable energy, *Nat. Mater.* 9 (2010) 871. <http://dx.doi.org/10.1038/nmat2887>.
- [54] R.M. Cuéllar-Franca, A. Azapagic, Carbon capture, storage and utilisation technologies: A critical analysis and comparison of their life cycle environmental impacts, *J. CO₂ Util.* 9 (2015) 82–102. doi:10.1016/j.jcou.2014.12.001.
- [55] M. Aresta, Carbon Dioxide: Utilization Options to Reduce its Accumulation in the Atmosphere, *Carbon Dioxide as Chem. Feed.* (2010) 1–13. doi:10.1002/9783527629916.ch1.
- [56] C. Song, Global challenges and strategies for control, conversion and utilization of CO₂ for sustainable development involving energy, catalysis, adsorption and chemical processing, *Catal. Today.* 115 (2006) 2–32. doi:10.1016/j.cattod.2006.02.029.
- [57] N. von der Assen, J. Jung, A. Bardow, Life-cycle assessment of carbon dioxide capture and utilization: avoiding the pitfalls, *Energy Environ. Sci.* 6 (2013) 2721–2734.

doi:10.1039/C3EE41151F.

- [58] M. Peters, B. Köhler, W. Kuckshinrichs, W. Leitner, P. Markewitz, T.E. Müller, Chemical technologies for exploiting and recycling carbon dioxide into the value chain, *ChemSusChem*. 4 (2011) 1216–1240. doi:10.1002/cssc.201000447.
- [59] E.T.C. Vogt, B.M. Weckhuysen, Fluid catalytic cracking: recent developments on the grand old lady of zeolite catalysis, *Chem. Soc. Rev.* 44 (2015) 7342–7370. doi:10.1039/C5CS00376H.
- [60] D. Bai, J.X. Zhu, Y. Jin, Z. Yu, Simulation of FCC catalyst regeneration in a riser regenerator, *Chem. Eng. J.* 71 (1998) 97–109. doi:10.1016/S1385-8947(98)00110-7.
- [61] D. Yadav, R. Banerjee, A review of solar thermochemical processes, *Renew. Sustain. Energy Rev.* 54 (2016) 497–532. doi:10.1016/j.rser.2015.10.026.
- [62] C. Graves, S.D. Ebbesen, M. Mogensen, K.S. Lackner, Sustainable hydrocarbon fuels by recycling CO₂ and H₂O with renewable or nuclear energy, *Renew. Sustain. Energy Rev.* 15 (2011) 1–23. doi:10.1016/j.rser.2010.07.014.
- [63] S. Abanades, M. Chambon, CO₂ dissociation and upgrading from two-step solar thermochemical processes based on ZnO/Zn and SnO₂/SnO redox pairs, *Energy and Fuels*. 24 (2010) 6667–6674. doi:10.1021/ef101092u.
- [64] X.L. Yan, R. Hino, Nuclear Hydrogen Production, (2011) 1–898. <http://libgen.info/view.php?id=675680%5Cnpapers3://publication/uuid/A01136AA-53C8-4316-8194-9371BF152FFF>.
- [65] M. Roeb, M. Neises, N. Monnerie, F. Call, H. Simon, C. Sattler, M. Schmecker, R. Pitz-Paal, Materials-related aspects of thermochemical water and carbon dioxide splitting: A review, *Materials (Basel)*. 5 (2012) 2015–2054. doi:10.3390/ma5112015.
- [66] C. Agrafiotis, M. Roeb, C. Sattler, A review on solar thermal syngas production via redox pair-based water/carbon dioxide splitting thermochemical cycles, *Renew. Sustain. Energy Rev.* 42 (2015) 254–285. doi:10.1016/j.rser.2014.09.039.
- [67] R. Palumbo, J. Lédé, O. Boutin, E.E. Ricart, A. Steinfeld, S. Möller, A. Weidenkaff, E.A. Fletcher, J. Bielicki, The production of Zn from ZnO in a high-temperature solar decomposition quench process - I. The scientific framework for the process, *Chem. Eng. Sci.* 53 (1998) 2503–2517. doi:10.1016/S0009-2509(98)00063-3.
- [68] P. Charvin, S. Abanades, G. Flamant, F. Lemort, Two-step water splitting thermochemical cycle based on iron oxide redox pair for solar hydrogen production, *Energy*. 32 (2007) 1124–1133. doi:10.1016/j.energy.2006.07.023.
- [69] K.S. Kang, C.H. Kim, W.C. Cho, K.K. Bae, S.H. Kim, C.S. Park, Novel two-step thermochemical cycle for hydrogen production from water using germanium oxide: KIER 4 thermochemical cycle, *Int. J. Hydrogen Energy*. 34 (2009) 4283–4290. doi:10.1016/j.ijhydene.2009.03.017.
- [70] M. Roeb, C. Sattler, R. Klüser, N. Monnerie, L. de Oliveira, A.G. Konstandopoulos, C. Agrafiotis, V.T. Zaspalis, L. Nalbandian, A. Steele, P. Stobbe, Solar Hydrogen Production by a Two-Step Cycle Based on Mixed Iron Oxides, *J. Sol. Energy Eng.* 128 (2006) 125. doi:10.1115/1.2183804.
- [71] C. Agrafiotis, M. Roeb, A.G. Konstandopoulos, L. Nalbandian, V.T. Zaspalis, C.

- Sattler, P. Stobbe, A.M. Steele, Solar water splitting for hydrogen production with monolithic reactors, *Sol. Energy*. 79 (2005) 409–421. doi:10.1016/j.solener.2005.02.026.
- [72] Y. Tamaura, A. Steinfeld, P. Kuhn, K. Ehrensberger, Production of solar hydrogen by a novel, 2-step, water-splitting thermochemical cycle, *Energy*. 20 (1995) 325–330. doi:10.1016/0360-5442(94)00099-O.
- [73] S. Lorentzou, C.C. Agrafiotis, A.G. Konstandopoulos, Aerosol spray pyrolysis synthesis of water-splitting ferrites for solar hydrogen production, *Granul. Matter*. 10 (2008) 113–122. doi:10.1007/s10035-007-0069-8.
- [74] T. Kodama, N. Gokon, R. Yamamoto, Thermochemical two-step water splitting by ZrO₂-supported Ni_xFe_{3-x}O₄ for solar hydrogen production, *Sol. Energy*. 82 (2008) 73–79. doi:10.1016/j.solener.2007.03.005.
- [75] A. Statnatiou, P.G. Loutzenhiser, A. Steinfeld, Solar syngas production via H₂O/CO₂-splitting thermochemical cycles with Zn/ZnO and FeO/Fe₃O₄ redox reactions, *Chem. Mater*. 22 (2010) 851–859. doi:10.1021/cm9016529.
- [76] A. Statnatiou, P.G. Loutzenhiser, A. Steinfeld, Solar syngas production via H₂O/CO₂-splitting thermochemical cycles with Zn/ZnO and FeO/Fe₃O₄ redox reactions, *Chem. Mater*. 22 (2010) 851–859. doi:10.1021/cm9016529.
- [77] S. Abanades, G. Flamant, Thermochemical hydrogen production from a two-step solar-driven water-splitting cycle based on cerium oxides, *Sol. Energy*. 80 (2006) 1611–1623. doi:10.1016/j.solener.2005.12.005.
- [78] E.A. Kümmerle, G. Heger, The Structures of C-Ce₂O_{3+δ}, Ce₇O₁₂, and Ce₁₁O₂₀, *J. Solid State Chem*. 147 (1999) 485–500. doi:10.1006/jssc.1999.8403.
- [79] C. William C., H. Sossina M., Ceria as a Thermochemical Reaction Medium for Selectively Generating Syngas or Methane from H₂O and CO₂, *ChemSusChem*. 2 (2009) 735–739. doi:doi:10.1002/cssc.200900138.
- [80] N. Gokon, S. Sagawa, T. Kodama, Comparative study of activity of cerium oxide at thermal reduction temperatures of 1300–1550 C for solar thermochemical two-step water-splitting cycle, *Int. J. Hydrogen Energy*. 38 (2013) 14402–14414. doi:10.1016/j.ijhydene.2013.08.108.
- [81] J.R. Scheffe, A. Steinfeld, Thermodynamic analysis of cerium-based oxides for solar thermochemical fuel production, *Energy and Fuels*. 26 (2012) 1928–1936. doi:10.1021/ef201875v.
- [82] S. Abanades, A. Legal, A. Cordier, G. Peraudeau, G. Flamant, A. Julbe, Investigation of reactive cerium-based oxides for H₂ production by thermochemical two-step water-splitting, *J. Mater. Sci*. 45 (2010) 4163–4173. doi:10.1007/s10853-010-4506-4.
- [83] Q. Jiang, G. Zhou, Z. Jiang, C. Li, Thermochemical CO₂ splitting reaction with C_xM_{1-x}O_{2-δ} (M=Ti⁴⁺, Sn⁴⁺, Hf⁴⁺, Zr⁴⁺, La³⁺, Y³⁺ and Sm³⁺) solid solutions, *Sol. Energy*. 99 (2014) 55–66. doi:10.1016/j.solener.2013.10.021.
- [84] A. Le Gal, S. Abanades, Catalytic investigation of ceria-zirconia solid solutions for solar hydrogen production, *Int. J. Hydrogen Energy*. 36 (2011) 4739–4748. doi:10.1016/j.ijhydene.2011.01.078.

- [85] Y. Tamaura, A. Steinfeld, P. Kuhn, K. Ehrensberger, Production of solar hydrogen by a novel, 2-step, water-splitting thermochemical cycle, *Energy*. 20 (1995) 325–330. doi:10.1016/0360-5442(94)00099-O.
- [86] M. Roeb, M. Neises, J.P. Säck, P. Rietbrock, N. Monnerie, J. Dersch, M. Schmitz, C. Sattler, Operational strategy of a two-step thermochemical process for solar hydrogen production, *Int. J. Hydrogen Energy*. 34 (2009) 4537–4545. doi:10.1016/j.ijhydene.2008.08.049.
- [87] N. Gokon, T. Mataga, N. Kondo, T. Kodama, Thermochemical two-step water splitting by internally circulating fluidized bed of NiFe₂O₄ particles: Successive reaction of thermal-reduction and water-decomposition steps, *Int. J. Hydrogen Energy*. 36 (2011) 4757–4767. doi:10.1016/j.ijhydene.2011.01.076.
- [88] S. Kawakami, T. Myojin, H.S. Cho, T. Hatamachi, N. Gokon, T. Kodama, Thermochemical two-step water splitting cycle using Ni-ferrite and CeO₂ coated ceramic foam devices by concentrated Xe-light radiation, *Energy Procedia*. 49 (2013) 1980–1989. doi:10.1016/j.egypro.2014.03.210.
- [89] H.S. Cho, T. Myojin, S. Kawakami, N. Gokon, T. Kodama, Y.H. Kang, S.N. Lee, K.K. Chai, H.K. Yoon, H.J. Lee, Solar demonstration of thermochemical two-step water splitting cycle using CeO₂/MPSZ ceramic foam device by 45kWth KIER solar furnace, *Energy Procedia*. 49 (2013) 1922–1931. doi:10.1016/j.egypro.2014.03.204.
- [90] W.C. Chueh, M. Abbott, D. Scipio, S.M. Haile, High-flux solar-driven thermochemical dissociation of CO₂ and H₂O using ceria redox reactions, *Science* (80-.). 63 (2010) 2010. doi:10.1126/science.1197834.
- [91] P. Furler, J.R. Scheffe, A. Steinfeld, Syngas production by simultaneous splitting of H₂O and CO₂ via ceria redox reactions in a high-temperature solar reactor, *Energy Environ. Sci*. 5 (2012) 6098–6103. doi:10.1039/C1EE02620H.
- [92] H. Kaneko, T. Miura, A. Fuse, H. Ishihara, S. Taku, H. Fukuzumi, Y. Naganuma, Y. Tamaura, Rotary-type solar reactor for solar hydrogen production with two-step water splitting process, *Energy and Fuels*. 21 (2007) 2287–2293. doi:10.1021/ef060581z.
- [93] R.B. Diver, J.E. Miller, M.D. Allendorf, N.P. Siegel, R.E. Hogan, Solar Thermochemical Water-Splitting Ferrite-Cycle Heat Engines, *J. Sol. Energy Eng.* 130 (2008) 041001. doi:10.1115/1.2969781.
- [94] J. Kim, J.E. Miller, C.T. Maravelias, E.B. Stechel, Comparative analysis of environmental impact of S2P (Sunshine to Petrol) system for transportation fuel production, *Appl. Energy*. 111 (2013) 1089–1098. doi:10.1016/j.apenergy.2013.06.035.
- [95] P. Pantu, K. Kim, G.R. Gavalas, Methane partial oxidation on Pt/CeO₂-ZrO₂ in the absence of gaseous oxygen, *Appl. Catal. A Gen.* 193 (2000) 203–214. doi:10.1016/S0926-860X(99)00429-9.
- [96] K. Otsuka, Y. Wang, E. Sunada, I. Yamanaka, Direct partial oxidation of methane to synthesis gas by cerium oxide, *J. Catal.* 175 (1998) 152–160. doi:10.1006/jcat.1998.1985.
- [97] K. Otsuka, Y. Wang, M. Nakamura, Direct conversion of methane to synthesis gas through gas–solid reaction using CeO₂-ZrO₂ solid solution at moderate temperature,

- Appl. Catal. A Gen. 183 (1999) 317–324. doi:10.1016/S0926-860X(99)00070-8.
- [98] K. Otsuka, E. Sunada, T. Ushiyama, I. Yamanaka, The production of synthesis gas by the redox of cerium oxide, in: M. de Pontes, R.L. Espinoza, C.P. Nicolaidis, J.H. Scholtz, M.S.B.T.-S. in S.S. and C. Scurrill (Eds.), *Nat. Gas Convers. IV*, Elsevier, 1997: pp. 531–536. doi:https://doi.org/10.1016/S0167-2991(97)80386-2.
- [99] K. Otsuka, T. Ushiyama, I. Yamanaka, Partial Oxidation of Methane Using the Redox of Cerium Oxide, *Chem. Lett.* 22 (1993) 1517–1520. doi:10.1246/cl.1993.1517.
- [100] T. Kodama, H. Ohtake, S. Matsumoto, A. Aoki, T. Shimizu, Y. Kitayama, Thermochemical methane reforming using a reactive WO₃/W redox system, *Energy*. 25 (2000) 411–425. doi:10.1016/S0360-5442(99)00084-5.
- [101] K. Li, H. Wang, Y. Wei, D. Yan, Syngas production from methane and air via a redox process using Ce–Fe mixed oxides as oxygen carriers, 2010. doi:10.1016/j.apcatb.2010.04.018.
- [102] K.J. Warren, J. Reim, K. Randhir, B. Greek, R. Carrillo, D.W. Hahn, J.R. Scheffe, Theoretical and Experimental Investigation of Solar Methane Reforming through the Nonstoichiometric Ceria Redox Cycle, *Energy Technol.* 5 (2017) 2138–2149. doi:10.1002/ente.201700083.
- [103] P.T. Krenzke, J.R. Fosheim, J.H. Davidson, Solar fuels via chemical-looping reforming, *Sol. Energy*. 156 (2017) 48–72. doi:10.1016/j.solener.2017.05.095.
- [104] P.T. Krenzke, J.R. Fosheim, J. Zheng, J.H. Davidson, Synthesis gas production via the solar partial oxidation of methane-ceria redox cycle: Conversion, selectivity, and efficiency, *Int. J. Hydrogen Energy*. 41 (2016) 12799–12811. doi:10.1016/j.ijhydene.2016.06.095.
- [105] L.M. Serra, M.A. Lozano, J. Ramos, A. V. Ensinas, S.A. Nebra, Polygeneration and efficient use of natural resources, *Energy*. 34 (2009) 575–586. doi:10.1016/j.energy.2008.08.013.
- [106] Y.K. Salkuyeh, T.A. Adams, A new power, methanol, and DME polygeneration process using integrated chemical looping systems, *Energy Convers. Manag.* 88 (2014) 411–425. doi:10.1016/j.enconman.2014.08.039.
- [107] Z. Chen, H. Zhang, W. Ying, D. Fang, Global Kinetics of Direct Dimethyl Ether Synthesis Process from Syngas in Slurry Reactor over a Novel Cu-Zn-Al-Zr Slurry Catalyst, *World Acad. Sci. Eng. Technol.* 68 (2010) 1426–1432.
- [108] Q. Yi, Y. Fan, W. Li, J. Feng, CO₂ capture and use in a novel coal-based polygeneration system, *Ind. Eng. Chem. Res.* 52 (2013) 14231–14240. doi:10.1021/ie401767b.
- [109] H. Lin, H. Jin, L. Gao, W. Han, N. Zhang, Thermodynamic and economic analysis of the coal-based polygeneration system with CO₂ capture, *Energy Procedia*. 1 (2009) 4193–4199. doi:10.1016/j.egypro.2009.02.229.
- [110] L. Zhu, Z. Zhang, J. Fan, P. Jiang, Polygeneration of hydrogen and power based on coal gasification integrated with a dual chemical looping process: Thermodynamic investigation, *Comput. Chem. Eng.* 84 (2016) 302–312. doi:10.1016/j.compchemeng.2015.09.010.

- [111] K.S. Ng, N. Zhang, J. Sadhukhan, Techno-economic analysis of polygeneration systems with carbon capture and storage and CO₂ reuse, *Chem. Eng. J.* 219 (2013) 96–108. doi:10.1016/j.cej.2012.12.082.
- [112] S. Li, H. Jin, L. Gao, X. Zhang, Exergy analysis and the energy saving mechanism for coal to synthetic/substitute natural gas and power cogeneration system without and with CO₂ capture, *Appl. Energy*. 130 (2014) 552–561. doi:10.1016/j.apenergy.2014.03.036.
- [113] Z. Azizi, M. Rezaeimanesh, T. Tohidian, M.R. Rahimpour, Dimethyl ether: A review of technologies and production challenges, *Chem. Eng. Process. Process Intensif.* 82 (2014) 150–172. doi:10.1016/j.cep.2014.06.007.
- [114] No Title, (n.d.). <http://www.toyo-eng.com/jp/en/products/energy/dme/>.
- [115] L. Bursanescu, F. Blais, NRC Publications Archive Archives des publications du CNRC, *Proc. Int. Conf. Recent Adv. 3-D Digit. Imaging Model.* (1997). <http://besmartbrand.com/download/8894951.pdf?187fdf>.
- [116] E.D. Larson, E.D. Larson, H. Jin, H. Jin, F.E. Celi, F.E. Celi, C. Engineering, C. Engineering, SUPPORTING INFORMATION to Large-Scale Gasification-Based Co-Production of Fuels and Electricity from Switchgrass, *Analysis.* (n.d.) 1–60.
- [117] L.R. Clausen, B. Elmegaard, J. Ahrenfeldt, U. Henriksen, Thermodynamic analysis of small-scale dimethyl ether (DME) and methanol plants based on the efficient two-stage gasifier, *Energy*. 36 (2011) 5805–5814. doi:10.1016/j.energy.2011.08.047.
- [118] D. Cocco, A. Pettinau, G. Cau, Energy and economic assessment of IGCC power plants integrated with DME synthesis processes, *Proc. Inst. Mech. Eng. Part A J. Power Energy*. 220 (2006) 95–102. doi:10.1243/095765006X76027.
- [119] S.H. Park, C.S. Lee, Combustion performance and emission reduction characteristics of automotive DME engine system, *Prog. Energy Combust. Sci.* 39 (2013) 147–168. doi:10.1016/j.peccs.2012.10.002.
- [120] J. McCandless, DME as an Automotive Fuel: Technical, Economic and Social Perspective, in: *Energy Front. Conf.*, 2001.
- [121] L. Ingvar, G. Rikard, M. Birgitta, G. Fredrik, F. Erik, L. Patrik, Ö.O.G. W., S.E. Lauge, S. Per, Two years experience of the BioDME project—A complete wood to wheel concept, *Environ. Prog. Sustain. Energy*. 33 (2014) 744–750. doi:doi:10.1002/ep.11993.
- [122] T.J. Kotas, Chapter 2 - Basic exergy concepts BT - The Exergy Method of Thermal Plant Analysis, in: *Butterworth-Heinemann*, 1985: pp. 29–56. doi:https://doi.org/10.1016/B978-0-408-01350-5.50009-X.
- [123] A.P. Hinderink, F.P.J.M. Kerckhof, A.B.K. Lie, J. De Swaan Arons, H.J. Van Der Kooi, Exergy analysis with a flowsheeting simulator - I. Theory; calculating exergies of material streams, *Chem. Eng. Sci.* 51 (1996) 4693–4700. doi:10.1016/0009-2509(96)00220-5.
- [124] J. Szargut, Chemical Exergies of the Elements, *Appl. Energy*. 32 (1989) 269–286.
- [125] J.Y. Xiang, M. Cal, M. Santarelli, Calculation for physical and chemical exergy of flows in systems elaborating mixed-phase flows and a case study in an IRSOFC plant,

- 115 (2004) 101–115. doi:10.1002/er.953.
- [126] Kristen Gerdes, John Haslbeck, Norma Kuehn, Eric Lewis, Lora L. Pinkerton, Mark Woods, James Simpson, Marc J. Turner, Elsy Varghese, Cost and Performance Baseline for Fossil Energy Plants Volume 1: Bituminous Coal and Natural Gas to Electricity, Doe/Netl-2010/1397. 1 (2010). doi:DOE/NETL-2010/1397.
- [127] K. Gerdes, W.M. Summers, J. Wimer, Cost Estimation Methodology for NETL Assessments of Power Plant Performance, Doe/Netl-2011/1455. (2011) 26. http://www.netl.doe.gov/File_Library/research/energy_analysis/publications/QGESSNETLCostEstMethod.pdf.
- [128] S. Lemmens, Cost engineering techniques & their applicability for cost estimation of organic rankine cycle systems, *Energies*. 9 (2016). doi:10.3390/en9070485.
- [129] J.A.S. Richard Turton, Richard C. Bailie, Wallace B. Whiting, Analysis, Synthesis and Design of Chemical Processes Third Edition, 2013. doi:10.1017/CBO9781107415324.004.
- [130] M. Yang, International Energy Agency Working Paper Series Modeling Investment Risks and Uncertainties with Real Options Approach Modeling Investment Risks and Uncertainties with Real Options Approach, Structure. 13 (2007) 1120–37. http://www.iea.org/Textbase/publications/free_new_Desc.asp?PUBS_ID=1857.
- [131] Eurostat, Natural gas price statistics, EU-28, (2016) 1–12. doi:http://ec.europa.eu/eurostat/statistics-explained/index.php/Natural_gas_price_statistics.
- [132] Statista wabe page, (n.d.). <https://www.statista.com/statistics/450146/global-reocerium-oxide-price-forecast/>.
- [133] G. Tsatsaronis, Definitions and nomenclature in exergy analysis and exergoeconomics, *Energy*. 32 (2007) 249–253. doi:10.1016/j.energy.2006.07.002.
- [134] G. Tsatsaronis, Computer-aided energy systems analysis: presented at the winter annual meeting of the American Society of Mechanical Engineers, Dallas, Texas, November 25-30, 1990, Amer Society of Mechanical, 1990.
- [135] A. Lazzaretto, R. Andreatta, Algebraic formulation of a process-based exergoeconomic method, *Am. Soc. Mech. Eng. Adv. Energy Syst. Div. AES*. 35 (1995) 2018.
- [136] M. Khaljani, R. Khoshbakhti Saray, K. Bahlouli, Comprehensive analysis of energy, exergy and exergo-economic of cogeneration of heat and power in a combined gas turbine and organic Rankine cycle, *Energy Convers. Manag.* 97 (2015) 154–165. doi:10.1016/j.enconman.2015.02.067.
- [137] A. Lazzaretto, G. Tsatsaronis, SPECO: A systematic and general methodology for calculating efficiencies and costs in thermal systems, *Energy*. 31 (2006) 1257–1289. doi:10.1016/j.energy.2005.03.011.
- [138] M.A. Lozano, A. Valero, Theory of the exergetic cost, *Energy*. 18 (1993) 939–960. doi:10.1016/0360-5442(93)90006-Y.
- [139] A. Valero, M. Lozano, M. Munoz, A general theory of exergy saving I. On the exergetic cost, 1986.

- [140] M.N. Khan, T. Shamim, Exergoeconomic analysis of a chemical looping reforming plant for hydrogen production, *Int. J. Hydrogen Energy*. 42 (2017) 4951–4965. doi:10.1016/j.ijhydene.2016.11.098.
- [141] M.M. Mekonnen, P.W. Gerbens-Leenes, A.Y. Hoekstra, The consumptive water footprint of electricity and heat: a global assessment, *Environ. Sci. Water Res. Technol.* 1 (2015) 285–297. doi:10.1039/C5EW00026B.
- [142] M. Egan, *The Water Footprint Assessment Manual. Setting the Global Standard*, Soc. Environ. Account. J. 31 (2011) 181–182. doi:10.1080/0969160X.2011.593864.
- [143] A.D. Martin, A. Delgado, A. Delgado Martin, Water Footprint of Electric Power Generation : Modeling its use and analyzing options for a water-scarce future, *Int. Congr. Adv. Nucl. Power Plants*. 44 (2012) 117. doi:10.1021/es802162x.
- [144] Kristen Gerdes, John Haslbeck, Norma Kuehn, Eric Lewis, Lora L. Pinkerton, Mark Woods, James Simpson, Marc J. Turner, Elsy Varghese, *Cost and Performance Baseline for Fossil Energy Plants Volume 1: Bituminous Coal and Natural Gas to Electricity, Doe/Netl-2010/1397*. 1 (2010). doi:DOE/NETL-2010/1397.
- [145] A.M. Eltony, H.G. Park, S.X. Wang, J. Kong, I.L. Chuang, Motional heating in a graphene-coated ion trap, *Nano Lett.* 14 (2014) 5712–5716. doi:10.1021/nl502468g.
- [146] D.-Y. Peng, D.B. Robinson, A New Two-Constant Equation of State, *Ind. Eng. Chem. Fundam.* 15 (1976) 59–64. doi:10.1021/i160057a011.
- [147] M.K. Cohce, I. Dincer, M.A. Rosen, Energy and exergy analyses of a biomass-based hydrogen production system, *Bioresour. Technol.* 102 (2011) 8466–8474. doi:10.1016/j.biortech.2011.06.020.
- [148] L. Fanxing, Z. Liang, V.L. G., Y. Zachary, F. Liang-Shih, Syngas chemical looping gasification process: Bench-scale studies and reactor simulations, *AIChE J.* 56 (2009) 2186–2199. doi:10.1002/aic.12093.
- [149] I. Barin, *Thermochemical data of pure substances*, (1995) 2 v.
- [150] H.M. Shim, S.J. Lee, Y.D. Yoo, Y.S. Yun, H.T. Kim, Simulation of DME synthesis from coal syngas by kinetics model, *Korean J. Chem. Eng.* 26 (2009) 641–648. doi:10.1007/s11814-009-0107-9.
- [151] G.H. Graaf, J.G.M. Winkelman, Chemical Equilibria in Methanol Synthesis Including the Water-Gas Shift Reaction: A Critical Reassessment, *Ind. Eng. Chem. Res.* 55 (2016) 5854–5864. doi:10.1021/acs.iecr.6b00815.
- [152] Politecnico di Milano - CAESER Project, European best practice guidelines for assessment of CO2 capture technologies, 2011.
- [153] M.N. Khan, T. Shamim, Influence of Specularity Coefficient on the Hydrodynamics and Bubble Statistics of an Annular Fluidized Bed Reactor, *Energy Procedia*. 105 (2017) 1998–2003. doi:10.1016/j.egypro.2017.03.573.
- [154] B.J.P. Buhre, L.K. Elliott, C.D. Sheng, R.P. Gupta, T.F. Wall, Oxy-fuel combustion technology for coal-fired power generation, *Prog. Energy Combust. Sci.* 31 (2005) 283–307. doi:10.1016/j.pecs.2005.07.001.
- [155] M. Pozzo, A. Lanzini, M. Santarelli, Enhanced biomass-to-liquid (BTL) conversion

- process through high temperature co-electrolysis in a solid oxide electrolysis cell (SOEC), *Fuel*. 145 (2015) 39–49. doi:10.1016/j.fuel.2014.12.066.
- [156] D. Version, based on gasification of biomass PhD Thesis, 2011.
- [157] K.L. Ng, D. Chadwick, B.A. Toseland, Kinetics and modelling of dimethyl ether synthesis from synthesis gas, *Chem. Eng. Sci.* 54 (1999) 3587–3592. doi:10.1016/S0009-2509(98)00514-4.
- [158] F. Dadgar, R. Myrstad, P. Pfeifer, A. Holmen, H.J. Venvik, Direct dimethyl ether synthesis from synthesis gas: The influence of methanol dehydration on methanol synthesis reaction, *Catal. Today*. 270 (2016) 76–84. doi:10.1016/j.cattod.2015.09.024.
- [159] C. Arcoumanis, C. Bae, R. Crookes, E. Kinoshita, The potential of di-methyl ether (DME) as an alternative fuel for compression-ignition engines: A review, *Fuel*. 87 (2008) 1014–1030. doi:10.1016/j.fuel.2007.06.007.
- [160] J. Sun, G. Yang, Y. Yoneyama, N. Tsubaki, Catalysis chemistry of dimethyl ether synthesis, *ACS Catal.* 4 (2014) 3346–3356. doi:10.1021/cs500967j.
- [161] T. Ogawa, N. Inoue, T. Shikada, Y. Ohno, Direct Dimethyl Ether Synthesis, *J. Nat. Gas Chem.* 12 (2003) 219–227.
- [162] K.M. Vanden Bussche, G.F. Froment, A Steady-State Kinetic Model for Methanol Synthesis and the Water Gas Shift Reaction on a Commercial Cu/ZnO/Al₂O₃ Catalyst, *J. Catal.* 161 (1996) 1–10. doi:10.1006/jcat.1996.0156.
- [163] G. Berčić, J. Levec, Catalytic Dehydration of Methanol to Dimethyl Ether. Kinetic Investigation and Reactor Simulation, *Ind. Eng. Chem. Res.* 32 (1993) 2478–2484. doi:10.1021/ie00023a006.
- [164] R.S. Schiffino, R.P. Merrill, A mechanistic study of the methanol dehydration reaction on γ -alumina catalyst, *J. Phys. Chem.* 97 (1993) 6425–6435. doi:10.1021/j100126a017.
- [165] K. Klier, V. Chatikavanij, R.G. Herman, G.W. Simmons, Catalytic synthesis of methanol from CO₂: IV. The effects of carbon dioxide, *J. Catal.* 74 (1982) 343–360. doi:https://doi.org/10.1016/0021-9517(82)90040-9.
- [166] G.R. Moradi, F. Yaripour, P. Vale-Sheyda, Catalytic dehydration of methanol to dimethyl ether over mordenite catalysts, *Fuel Process. Technol.* 91 (2010) 461–468. doi:10.1016/j.fuproc.2009.12.005.
- [167] Y. Zhao, H. Chen, M. Waters, D.N. Mavris, Modeling and Cost Optimization of Combined Cycle Heat Recovery Generator Systems, Vol. 1 Turbo Expo 2003. (2003) 881–891. doi:10.1115/GT2003-38568.
- [168] L.E. D., J. Haiming, C.F. E., Large-scale gasification-based coproduction of fuels and electricity from switchgrass, *Biofuels, Bioprod. Biorefining.* 3 (2009) 174–194. doi:doi:10.1002/bbb.137.
- [169] N. Berghout, T. Kuramochi, M. van den Broek, A. Faaij, Techno-economic performance and spatial footprint of infrastructure configurations for large scale CO₂ capture in industrial zones. A case study for the Rotterdam Botlek area (part A), *Int. J. Greenh. Gas Control.* 39 (2015) 256–284. doi:10.1016/j.ijggc.2015.05.019.

- [170] R. Porrazzo, G. White, R. Ocone, Techno-economic investigation of a chemical looping combustion based power plant, *Faraday Discuss.* 192 (2016) 437–457. doi:10.1039/C6FD00033A.
- [171] IPIECA, (n.d.). <http://www.ipieca.org/resources/energy-efficiency-solutions/power-and-heat-generation/turbo-expanders/>.
- [172] Market Observatory for Energy, Quarterly Report on European Electricity Markets, 2017.
- [173] T.A. Semelsberger, R.L. Borup, H.L. Greene, Dimethyl ether (DME) as an alternative fuel, *J. Power Sources.* 156 (2006) 497–511. doi:10.1016/j.jpowsour.2005.05.082.
- [174] P.N. Dyer, R.E. Richards, S.L. Russek, D.M. Taylor, Ion transport membrane technology for oxygen separation and syngas production, *Solid State Ionics.* 134 (2000) 21–33. doi:10.1016/S0167-2738(00)00710-4.
- [175] M. Martín, Artificial versus Natural Reuse of CO₂ for DME Production: Are We Any Closer?, *Engineering.* 3 (2017) 166–170. doi:10.1016/J.ENG.2017.02.002.
- [176] C.L. Muhich, B.D. Ehrhart, V.A. Witte, S.L. Miller, E.N. Coker, C.B. Musgrave, A.W. Weimer, Predicting the solar thermochemical water splitting ability and reaction mechanism of metal oxides: a case study of the hercynite family of water splitting cycles, *Energy Environ. Sci.* 8 (2015) 3687–3699. doi:10.1039/C5EE01979F.
- [177] N. Gokon, T. Suda, T. Kodama, Oxygen and hydrogen productivities and repeatable reactivity of 30-mol%-Fe-, Co-, Ni-, Mn-doped CeO_{2-δ} for thermochemical two-step water-splitting cycle, *Energy.* 90 (2015) 1280–1289. doi:10.1016/j.energy.2015.06.085.
- [178] D.L.-S. Fan, *Chemical Looping Partial Oxidation: Gasification, Reforming, and Chemical Syntheses*, Cambridge University Press, 2017.
- [179] B. Bulfin, A.J. Lowe, K.A. Keogh, B.E. Murphy, O. Lübben, S.A. Krasnikov, I. V. Shvets, Analytical Model of CeO₂ Oxidation and Reduction, *J. Phys. Chem. C.* 117 (2013) 24129–24137. doi:10.1021/jp406578z.
- [180] D. Arifin, Study of redox reactions to split water and carbon dioxide, University of Colorado, 2013. http://scholar.colorado.edu/chbe_gradetds/54.
- [181] D. Arifin, A.W. Weimer, Kinetics and mechanism of solar-thermochemical H₂ and CO production by oxidation of reduced CeO₂, *Sol. Energy.* 160 (2018) 178–185. doi:10.1016/j.solener.2017.11.075.
- [182] Aspen Technology, Aspen Plus Model for Moving Bed Coal Gasifier, 2010.
- [183] R. Dindorf, Estimating potential energy savings in compressed air systems, *Procedia Eng.* 39 (2012) 204–211. doi:10.1016/j.proeng.2012.07.026.